PB195763

QUARTERLY REPORTS

RAILWAY TECHNICAL RESEARCH INSTITUTE

1970

VOL. 11 NO. 3

Reproduced by
NATIONAL TECHNICAL
INFORMATION SERVICE
Springfield, Va. 22151

JAPANESE NATIONAL RAILWAYS

Published quarterly by Ken-yusha, Inc. under the supervision of the Railway Technical Research Institute, JNR
© Copyright 1970 Railway Technical Research Institute

Editorial Board

Chairman : Nobuo MATSUI, Vice-director RTRI
Co-chairmen : Noboru KUROKOCHI, Junichi MIYAKO
Editors : Sukekuni SHIBA, Toshio NAKANISHI, Yoshimasa KOBAYASHI, Sadaaki KURODA, Hideaki YOSHIMOTO, Kuranobu SUGITA, Hiroshi ARAI, Seinosuke ARAI, Yoko ISHII, Shigemichi SUZUKI, and Takeo SUGIMURA

Correspondence should be addressed to the Railway Technical Research Institute, JNR, Kunitachi, P.O. Box No. 9, Tokyo, Japan. Copies are obtainable on exchange basis.

QUARTERLY REPORTS

RAILWAY TECHNICAL RESEARCH INSTITUTE

REVIEW

121 · Modernization of Ticket Issuing and Inspection **Y. Ohno, T. Kikuchi**

129 · Corrosion Prevention of Track Materials **Y. Kose**

137 · Delayed Failure of High Strength Bolt **A. Ito, S. Matsuyama**

TECHNICAL PAPERS

142 · The Investigation of Cutting Slopes — Survey of Slope Soil Structure and Reappraisal of the Point-rationing System Evaluating Slope Failure **G. Yamada, S. Kobashi, H. Arai, A. Imai**

146 · Experiments on Arita River Railway Bridge with the Concrete Bed **Y. Warizawa, I. Iwasaki**

149 · Standing Test of Eddy Current Rail Brake Set to a New Test Electric Car **H. Sookawa, Y. Sato, E. Itakura, M. Miyairi**

153 · Computer Program for Analysis of the Feeder Circuit with Auto-Transformers on AC Electrified Railway **J. Mizuno, S. Hamayose, K. Ishikawa**

155 · Nondestructive Snapping Inspection of Stranded Wire in Jumper Cable of Railway Car **T. Matsunaga, M. Nakano, M. Miyairi**

158 · Fatigue Strength of Side Fillet Welded Joint **S. Ohta, S. Terada, Y. Eguchi, S. Deguchi**

160 · On the Thermal Effect of Tread Braking upon Car Wheels **T. Hirooka, H. Teramura, T. Saito, T. Kikawa, K. Ishii**

163 · A New Method of Measuring Fatigue and Fatigue Behaviors of Plastics **F. Ohishi**

TECHNICAL NOTES

167 · Some Data on Damage to Manganese Steel Crossing in Service **I. Ooi, N. Kimata**

168 · Rock Breaking with High Speed Water Jet Stream **T. Kinoshita, K. Hoshino**

169 · Measurement of Strese of Railway Bridge Stringers to which the Rail is Fastened without Sleeper **F. Itoh, T. Okuda**

170 · Surge Test on Test Car in SHIN KANSEN **K. Arai, K. Watahiki, T. Furuhata, T. Tajima**

171 · Discharge Characteristics of Nickel-Cadmium Cells Charged at Constant Voltage **S. Okuma, K. Sugita**

172 · Analysis of Combustion Process of DML 61 Series Diesel Engine **T. Uchibori, E. Kawashima, T. Arai**

173 · Experiment of the Automatic Valve Clearance Adjusting Device of the Diesel Engine for Rail Car **T. Uchibori, T. Arai**

174 · Construction of the New Alternating Load Type Adhesion Testing Machine **H. Maruyama, T. Oyama**

175 · Effect of Air Bag Type Car Holder on the Side Structure of Freightcar **M. Izumi**

176 · Noncontact Transmission of Signals Measured on Rotating Objects with Mutual Induction **H. Sugiyama, S. Wada**

177 · Package form Survey of JNR Baggage **R. Imanishi, T. Ohnuma, K. Maeda, K. Yamanaka**

179 · Statistical Estimates of Cumulative Failure Rate and Conditional Reliability from Short Term Observations **S. Abe**

September 1970 Vol. 11 No. 3

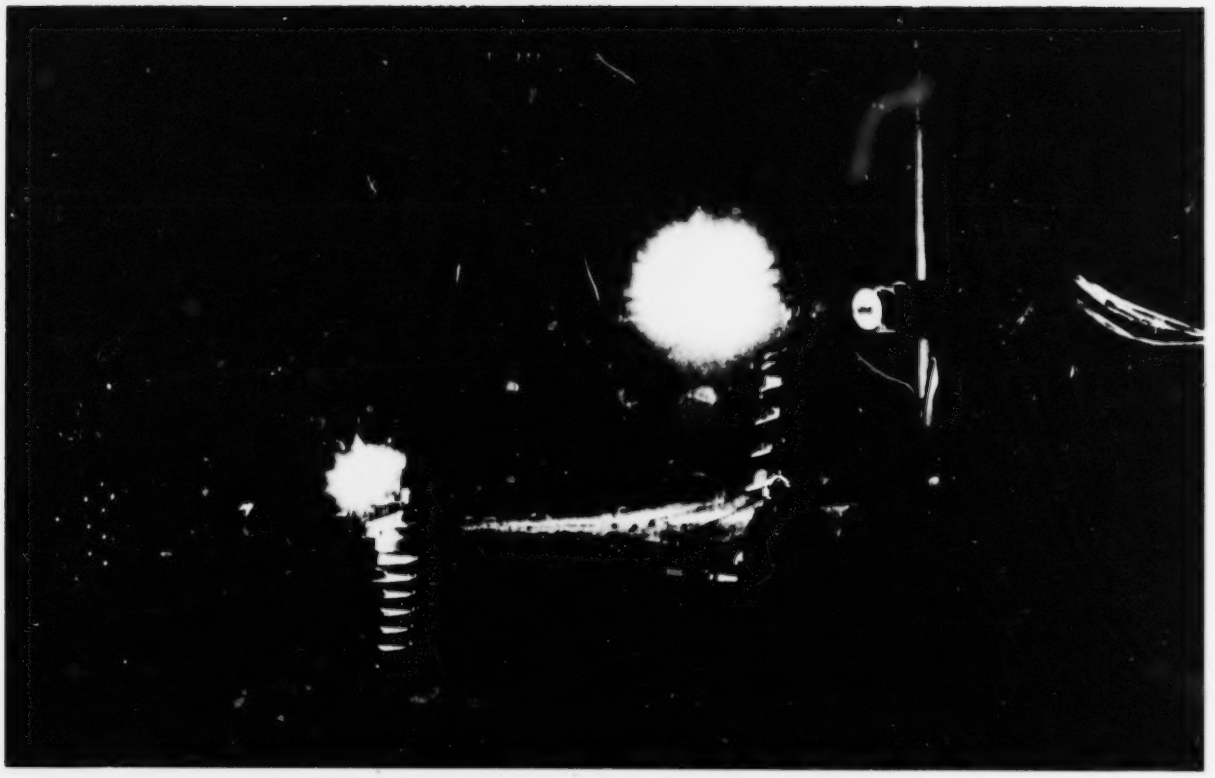

Artificial fault test of AT feeder circuit at Komenotsu Station

AT Feeder System Becomes Practical

AC electrification of Kagoshima Trunk Line between Yatsushiro and Kagoshima is under way for completion by October, 1970. The first AT feeder system in Japan will be adopted on this line. This system will also be adopted on SAN-YO SHIN KANSEN. Extending over a month from October to November, 1969, various tests were carried out to confirm its practicability.

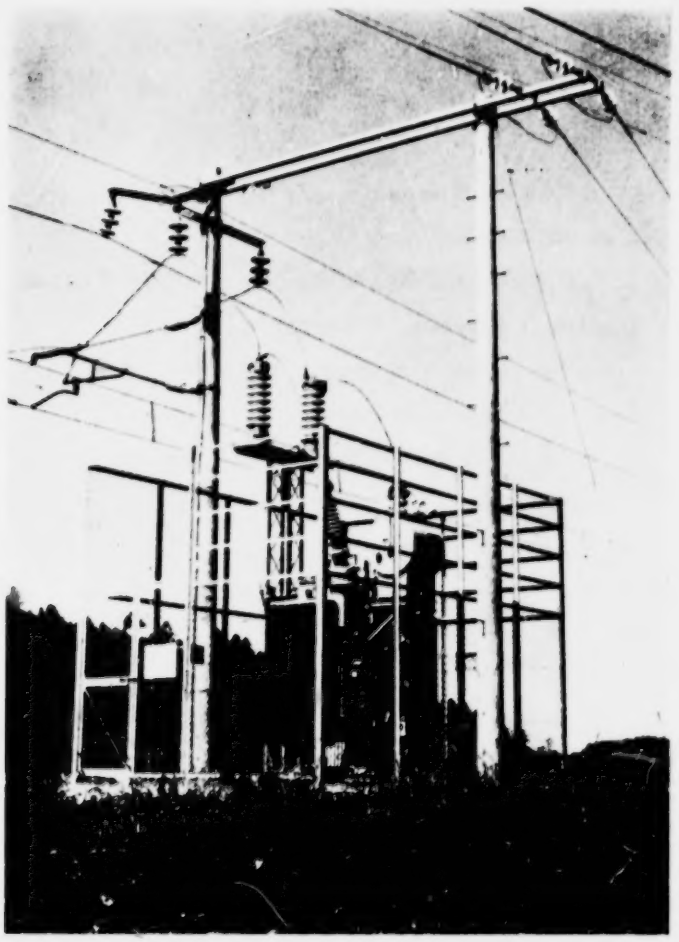

Way side autotransformer (AT)

Artificial fault test of AT feeder circuit in Tsunaki Tunnel

656.2.035.2/3—52 : 656.211.063 : 681.3

Modernization of Ticket Issuing and Inspection

Yutaka OHNO, Dr. Eng.*, Takashi KIKUCHI†

JNR is planning Automatic Wicket Gate System (AWGS), which is to be applied on Musashino line that is now under construction and is scheduled to be opened to traffic October 1972. In this connection, the most essential proflems are discussed; system analysis which is concerned with a backgroud for development of AWGS, an outline of ticket issuing and inspection jobs, progress future line for development of AWGS, etc.

Introduction

Modernization of ticket issuing and inspection, which are main business at passenger railway stations, has been positively pushed forward since about 1955. These efforts have brought about successful improvement of passenger service and rationalized exploitation of personnel such as the "Green Window", automatic ticket vending machines. In addition to seat reservation and sale of short distance tickets, the business of ticket issuing and inspection involves many other jobs, modernization of which presents a future task.

Among others, modernization of ticket inspection at the wicket is an area about which nothing has been done, mainly because it requires issue of tickets readable by machine and on account of necessary coordination with private railways the mechanization of ticket inspection cannot be limited to a specified scope at a specified station. However, the increase of personnel cost and the ever increassing difficulty of securing manpower for simple jobs under unattractive conditions are compelling JNR to venture on the modernization of ticket inspection.

The present paper purports to give a rough idea of modernization of ticket issuing and inspection as a whole and go into some details about ticket inspection.

1. Background to Modernization of Ticket Issuing and Inspection

As well known, the JNR finance has been continuously in the red since 1964 and in spite of tariff revisions in 1966 and again in 1969, the condition is now critically bad with no anticipated revenue increase realized and tremendous debts never dwindling. To tide over this crisis, JNR feels it necessary not only to resort to tariff revision but also to probe into the traffic cost structure itself.

Breakdown of expenses, as indicated in Fig. 2, shows that personnel cost is far in excess of materials cost; that is, the cost structure is labour-intensive.

It is the consensus of opinion that this financial crisis of JNR can be traced to a drop in the JNR share in the total traffic volume of Japan and a sharp rise in personnel expenses.

The first countermeasure would be drastic improvement of productivity through thoroughgoing streamlining of business. In other words what is to be done are industrial change from labour intensive to equipment-intensive basis and enlargement of share through modernized service and stepped-up activity of sales operation. Sales operation is just the activity that can be made only by humans. Personnel need for this activity should be filled by rationalizing the other operations that may be taken over by machines and thus humans ought to be utilized in such manner as "humans" should be.

Automation of ticket issuing and inspection

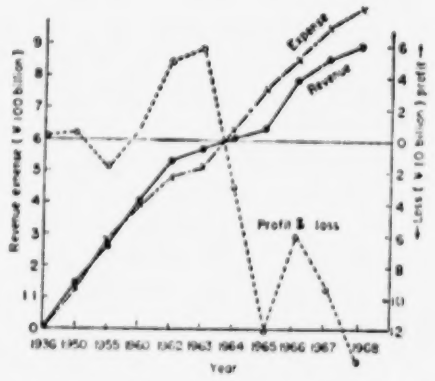

Fig. 1 Operation results (figure for 1968 is an estimate)

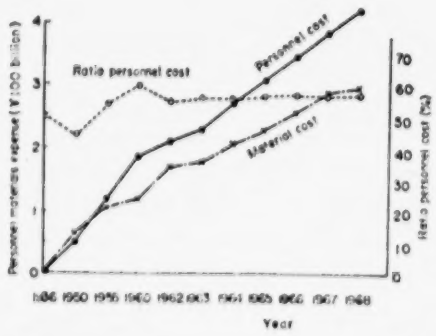

Fig. 2 Personnel vs. materials expenses (profit-loos account) (figure for 1968 is an estimate)

* System Laboratory, † Formerly, System Laboratory

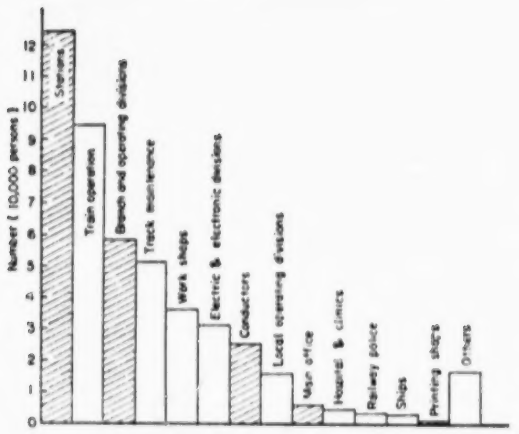

Fig. 3 Number of personnel by work areas (as of end of 1966) (cited from "JNR memo")

comes up as an important part of "equipment-industrialization" of JNR to save it out of financial distress.

According to Fig. 3 showing the numbers of employees by work divisions, the greatest number of workers are assigned to stations and of this number, according to a partial survey giving inaccurate figures, more than 50 % of personnel at passenger stations are represented by ticket clerks and inspectors. From this it may be estimated that there are over 35,000 ticket clerks working at stations and if many other employees related indirectly to ticket business, i.e., printing, examination and statistics are counted, the work volume will be equivalent to about 45,000 employees for the whole JNR, which means that the personnel related to ticket business has a high proportion of 10 % in JNR.

Thus, from a standpoint of personnel rationalization, modernization of ticket issuing and inspection might well be called one of the most vital tasks to be performed. Ticket issuing and inspection, which involves contact with customers, cash handling and decision-making, has been most labour-intensive, but the latest advances in electronics technology offer good prospects, technical and economic, of mechanizing this business.

JNR passenger traffic volume is estimated to exceed 300 billion passenger-kilometers in 1978, which is double the figure for 1965. Even at present, the traffic in rush hours is too busy to allow the ticket inspector to check the face of each ticket. If things are allowed to drift as they do, substantial increase in ticket clerks and inspectors will be imperative. Meanwhile, the relative monotony of this job in unfavourable work environment with dust, noise, heat (summer) and cold (winter) is becoming less and less alluring to job seekers. Already private railways begin to find difficulty in recruiting station personnel. Thus viewed, simplification, mechanization of ticket business or even its automation with no human attention may be called a natural course of development.

In Western countries, issuing of common tickets has long been mechanized; mechanized issuing began to be practiced early in the 20 th century. As for ticket inspection, subways under flat fare system were the first to automate ticket inspection, followed by other railways, which are now positively going ahead with automation. The Illinois Central of U. S. has completed full automation of ticket issuing and inspection (automatic fare collection system) at all its 49 stations. The London Board of Transport has finished automation of ticket business on the Victoria line and soon the automation will be extended to other lines. BART in the U. S., which is now under construction, is said to be going to realize automated ticket issuing and inspection with introduction of the "credit card" idea. Major railways in foreign countries, though later than JNR, now adopt automation of seat reservation.

Modernization of ticket business in private railways of Japan is going at nearly the same pace as that in JNR. As pointed out, however, the private railways are experiencing difficulty in personnel recruitment and accordingly they are more enthusiastic in automation of ticket inpsection; already Hankyu Electric puts tentative equipment in service test at two stations and Nagoya Railway at one station. Several other companies are now planning a test. All these railways seem to be waiting for JNR decision on its system to be adopted for reasons of coordination with JNR, so that they can put their equipment to practical use as soon as possible.

In the above, the necessity for modernization of ticket business and other related matters have been briefly discussed. It may be concluded that JNR should also be still more positive, comprehensive and drastic in its modernization efforts.

2. Outline of Ticket issuing and Inspection

At first, a rough idea of ticket business is to be given. Figure 4 illustrates a flow chart of ticket business centered around tickets.

Common tickets may be classified into ones (for short trip) handled by vending machines and ones (mainly for long trip) issued at manned ticket windows. The former are printed and issued in time of sale. The latter are already printed at printing shops and have values as negotiable tokens, which call for strictness in reception, inventory and delivery at stations.

Sold tickets are entered in respective accounts (destination numbers) of the ticket register; and together with retained pieces of supplementary tickets and others, they make materials for examination and statistics-taking. Sales records of the "Green Windows" are automatically taken by the central computer.

A ticket handed over to the passenger is inspected at the wicket. Aboard the train, if he goes beyond the original destinatiou or changes the direction of travel, he asks the conductor to issue

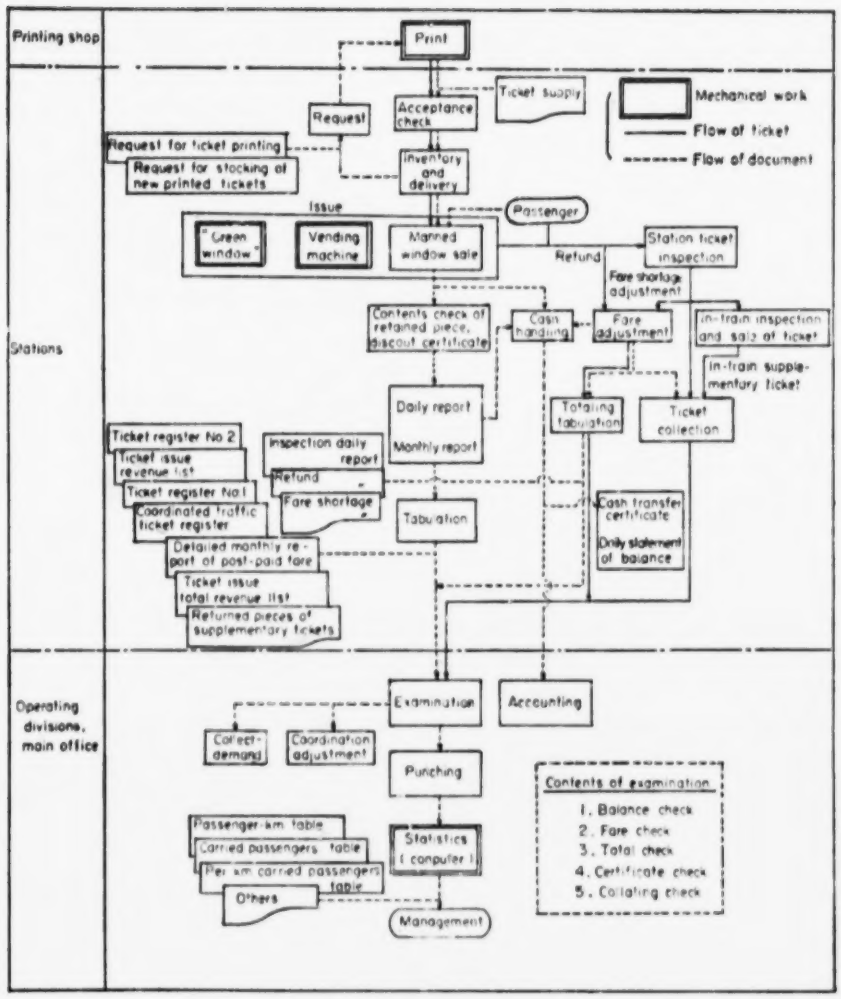

Fig. 4 Flow (existing) of ticket business

a supplementary ticket or he adjusts the fare at the destination. Passengers with a season ticket or a stopover ticket pass through the wicket without surrendering the ticket, but other tickets are collected there.

Mutual adjustments between coordinated railways are manually made by the Examination Department on the basis of ticket registers and retained pieces of supplementary tickets.

Annual passenger volume handled by JNR is about 7 billion as of 1967, of which about 5 billion are season-ticket holders accounting for 71 %. In terms of the number of tickets sold, the major 400 of about 4,500 stations in total of JNR sell approximately 70 % of the total tickets. There is thus a wide difference in ticket sales between major and minor stations and the greater part are minor stations. This situation dictates the need for a comprehensive review based not simply on mechanization but also on drastic reform of system.

3. Developments and Future Trends in Modernization of Ticket Business

As mentioned above, ticket business is broadly divided into window business, rear business and wicket business. Description will be made in accordance with this division.

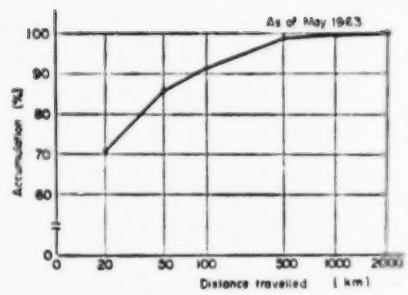

Fig. 5 Distance breakdown of passengers other than season ticket holders

3.1 *Window business*

Tickets are many and diverse and accordingly modernization of window business is being worked out to suit each feature of tickets. This trend will remain unchanged.

(1) Common short distance tickets

As illustrated in Fig. 5, among the passengers other than season ticket-holders the short travellers are predominant; for instance, low fares for short distances of less than 100 km account for more than 90 % (this involves use of coins). Thus, passenger-operated automatic sale of such tickets is possible and the adoption of automatic ticket vending machine has long been contemplated.

In 1929, a machine for selling hardboard platform tickets was for the first time tried, but under the circumstances prevailing in those days the necessity for such a machine was not felt strongly enough and for a long time afterward subsequent development was not witnessed. About 1953, a hardboard ticket vending machine, was introduced, but it was not yet fully utilized. Full utilization and dissemination of such machines came after successful development of a multipurpose soft ticket vending machine in 1966. Since October 1968, the sale of all tickets less than ¥ 100 worth for a ride on the Tokyo electric loop line has been mechanized by vending machines.

In future the dissemination and improvement of vending machines will continue and the problems to be solved will be alleviation of daily maintenance (supply of changes), cutdown of machine cost and extension of sales range (at present about 50 km).

Solutions of these problems are already being tried. Namely, prototypes of a machine with automatic supply of changes and one with centralized printing have been worked out and are now under test.

Extension of sales range of the machine poses specific problems, one of which is how to print the ticket face. With an increased sales range, it

would be disadvantageous to draw a map on the ticket; but a mere indication of departure station would require the inspector at the destination to remember fares to his station from many others. This inconvenience would be liquidated by automation of ticket inspection as described later. It offers a good example of mechanization of one area giving favourable conditions for mechanization at other areas.

(2) Common long distance tickets

Tickets other than ones for short distances (that is, unfit for vending machines) are called long distance tickets. With an increased sales range of vending machines, the number of long distance tickets is bound to decrease. These tickets have contrary features to short distance ones: small number, extremely wide variety of destinations, and high prices. On account of these features, they do not permit modernization in such a simple manner as by use of the vending machine. Modernization of these tickets, therefore, should be directed toward a shortening of the ticket processing time at the window or simplification of rear business; and actual it is moving in this direction. Since 1957, deliberations had been made mainly by the Ticket Business Modernization Committee and the year 1961 marked a tentative manufacture of a ticket printer-issuer on a relief-printing system. Because of noisiness, bulkiness and other troubles, however, this machine stopped short of practical application.

With subsequent progress in technology, in 1967 a mechanical ticket printer-issuer with an improved relief printing of the same system as before was worked out and submitted to various tests and as the result its practicability was fully established. Several units of this machine are to be placed in regular service at stations this year. In the same year of 1967 a machine of electrostatic printing system was perfected; being intended for service at particularly big stations, it employs a technically most advanced system. Also a set of this machine will be put on trial this year; this machine has the drawback of being bulky.

The microfilm method earlier conceived for simplification of printing had become promising as applicable to the printer-issuer through technical progress. Thus, in 1968 a prototype of the machine was built. This system seems to be suitable as a simplified printer-issuer to serve at medium and small stations.

Adoption of these machines will not only make it possible to automate and promptly execute discount calculations which are presently the most time-consuming of all window jobs, but also will bring great benefits through simplification and automation of rear business. But such modernization effects will appear only at major stations; and medium and small stations will not be modernized by a mere mechanization of ticket issuing. For small stations hard to mechanize, a different approach like basic change of ticket sales system must be taken.

It would be conceivable to set only a vending machine at small stations and urge the prospective long distance travellers to buy their tickets at the nearest major station. This is quite a realistic approach. As for seat reservation, telephone request system as described later may be adopted. This would not look unreasonable, when it is considered that long-distance travellers generally take superior trains, at least express trains, which skip minor stations.

Discontinuance of long-distance ticket sale is controversial. It is thinkable at some stations of considerable size to mitigate the work load on the ticket agent through installation of a most simplified printer-issuer and, through combination with automation of ticket inspection, put the whole station on a one man operation basis. As a matter of fact, stations of this size are quite numerous; private railways seem to be planning to make practically all stations one-man operation.

Anyway, modernization of ticket business at medium and small stations (majority of stations) calls for comprehensive studies including the system and the work shift pattern and only these studies will be able to realize effective modernization.

(3) Season tickets

Season tickets are characterized by small number of sales on account of long-term validity for each (though passenger volume is large), very wide variety and complexity of fare calculation. For these reasons, mechanization of sale of these tickets would be expensive and accordingly with no investment effect assured, it has practicaliy been neglected in modernization program.

Because of expenses, modernization of season ticket sale in the form of installing a machine at the present season ticket window would be unrealizable, so an adequate approach would be to concentrate at a single spot the sales of season tickets at several to some ten stations or to expand a group sale of tickets for individual companies, as partially practiced even now. The most preferable system would be to put the sale of all season tickets on a group sale basis. Upon adoption of this system, all ticket windows of stations will be closed and instead a season ticket issue certer equipped with a season ticket issuer will be established at several operating division offices.

In that case if the application form were to be filled in for employee as before, the trouble on the company side would be tremendous, while enormous time and labour would be required to give input to the machine. Thus it is conceivable to establish a master file of season ticket holders to be revised for every change in personal data such as transfer and to issue their season tickets automatically and systematically every month. The benefits accruing from such a reform will be not only a remarkable simplification of business related to season ticket

issuing but also an improved service to passengers and a rationalization of company business.

Group sale of season tickets, however, cannot be realized all at once and for the time being, we must be content with concentration of sales for several stations at one spot, the ticket window of each station accepting only the sales request. Thereby an alternative will be to refuse acceptance of request at each station and turn all the customers to a single issuing station. Many bus companies already adopt this sales system for season tickets.

Telephone acceptance of requests is also possible and this would be preferable for future; it is practically the same as group sale. In this case, too, a master file of customers will be established and customers have only to ring up the station on a preset day of every month, telling it to continue or change their tickets. Then they will be able to get their season tickets at a preset station on a preset day. The amount of data on one customer is such as can be stored on one 80-column card and a single reel of magnetic tape will be able to hold data on several tens of thousands of persons. Payment can be made by transfer from bank deposit account.

The above is a discussion on how to sell season tickets. Anyway with automation of ticket inspection expected as described later, mechanization of season ticket issuing is unavoidable.

Printed entries differ from one season ticket to another and therefore a special technique is needed in mechanical printing of season tickets. Prior to deciding on the system of season ticket sale, the prototype of a microfilm type season ticket printing mechanism was developed in 1968 as a step to perfection of the necessary printing technology and in 1969 one more step was taken in construction of a prototype season ticket issuer for automatic inspection.

(4) Reservation tickets

As the name suggests, the reservation ticket is characterized by its sale depending on availability of vacant seat; therefore a control center for availability of seats must be established. As early as 1955, JNR embarked on research for computerization of this conventionally manual work of seat reservation and now every one knows that JNR automatically reserves 340,000 seats per day. Handling of such a volume of seat reservations would be an utter impossibility without computerization. JNR plans to make a sharp increase in the number of seat reservations and offer more comfortable travel to passengers in future (see Fig. 6)

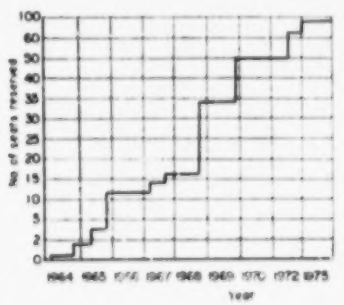

Fig. 6 Trends in seat reservation (MARS)

Future trends point not only to quantitative expansion mentioned above but also to qualitative improvement. Namely, reservation system will evolve into a consistent "travel sale" system covering not only train seats but also hotel rooms and seats on other means of transport. As for the acceptance of reservation request, instead of waiting lines before ticket windows the telephone request (as practiced by air-line companies) ought to be allowed. In this connection studies and planning are already under way.

For reservation of seats for relatively short trips, a customer-operated automatic reservation seat vender similar to the one presently in use may be used to alleviate the work load at the ticket window. A prototype apparatus for this purpose was built and tested in 1968.

In connection with the above-mentioned telephone request for reservation, a system of the computer answering the request with an intelligible "voice" instead of humans is now being studied. Prototype of this apparatus as a computerized audio-responder was built in 1969.

When all these attempts turn out successful, a comprehensive modernization of passenger service will be completed.

3.2 *Rear business*

Rear business is in a word the ticket business hidden from the sight of passengers; its volume is estimated at 20—30% of the total ticket work volume. Essentially it is a business in the nature of processing the business data.

Naturally use of computer is thinkable for modernization of this business, too. Of the business conducted by operating division offices, the statistical part has been computerized, but at present all the business from collection of data at stations to input to the computer is manually being carried out (except seat reservation); the reason is the delay in mechanization of window business. Upon, however, mechanization of window business through adoption of printer-issuers, data collection will be automated and this will be followed by automation of the succeeding business, i.e., rear business. Rear business behind the "Green Window" which is linked on-line with the computer is then naturally automated.

For rear business related to common tickets and season tickts one method conceivable is utilization of OCR (optical character reader); it is possbile to process the output from the printer-venders to be placed in regular service beginning from 1969 also by OCR. Under use of OCR, each sale or each account is printed for recording on a paper tape

about 10 cm wide using special characters intelligible to both man and machine. This tape is put through the OCR reader to transfer the records to a magnetic tape, which is then processed by the computer. The primary merit of this method is that the records are intelligible to both man and machine. Other merits are higher recording density of OCR tape than paper tape and cheapness of tape. The only slight drawback to it is that manpower is required for transport of tape and upon completion of data transmission network in future a transmission line for direct link to the central computer will come into being.

Group sale of season tickets will not only liquidate window business at stations but also simplify the rear business to a maximum extent. Because data for statistics and coordination adjustment of fares can be directly taken from the master file; and together with transfer payment of fare from bank deposit account, this will render examination needless. Thus group sale of season tickets has a number of merits in all respects and it deserves all-out efforts for dissemination.

3.3 *Wicket business*

As pointed out above, nothing worthy of note has been done about modernization of ticket inspection. About three years ago, the necessity for its modernization began to be appreciated in certain quarters and investigation about ticket inspection was opened. A prototype inspection apparatus intended solely for season tickets was developed to be put to practical test at a station. Automated inspection of season ticket alone, however, cannot be expected to have any great effect of rationalization, because the problem of separating season ticket holders from the general flow of passengers remains unsolved. Thus, automated inspection must be extended to common short distance tickets. And in 1968, a prototype inspection apparatus available for both season tickets and common tickets was built for a test. Summing up the results of these tests of JNR and field tests conducted by private railways, it may be said that there are good prospects of realizing automation of ticket inspection without largely modifying the existing restrictions of the system.

Study on modernization of ticket inspection has only just started and its future course is not yet authorized. Thereupon, discussion will go into details including the tariff system.

(1) Tariff system

The present rule of tariff collection is to deliver a ticket to the passenger in exchange for the necessary cash paid. Future rule, however, is conceivably either to calculate a fare for each ride by the ticket inspecting machine, enter it on the ticket face and after a definite period collect the accumulated fares; or to collect an appropriate lump sum at first and at the same time put down the collected sum on the ticket face, and subtract a fare for each from this sum by the ticket inspection machine. The latter method is adopted in the BART plan.

Study shows that these two methods are in principle not infeasible but rather may be found effective in realizing the most sophisticated comprehensive automation including ticket issuing. On account of various restrictions of the existing tariff system such as many kinds of discounting, validity limited to the nominal ticket holders (season tickets) and other factors, their adoption would be difficult. Nevertheless, the efforts now rendered in the direction of solving these basic problems would not be premature, if the railway ticket business had to be adapted to the future "cashless" society. As evidenced by subways in Western countries, uniform tariff system for the whole line permits complete automation of ticket business (with no human attention) and it would be advisable to introduce such a system in many JNR lines with slack traffic. In modernization of ticket business on slack lines, investment effect can not be expected from it unless the present system is corrected; it would be essential to carry out drastic changes in the present system including the tariff structure.

(2) Ticket shape

Even if the ticket inspection is to be automated without any substantial alteration of the present system, it will be unavoidable to make certain modification of the existing ticket; the least thing to be done would be to make the entry on the ticket face "intelligible" to the machine.

For this purpose, the ticket may be provided with punched hole without modifying the whole shape of ticket or it may be provided with a magnetic coat for magnetic recording. Some other methods are also conceivable. In all these methods it is necessary to put a ticket through an inspection machine, in which the ticket is carried on in contact with or in proximity to the reading unit of the machine. This will make it necessary for the passenger to put his ticket into the machine and take it out of the machine and for a season-ticket holder this would be a little less convenient than the existing procedure of being checked by a human inspector. Accordingly the season ticket handling capacity of the machine will be 20—30 % less than that of a human inspector. In terms of the capacity per wicket, the efficiency will be nearly the same, because in the case of an inspection machine which needs no latch, passage space can be expanded.

It is not inconceivable to realize automatic ticket inspection on a noncontact reading basis with the passenger handling remaining unchanged (the passenger has only to show his ticket). For instance, the ticket may be provided with an electric circuit which oscillates or resonates to a specific frequency. This method is technically feasible; such a ticket can be made in an appropriate size; and the passenger with his ticket in the pocket may

pass through the wicket. Economically, however, it is not feasible, because such a ticket costs several thousand yen.

After all, the recommendable method will be to retain the shape of ticket practically as it is and provide punched holes or magnetic entry on the ticket to be read by the machine; prototypes so far developed are either punched hole type or magnetic type. In future it is advisable to prefer the latter, because it is more difficult to forge, easier to write in or erase; can hold information with greater density; and is reasonably durable.

(3) Composition of inspection machine

The major functions to be performed by an inspection machine are reading of ticket information, checking of ticket validity (travel section, period of use) and action besed on the results thereof (for instance, opening and closing of the gate). To perform these functions satisfactorily the machine is composed such as schematically shown in Fig. 7, where (a) and (c) are supposed to be occupied by a passenger while he is passing through the gate

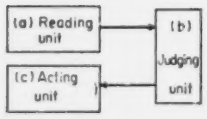

Fig. 7 Composition of inspection machine

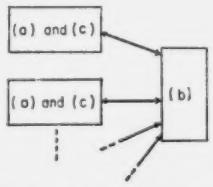

Fig. 8 Composition of inspection machine (of sampling system)

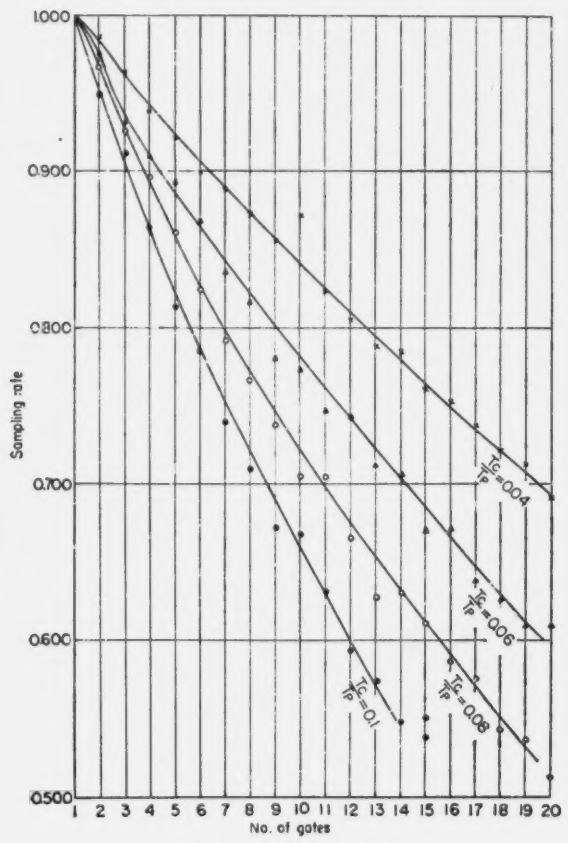

Fig. 9 Sampling rate

(passage time is put as T_p); and (b) acts only until the ticket information is read off and judgment is made on the reading (this time lapse is put as T_c). T_c is far shorter than T_p, usually $T_c/T_p =$ less than 0.1. This means that the judging unit (b) is idle most of the time; therefore, as indicated in Fig. 8, it would be appropriate to provide a single set of (b) for several sets of (a)(c). In that case, it would also be possible to make temporary storage of ticket information and then proceed to judgment on all the tickets read, but it would be advisable to make the machine do the same sampling and judgment as the human inspector does in present practice. Namely, when (b) is busy, all the other tickets are cleared without checking. Thus the machine will be extremely simplified, Figure 9 illustrates a simulation to show what is the sampling rate of this method; it is seen therefrom that there will be practically no trouble when a single judging unit controls several gates.

Now one of the problems in automation of ticket inspection is the machine cost, but it will be almost solved through adoption of the above-mentioned sampling method.

(4) Method of judging

Major items to be judged by the inspection machine are ones related to travel section and ones to period of availability. Judgment can be easily made on the period, but in selection of the method of judgment-making on the travel section, various factors must be considered such as system scale, adaptation to change, related business and information volume.

At present there are several proposals which follow:

(a) Stations are set at positions determined by X, Y coordinates on the ticket face and judgment is made depending on whether the bit stands on these positions on the ticket face. This is the most simplified mechanism of judgment-making; it may be applicable to automatic ticket inspection of a line with only several tens of stations, but it is inapplicable to JNR.

(b) A network of lines is cut like a tree and each cut point is given a cut mark. Thereby the travel course can be represented by combination of departure-destination code and cut position code.

This is the best method in that it needs little information, but it has a number of drawbacks such as difficulty of network encoding, less adaptability to system change, difficulty of automating fare adjustment. The season ticket inspection machine developed in 1967 is based on this method.

(c) The rail network is split into individual lines. Each line is numbered (line code) and all stations on this line are successively numbered (station sequence code). Thus each station is assigned a station code which is a combination of its line code and its station sequence code. Travel course can be expressed as a successive arrange-

ment of departure, midway and destination station codes.

In all respects except a slight increase in information volume, this method is excellent and it was adopted in the 1968 prototype. With an algorithm for fare adjustment worked out, a new prototype was built in 1969.

(5) Prevention of illegal riding

Intermediate free ride or the so-called "Kiseru* (Japanese smoking pipe) which is the most popular form of illegal riding can be prevented only by more strict enforcement of in-train ticket inspection and extraordinary inspection (at transfer stations only). Realization of automatic ticket inspection would offer a powerful means to prevent "Kiseru".

For this purpose a symbol is entered on the ticket face when the ticket bearer goes in; and it is erased when he goes out. When he goes out, the entrance symbol on his ticket is checked; and if there is no such a symbol, he must be a "Kiseru" case or he ought to carry another legitimate ticket. In this way "Kiseru" using two season tickets can also be apprehended.

3.4 *Modernized ticket business*

Figure 10 shows the future flow of ticket business when it has been modernized perfectly. Major differences from the present practice are as follows:

(a) Machines are ubiquitous with only a few personnel —— perfect transition from labor-intensive to equipment-intensive basis.

(b) No customers standing for a long time in a waiting line before ticket windows —— modernized service.

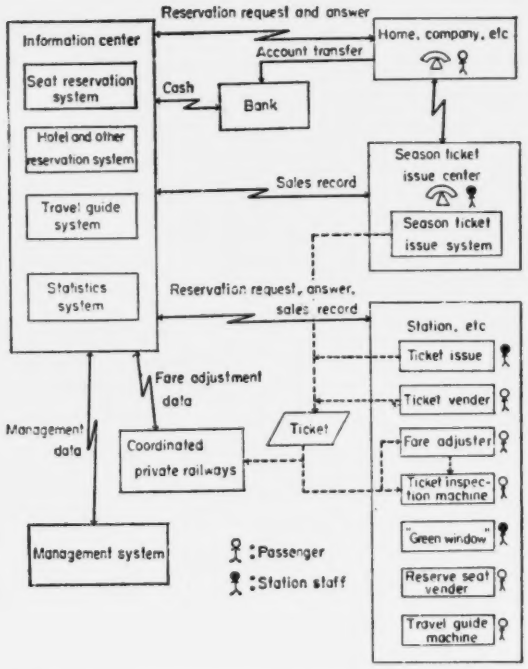

Fig. 10 Comprehensive ticket issue-inspect system in future

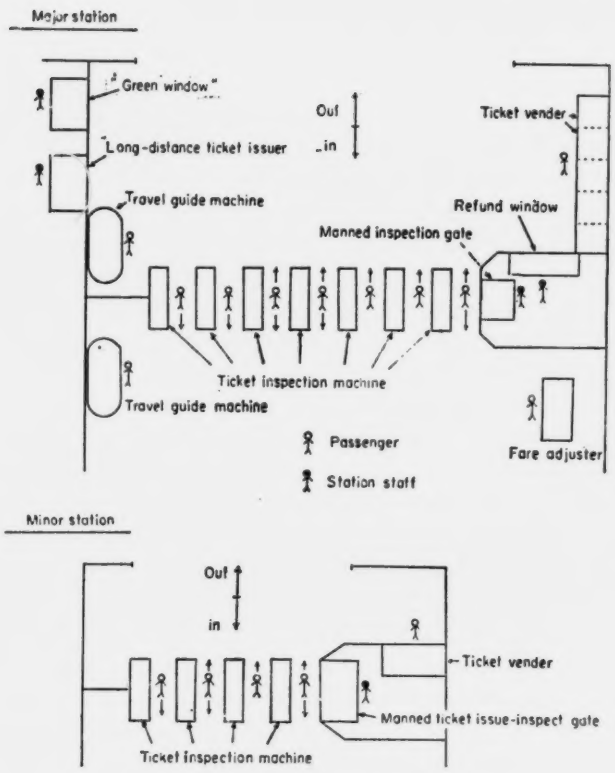

Fig. 11 Platform entrance and exit at modernized stations

(c) Complete automation of rear business —— conversion of management system to a subsystem.

Thus it will be understood what a powerful means for rejuvenation of railway is offered by modernization of ticket business.

The image of a modernized station as represented by the layout of platform entrance and exit will be broadly as schematically shown in Fig. 11. Namely, major stations are equipped with a variety of machines and automatically operated. Announcements to passengers will be computerized and adequate information will be offered rapidly to them; and thereby an audio-responder or a graphic display will be liberally utilized. Fare adjustment for irregular travel will be automatically made. No longer will have station clerks to stand in the crowd; they will sit comfortably in an office and attend to respective jobs.

At most of the stations with no "Green window", each wicket will be manned by a single worker (on watch duty), whose duty it is to control the machine and handle some tickets unfit for automatic inspection; and his work load will be substantially alleviated.

Concluding Remark

Various problems in modernization of ticket issuing and inspection have been discussed. Some have been solved and for some others the future policy has been established. Apart from these problems, the problems waiting for solution, that is, those centered around modernization of ticket in-

* "Kiseru" consists of tow metal pieces (two tickets) at both ends and a bamboo piece in between (no ticket).

spection should be solved in the following steps.

First step (test period)

To test automatic inspection of common short-distance tickets and season tickets on a scale of several stations. During this period, "debugging" must be made. This will take about two years including the preparation.

Second step (trial period)

To try automation of one line or a certain extent of rail network. During this period, stress should be placed on familiarization and retraining of passengers for the new system, so that no problem may be carried over to the next period of regular practice. This, too, will take about two years and in the meantime it would be practically impossible to expect any investment effect.

Third step (practice period)

All technical and passenger-handling problems must have been solved in the preceding periods. Besides, the system may have been improved. Therefore, automation should be put into practice positively beginning with lines likely to show investment effect. Only in this stage, the effect of modernization will emerge.

Lastly it should be noted that modernization of ticket business is associated with many other problems which failed to be treated here and further research must be carried on with intimate contact with related quarters.

625.144.620.197

Corrosion Prevention of Track Materials

Yutaka KOSE, Dr. Eng.*

Following the previous report on corrosion prevention of rail joints, the present paper describes mainly the anti-corrosion tests of tie-plates with reference to corrosive wear and electrolytic corrosion of track materials. Tests have been carried out for about five years on tentative tie-plates, plastic-coated, metal-coated, weatherproof steel-made or stainless steel-made, as laid in tunnels. Corrosive wear, expressed in terms of weight loss, is worst in tunnels of non-electrified lines. In tunnels of electrified lines electrolytic corrosion is more of the problem in connection with the voltage between rail and earth. In all tunnels stainless steel suffered the least weight loss. Nyloncoated, chrome-impregnated tie-plates exhibited excellent performance with a considerable extension of service life expected.

1. Introduction

Rail and the most of other track materials are made of common steel. Common steel is cheap and excellent in properties, but it has a great disadvantage of being liable to corrosion. Nevertheless, up to the latest times track materials have been fabricated of common steel with no anti-corrosive treatment provided. This is contrasted to the painting and other anti-corrosive treatments having been practiced on the most of railway structures including bridges. Now that long rails are used, the track structure is complicated, with a speed up of train operation the structural precision of track is increasingly demanded and the personnel cost is mounting, naturally the track is required to be maintenance-free and durable and the track materials too are required to be equally durable.

It is in 1959 that corrosion prevention of track materials came up for the first time as a technical project and since then long-range comprehensive tests for corrosion prevention have been carried out. Five laboratories, i.e., Electric Testing, Machinery Equipment, Steels & Alloys, Chemistry and Chemical Testing are involved in these tests and the project has been pushed as a Group Study. The results of these tests are summarized in a series of 18 Pre-reports and Reports. Concerning the rails, the final report[1] was submitted and a technical review[2] was carried by the present journal.

The present paper summarizes the results of anti-corrosion tests on the F-type tie-plates which extended over a long period, and refers to corrosive wear and electrolytic corrosion of them. Tie-plates are also subject to breakage (cracking), but the technical review[2] has dealt with this problem, mainly about damage due to corrosion fatigue and this problem will not be taken up in this paper.

2. Anti-Corrosive Tests of Tie-Plates

The first series of anti-corrosion tests began in 1959 and the second series in 1963. In the first

* Chemical Testing Laboratory

series of tests aimed at selection of effective anti-corrosion measures, though small in the number of specimens per one method, a wide variety of anti-corrosion methods (painting 10, plastic lining 9, metallic coating 12 and stainless steel 2) were tried.

The tested tie-plates were C-type and test sites were taken in three non-electrified tunnels of Oyashirazu, Koshirazu and Katsuyama on the Hokuriku Line and in one electrified tunnel of Tanna on the old Tokaido line. These tie-plates were taken off after a definite period of service to check the deterioration of coating or the breakage of springs. For lack of space, full details of the results are omitted and only an outline is given here.

(1) Painting is the least expensive of all preventive methods. Coating is, however, liable to mechanical damage; the paint coat was broken in transit or when the plate was fitted. Except the initial defects or damage to the part in direct contact with the rail base or tie, the paint coat of tie-plate remained intact for a relatively long time.

Of all the forms of paint coat, the one executed on a ground coat of zinc-rich paint proved notably sound; under this coat even when the top coat had been mechanically destroyed, the progress of corrosion was slow. This zinc-rich painting was later applied to the spring clips of SHIN KANSEN. It was adopted because of low cost; besides, the conventional molten zinc plating could not prevent early failure of spring due to embrittlement.

(2) Plastic lining film is considerably thicker than paint film and accordingly it is less liable to mechanical damage, but it has the drawback that on account of insufficient adhesion to the metal ground, the film floats and even if it is retained, corrosion progresses under it. For execution of lining, brushing and fluid immersion were tried; the latter produced a thicker coat, which was less perfect in adhesion than the coat given by the former. Among the plastics, the nylon-coating turned out the most abrasion-resistant.

(3) For metallic coating, molten plating (Zn. Al) metalikon (Zn, Al) and electrolytic plating (Zn, Cd, Cr, Pb, Sn) were tested. Metallic coat is less liable to mechanical damage, but except zinc and cadmium, it suffers heavy corrosion originating from a pinhole. Particularly in the case of Cr and Pb, iron leached out through pinholes; and even if the coat remained, the inside had been corroded as if eaten by worms.

A second disadvantage of metallic coating is that on account of its electroconductivity it is vulnerable to electrolytic corrosion. Among the coats tested, the most recommendable taking into consideration the cost, was the molten zinc-plated one.

(4) As stainless steels, 13 Cr steel and 18—8 austenitic steel were used. Both were found highly corrosion resistant, except slight tendency of pitting recognized in 13 Cr steel.

The results of the first series of tests with cost consideration recommend the following as adequate processes for making the tie-plates anti-corrosive:

(1) Zinc-rich painting
(2) Molten zinc-plating
(3) Nylon coating
(4) Stainless steel

The process (3) leaves room for improvement in the coating method and (4) is found considerably expensive; for these processes, a long-range test of practical use is required.

In the second series of tests aimed at long period service lift testing, the variety of anti-corrosive processes was limited and the number of specimens for each process was increased.

Table 1 summarizes the details of testing. Tie-plates of F type were submitted to test, because a

Table 1 Outline of second series corrosion tests on tie-plates

Test tunnels				Kobotoke		Uto	Kamuriki
Lines				Chuo		Chuo	Shinonoi
Electrified, non-electrified				Electrified		Electrified in mid-test	Non-electrified
Tunnel length (m)				2,574		1,658	2,656
Test period (year, month)				1963. 4～1967. 10		1963. 5～1967. 10	1963. 4～1968. 10
Quantities of test tie-plates	F-type	A	Nylon coat (1)	Dry 20	Wet 20	20	20
		B	〃 (2)	〃 20	〃 20	20	20
		S	Chrome-impregnated steel	〃 20	〃 20	20	20
		Y	Weatherproof steel (1)	〃 20*	〃 20*	20	20
		K	〃 (2)	〃 20*	〃 20*	20	20
		O	Control (conventional SS-41)	〃 20	〃 10	20	20
	C-type	3 A	13 Cr stainless steel	〃 8	〃 10	—	16
		8 A	18—8 stainless steel	〃 8	〃 10	—	18

* Coupled with nylon insulation pad

Table 2 Anti-corrosive processes for test tie-plates

Symbols	Processes	Descriptions
A	Nylon coat (1)	Trichlorethylene wash, degrease—300°C preheat, air cool—230°C nylon fluid immersion—air cool—rapid water cool, coat 0.35 mm thick
B	Nylon coat (2)	Grinder--sandblast--wash, degrease—phosphatization--nylon baking; coat 0.4 mm thick
S	Chrome-impregnated steel	Derust, degrease—900 ~ 1,000°C, 2 ~ 10 hours chrome impregnation Impregnated thickness 0.11 mm (tie-plete)
Y	Weatherproof steel (1)	Chemical composition (%) C 0.09, Mn 0.75, Si 0.23, P 0.088, S 0.008, Cu 0.36, Ti 0.046
K	Weatherproof steel (2)	Chemical composition (%) C 0.07, Mn 0.42, Si 0.45, P 0.080, S 0.010, Cu 0.30, Ni 0.45, Cr 0.88
O	Control (conventional tie-plate)	Structural carbon steel SS-41
3 A	13 Cr stainless	SCS 1, 1,000°C oil cooled
8 A	18—8 stainless	SCS 13, 1,100°C oil cooled

tendency of F type superseding C type was evident. It is on account of the specimens for the first series continuing to be used that the stainless steel specimens are in C type.

A great difference between F type and C type from a standpoint of corrosion prevention is that a rubber tie-pad is inserted between rail base and the body of F type tie-plate and this is effective in considerably mitigating mechanical damage to the anti-corrosive coat of this area.

Table 2 describes the anti-corrosive processes. In B, i.e., nylon coating (2), the ground is treated with phosphatization; this is executed to strengthen the bond between coat and ground. Meanwhile, S, i.e., chrome-impregnated steel aims at eliminating pinholes in chrome-plating and securing the corrosion resistance equivalent to stainless steel at relatively low cost.

Weatherproof steel was a new grade of steel, domestic production of which had been well advanced in Japan when the second series of tests were opened. Costing about 1.2 times as much as the structural steel SS—41, it was regarded as one of the prospective materials for tie-plates.

In addition to the methods listed in Table 2, a nylon insulation pad was tentatively prepared as a countermeasure for electrolytic corrosion. In the conventional rubber tie-pad, with no insulation provided between spring clip and rail or between tie-plate shoulder and rail though rail base is electrically insulated from the tie-plate, the current leaks to the earth, causing an electrolytic corrosion.

To prevent this, the tie-pad was extended 50 mm on both sides to cover up the rail base. The material was 6—Nylon, the base being 6 mm thick and the extensions on both sides being 1.0—1.5 mm thick. This nylon insulation pad was tried on tie-plates of Y and K weatherproof steels used in Kobotoke Tunnel.

The tentative tie-plates were checked once every year; the results of checking are briefly stated here, the details being reserved for a full report.

Figures 1, 2 and 3 indicate weight losses in the tie-plates as used in Kobotoke, Uto and Kamuriki tunnels. The F type tie-plate weighed 4.93—5.44 kg or 5.21 kg on the average as measured on the control (SS—41). Anti-corrosive treated tie-plates slightly increased in weight and their weight losses are indi-

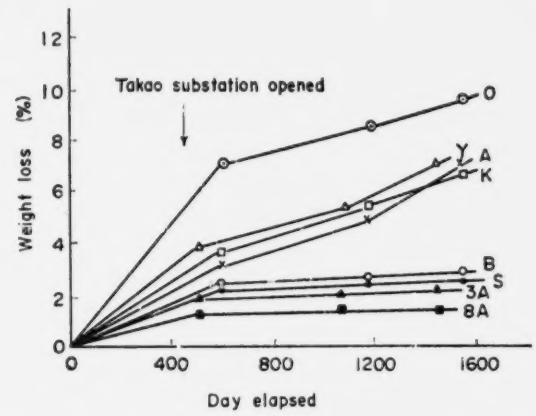

Fig. 1 Weight loss in tie-plates at Kobotoke tunnel (average for dry & w)

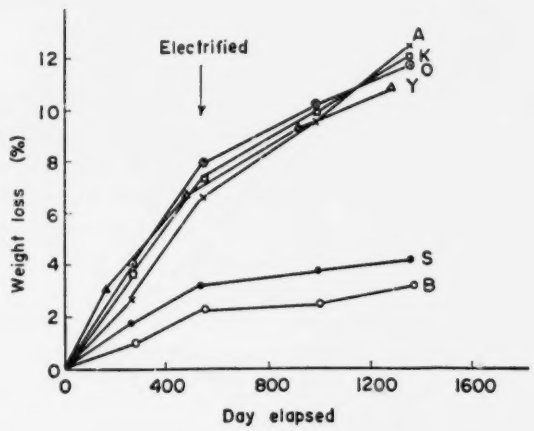

Fig. 2 Weight loss in tie-plates at Uto tunnel

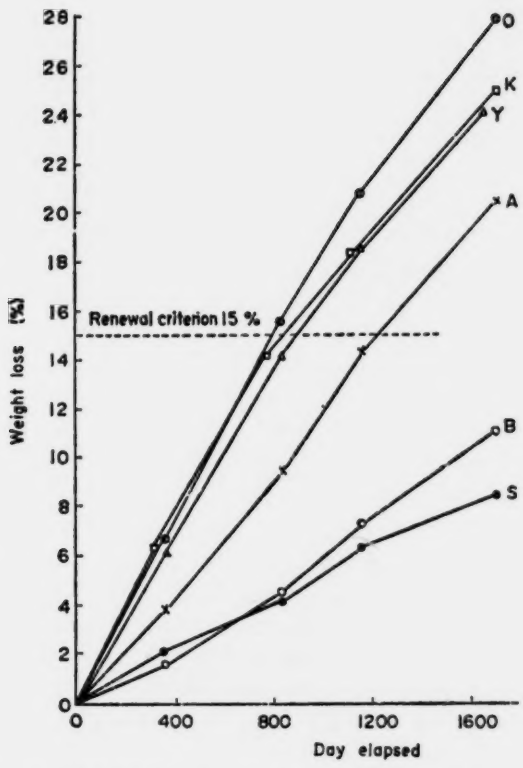

Fig. 3 Weight loss in tie-plates at Kamuriki tunnel

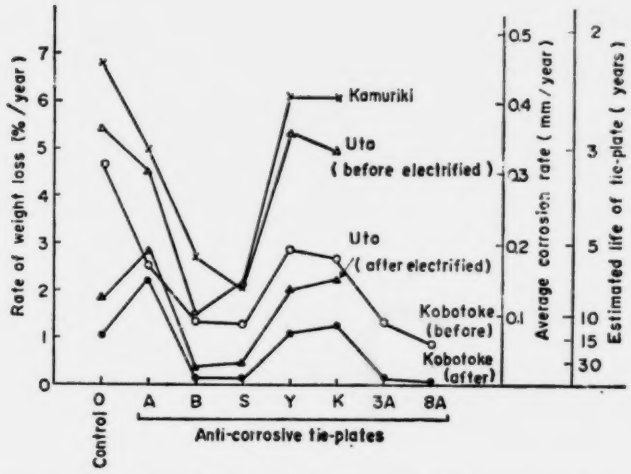

Fig. 4 Rate of weight loss vs. estimated life for tie-plates

catedas ratios (%) to the pre-test weight. As clearly seen from Figs. 1 and 2, the progress in weight losses in Kobotoke and Uto tunnels flattened during the test; this is due in Kobotoke to mitigation of electrolytic corrosion as the result of the rail-earth voltage having dropped on account of Takao Substation being newly constructed; and due in Uto to the corrosive conditions being improved as the result of the tunnel being electrified and liberated from the smoke of steam locomotives.

In view of substantial improvement of environmental conditions during the test in Kobotoke and Uto tunnels, the progress in weight loss was plotted as in Fig. 4, dividing the results as before and after the first survey (actually the opening of Takao Substation was slightly earlier than the first survey period) in Fig. 1 and as before and after the second in Fig. 2.

Including the control, i.e., non-treated tie-plates and the anti-corrosive treated tie-plates, the fastest rate of weight loss was exhibited by Kamuriki tunnel followed by Uto before electrification. In both tunels the extremely corrosive conditions may be attributed to the smoke from steam locomotives.

As for electrified tunnels, Kobotoke before operation of Takao Substation registered the fastest rate of weight loss, followed by Uto and Kobotoke after opening of Takao Substation. The difference in the rate of weight loss in electrified tunnels is caused by the effect of electrolytic corrosion. As testified by the results of rail earth voltage measurement to be described later, Kobotoke prior to operation of Takao Substation showed a notably high voltage (Table 3).

Among the anti-corrosive treated tie-plates, 8 A and 3 A made of stainless steel exhibited the least weight loss, though their data are limited to Kobotoke. Among the stainless steels, the best one was 8 A, i.e., 18—8 austenitic steel, which suffered only slight pitting. In good performance stainless steel was followed by B, i.e., nylon coating, and S, i.e., chrome impregnation. The weight loss in B results from corrosion of a defective coat. S, just like 3 A, exhibited pitting, which was considerably deep under electrolytic corrosion.

As for the nylon coating, A suffered early deterioration of coat and in many cases the coat floated off the ground on account of poor bonding between coat and ground. Difference between A and B is largely attributable to the ground preparation. In B, phosphatization has vastly contributed to increased durability of coat.

The corrosion rate in ordinary outdoor exposure of Y, K weatherproof steels was 1/3—1/5 of that in SS—41; in tunnels these steels exhibited no wide difference in weight loss from SS—41. It was due to the effect of nylon pads mitigating electric corrosion that the results at Kobotoke turned out satisfactory.

The average corrosion rate in Fig. 4 was calculated from the rate of weight loss, taking the original weight of tie-plate as 5,210 kg (average of test tie-plates (O)), the surface area as 1,000 cm^2 and the specific gravity of iron as 7.87.

Depending on the anti-corrosive treatment applied, the test tie-plates varied somewhat in the body weight. Moreover, in the case of coating, the body weight included the weight of coat, so the average value of corrosion rate in mm/year is nothing more than rough estimate. In the case of localized corrosion, the corrosion rate in that locality may be several times the average.

The estimated life is defined as the years in which the weight loss amounts to 15 %, this value of 15 % being set as the criterion for discarding a tie-plate. As Fig. 3 shows, many of the tie-plates

in Kamuriki tunnel exceeded 15 % in mid-test, some of them developing cracks. Thus the 15 % limit is considered reasonable.

The estimated life is based merely on the results of service tests extending over a period of about five years and a large error may occur in prediction of long-term service life. Nevertheless, 5—10 times or even more than 10 times as long as the life of the conventional tie-plates may be predicted for the anti-corrosive treated ones which exhibited good performance.

3. Corrosive Wear

Wear is counted as one of the important factors governing the service life of track materials. Wear is a phenomenon taking place when two objects in contact move relatively to each other.

There are relative movements such as a unidirectional one when wheels roll on the rails and a reciprocating one which happens on the contact surface of fish plate with rail, that is, a vibration.

Corrosive wear is a wear accompanied by corrosion. "Fretting corrosion", a different term from corrosive wear, is applied to the corrosive wear caused by vibration, but here the term "corrosive wear" is interpreted to cover fretting corrosion.

A typical case of corrosive wear in track materials is observed in rail top. Figure 5 shows the results of a British survey[3], in which the specific wears of rail top are classified in three divisions depending on the environments; They concern straight stretches of track with few applications of brake. The highest value of specific wear is recorded in tunnels where steam locomotives work; and the longer the tunnels, the worse the wear.

The second division is an open section out of tunnels, in which the specific wear increases from country side to industrial zone. The lowest specific wear is manifested by electrified tunnels and the London Underground Railway, the value being lower than that in non-tunnel sections.

Data on water leakage are not available, but the corrosion in tunnels which are free from rainfall — if no water leaks — is supposed to be less than in open sections.

In all divisions, the specific wear tends to diminish with an increased number of axles passing over them in a year; this is because an increase in annual axle passage shortens the time for the accumulated number of axles passed to reach 10^6 and in consequence the effect of corrosion drops.

Putting the annual axle passage as 10^6, the specific wear in steam traction tunnels will be 0.7—2.5 mm, in open sections 0.15—0.7 mm and in electrified tunnels less than 0.15 mm.

These values of weight loss are substantially larger than the values of corrosion rate, but generally proportional to the latter. The reason lies in that the amount of corrosive wear obeys not the relation of corrosive wear being equal to (corrosion + wear), but that of it being equal to (corrosion $\times \alpha$) ($\alpha \geqq 1$, which depends on the physical conditions of wear); when the corrosive wear of rail top alone is considered, the change of α is small and the change of corrosion rate due to environment is supposed to be more decisively influential on the amount of corrosive wear.

Weight loss in tie-plates mentioned in the anti-corrosion test above is considered an example of corrosive wear. In the F type tie-plate the bottom surface contacts the tie, the top surface does the rubber pad and the train load falls on it through the rails. Accordingly, over 2/3 of the surface area of tie-plate is in contact with other objects and is subject to vibration.

Weight loss curves in Fig. 1—3 differ from those of common exposure tests in that the rate of weight loss in the former is constant (Kobotoke and Uto are respectively considered in terms of before and after construction of a substation and before and after electrification).

In common exposure test of iron and steel, ordinarily the metal surface is steadily passivated over a long period or a formed layer of rust acts as an anti-corrosive barrier, thereby the corrosion rate tending to lessen gradually.

In the case of tie-plates which are subjected to vibration in contact with the tie or pad, passivation is hard to occur and an anti-corrosive layer of rust is hard to form.

Similar reason may be given for little difference being observed in weight loss between the exisitng SS—41 tie-plate and tie-plates of weatherproof steels. As shown in Fig. 4, the rate of corrosive wear of tie-plate is 0.07—0.46 mm/year for the conventional SS—41. (of the whole area of surface of tie-plate, about 2/3 suffers corrosive wear; therefore the actual rate of corrosive wear will be somewhat greater than the above value).

As compared with the wear on rail top in Fig. 5,

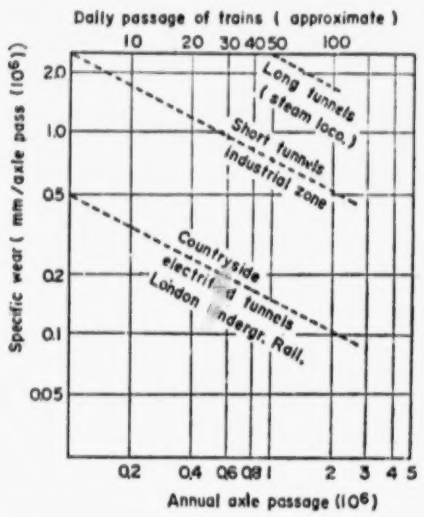

Fig. 5 Specific wears of rails by environments (Great Britain)

this value is considerably low. Namely, α being small, the physical conditions of wear are considerably less severe than on rail top; accordingly even a relatively low-hardness stainless steel or nylon coating has proved sufficiently effective.

As a rather peculiar case of corrosive wear in track materials may be cited the red rust developed on the contact zone between fishplate and rail. This rust looks more tinged with red than the common iron rust; the rust flowing from the contact zone between fishplate and rail is occasionally observed to render the fishplate reddish.

It is called peculiar for the following reason: Conventional corrosion is a corrosion associated with moisture, i.e. "wet corrosion", but this red rust is a dry corrosion. Namely this rust is a water-free oxide ($\alpha\ Fe_2O_3$) developed in direct combination with the atmospheric oxygen of the metal in the contact zone between fishplate and rail under vibration caused by train passage. For prevention of this type of corrosive wear, use of lubricant oil or solid lubricant (graphite, molybdenum sulfite) or coupled use of phosphatization and lubricant oil is recommended.

4. Electrolytic Corrosion

Electrolytic corrosion is a great menace to the track materials used in d—c electrified sections. In the common d—c electric railway, the overhead line has a positive potential to the rail and the current flows along the course: overhead line—pantograph —motor—wheels—rails—substation.

Though with a large sectional area, the rail has some electric resistance, while the rail joint connected with a copper bond offers also some electric resistance. As it becomes farther from the substation, the electric resistances of a large number of rails and joints are added in series; and when a large current flows, a potential difference occurs and the farther it is from the substation, the higher the voltage becomes. The rail voltage is measured in reference to the nearby earth and is expressed as rail-earth voltage; it is not rare that the value amounts to several tens of volts at a spot far removed from the substation.

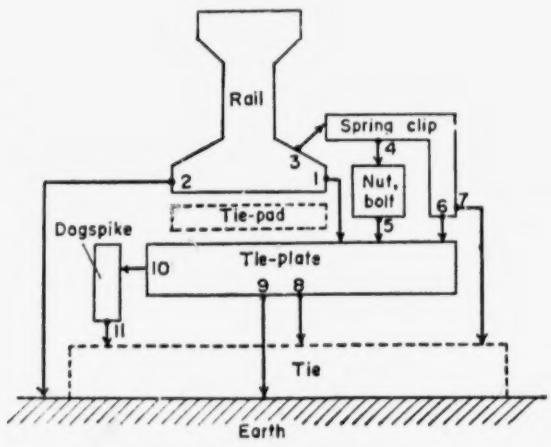

Fig. 6 Path of current leakage from rail

If the rail-earth voltage is positive and the rail is not well insulated to the earth, a part of the current may leak from rail to earth, causing electrolytic corrosion. Figure 6 models the path of a leak current from rail to earth.

1. Leakage from rail to tie-plate occurs through the whole area of rail bottom when a tie-pad is not provided; and even a good insulating tie-pad is provided, it will take place through the shoulder of tie-plate or through the contaminated surface of tie-pad.

2. When the rail is contacted with dirty ballast, the current directly leaks into the earth and that part of rail is electrolytically corroded. Ballast itself is an insulator, but when dirty with iron particles or wet, the current is conducted over the surface. Such cases of electrolytic corrosion are frequent.

3. Current path from rail base to spring clip

Elasticity of spring clip assures full contact between metals and there is no hazard of electrolytic corrosion even if the current flows.

4, 5. Path from spring clip via bolts and nuts to tie-plate. Electrolytic corrosion of this path is also rare because of the metal contact being assured by the elasticity of clip.

6. Path from spring clip tail to tie-plate

For the same reason as above, this path is also subject to little electrolytic corrosion.

7. Path from the tail projection of spring clip via contamination to the tie.

This path is occasionally observed as electrolytically corroded with the tail projection of clip being worn thin.

8, 9. Path from tie-plate via tie or contaminated surface of it directly to earth. This is one of the most vulnerable spots to electrolytic corrosion.

10, 11. Path from tie-plate via dogspike to tie

This path is also vulnerable to electrolytic corrosion. Metal contact ought to be maintained at 10, but in reality the dogspike gets loosened to break the metal contact and as the result a heavy electrolytic corrosion develops.

In the above the paths of current leakage and the vulnerable spots to electrolytic corrosion are described. As a matter of fact, however, even with identical rail-earth voltage certain tie-plates are heavily corroded, whereas others adjoining them may often be free from corrosion.

Next, the mechanism of electrolytic corrosion is to be a little more scrutinized.

(1) Rail-earth voltage

When this voltage is positive and higher, the electrolytic corrosion is more serious. This tendency is more accentuated with an increased distance from the substation (even if the voltage is negative, electrolytic corrosion is possible; but actually a high negative value rarely occurs and the damage inflicted

Table 3 Rail-earth voltage in Kobotoke and Uto tunnels

Tunnels	Measured date	Site	Rail-earth voltage	
			Variance	Average
Kobotoke	1963. 3.19 ~ 20 (before opening of Takao substation)	Downbound, center portal	55 ~ −5	6.4
			100 ~ −3	—
	1964.10.27 ~ 28 (aftor opening of Takao substation)	Downbound, center portal	17 ~ −16	−4.0
			15 ~ −19	−3.9
	1968. 7.24 ~ 25 (at last survey)	Downbound, center portal	8.5 ~ −1.5	0.7
			5.5 ~ −1.1	−2.5
Uto	1965. 7.13 ~ 15	9 spots throughout the tunnel		0.1 ~ 1.0
	1965.10.26 ~ 28			1.2 ~ −0.9
	1967. 2.20 ~ 20			1.0 ~ −2.0

by it is less than that by the positive voltage).

Table 3 cites measurements of voltages in Kobotoke and Uto tunnels where the tie-plate corrosion tests were carried out. Before construction of a substation, the rail-earth voltage at Kobotoke averaged 6.4 V and as stated above a heavy electrolytic corrosion developed.

(2) Leakage resistance

Even for the same rail-earth voltage, the lower the leakage resistance, the larger the current leakage. The relation among the earth voltage, the leakage resistance and the current leakage does not always follow the Ohm's Law, but generally this law is applicable. The factors affecting the leakage resistance include ties, ballast, water leakage in tunnels and dirtiness.

Electric conductivity of tie is attributable to moisture, but in fresh ties with impregnated preservative the moisture is low. As they become aged, the preservative content is lost or a crack develops; and the moisture increases.

Water leaking in tunnels is a relatively pure underground water with a high value of specific resistance. Where the leakage is heavy, the ballast is washed and the leakage resistance becomes often higher than in places of small leakage. After all, the most vulnerable spot to electrolytic corrosion is a place adequately moist.

(3) Fastened state of tie-plate

In Fig. 6 the path of current leakage in tie-plate is shown and the spots liable to electrolytic corrosion are pointed out. It is stated that electrolytic corrosion cannot occur where the metal contact is perfect.

When the metal contact is disturbed by, say, rusting, the path metal→rust→metal is formed; the rust being a poor conductor, the moisture in the rust conducts electricity, which flows following the route metal→water→metal; and the first metal suffers electrolytic corrosion.

The contact between spring clip and rail or tie-plate is kept relatively well by virtue of clip elasticity; but the contact between dog spike and tie-plate body is poor and electrolytic corrosion develops frequently. For the primary purpose of it too, the tie-plate has to be fully fastened without looseness.

(4) Material quality

Be it rail or tie-plate, track materials are made of carbon steel and there is supposed no great variance in quality between different grades of carbon steel. For this reason, the relation between material quality and electrolytic corrosion has not been examined very much.

In the tie-plate corrosion tests mentioned above, however, chromeimpregnated steel and stainless exhibited a considerably good performance against electrolytic corrosion. The reason for this is to be studied here.

Earlier it is stated that electrolytic corrosion occurs as the metal is submitted to electrolysis under d—c passage from metal to water. As wellknown, in metals, the electrons carry an electric charge and thereby an electric current flows (electronic conduction), but in water the electric charge is carried by ions (ionic conduction).

On the metal-water boundary surface, electrolysis takes place and, if the metal is iron, the metal is decomposed into positive ions and electrons as follows:

$$\mathrm{Fe\ (metallic\ iron)} \rightarrow \mathrm{Fe^{++}\ (iron\ ion)} + 2\,\mathrm{e\ (electron)}.$$

Thus, the ions play the role of a carrier for electric charge in water and the electrons do the same role in metals. Electrolytic corrosion is a phenomenon of metal turning into ions in an electrolytic reaction and gradually being dissolved and lost (in the common wet corrosion the same reaction promotes the corrosion).

In the electrolytic reaction of the current flowing from metal to water, however, the reaction is not simply a dissolution of metal. For instance, the following process happens:

$2\,OH^-$ (hydroxide ion in water) $\rightarrow H_2O$ (water) $+ 1/2\,O_2$ (oxygen gas) $+ 2\,e$ (electron)

Thereby the hydroxide ions, i.e., carriers of electric charge in water, reach the metal surface and deliver the electrons to the metal. They themselves break into water and oxygen. In that case, with on dissolution of metal taking place, electrolytic corrosion cannot occur. After all, electrolytic reactions caused by the current flow from metal to water in some cases develop electrolytic corrosion and in others do not. Usually, both reactions happen together and it is important to know what % of the current leads to electrolytic corrosion. This depends upon the kind of metal, the ions in water and the voltage; in common carbon steel, nearly 100 % of the current develops electrolytic corrosion, but the proportion is considerably low in stainless steel. Thus the stainless steel is less subject to electrolytic corrosion even under the same extent of current leakage.

(5) Acidification by leak current

Rail-earth voltage rises under train passage and drops after train passage. In places electrolytically corroded, however, the water is acidified; and even when the rail-earth voltage has dropped and the current flows no longer, a common corrosion other than electrolytic one progress. Stainless steel is resistant to the common corrosion, too; and it is expected from this standpoint to behave well in relation to electrolytic corrosion.

Five aspects of electrolytic corrosion have been discussed with some reference to countermeasures for electrolytic corrosion. Lastly, the preventive measures are to be briefly summarized.

(1) Reduction of rail-earth voltage

For this purpose, the number of substations is to be increased to shorten the distance between them. Tunnels particularly liable to electrolytic corrosion are numerous in mountainous regions and they are mostly located far from the substation. Thus, it becomes necessary to consider the location of substation.

Besides, the electric resistance at rail joints may be minimized or a return circuit to the substation without passing the rails may be formed. As an example of the latter, utilization of the sea has been tried.

(2) Increase of leakage resistance

The results of anti-corrosion tests revealed that both nylon coating and nylon pad were effective for electric insulation between rail and earth. Also the leakage resistance can be improved through renewal of ties or ballast or a simple washing of tie-plates with pressurized water may be effective.

(3) Other preventive measures

Cathodic protection is highly effective but its application calls for consideration of influences on other buried objects. Corrosion-free metallic material is stainless steel of more than 13 Cr. Test results show that a low alloy steel such as weather-proof steel is not so effective.

5. Concluding Remark

It goes without saying that the purpose of anti-corrosive treatment of track materials lies in the prolongation of their service life. For this purpose, the important thing is not merely prevention of corrosion but prevention of corrosive wear, corrosion fatigue and electrolytic corrosion. These points are discussed mainly referring to the results of long-range tests for corrosion prevention on rail and tie-plates, including the discussions given in the previous report.

The results of corrosion tests testify that anti-corrosive measures can remarkably extend the service life of track materials and the benefits accruing from them more than redeem the expenses needed.

Some of the measures are already being practiced, and a more extensive application of them must be considered. In the present tests, prevention of crack or corrosive wear on rail top has not been studied, but they pose a problem of equal importance and wait for future solution.

References

(1) "Life test on rails submitted to anti-corrosive treatment" RTRI Technical Report No. 599 1/32(1967. 07)

(2) "Anti-corrosive treatment of rails to prevent rail end failures" Journal of RTRI Vol. 24 No. 6 43/48(1967. 06)

(3) "Wear and Corrosion of Rails" Railway Gazette, Vol. 121 No. 1 18/21(1965. 01)

539.42 : 621.882.6 : 669.14.018.29

Delayed Failure of High Strength Bolt

Atsushi ITO*, Shinsaku MATSUYAMA*

It comes recently into question that some high strength bolts applied in structures result in delayed failures.

In this review, the conceptior of delayed failure and the predominant fractu·e mechanisms, that is, hydrogen embrittlement and stress corrosion cracking, are explained, and then two cases of bolt failures in service are explained.

1. Introduction

It is about fifteen years since friction-type joints with high strength bolts were applied in practical steel construction, and these applications are recently remarkably increasing. For instance, we expect that a large amount of high strength bolts will be used in the great suspension bridge between Honshu and Shikoku under contemplation. The tendency toward such a large construction has resulted in demands of bolting of higher and higher strength.

In 1964, a bolt with ultimate tensile strength (U. T. S) of 130 kg/mm² (designated as 13 T bolt) was recommended in JIS B 1186. However, the trouble that some of 13 T bolts failed in some months after tightening has encountered in all bridges applying them. A few 11 T bolts, also failed. This suggests that the resistance to delayed fracture should decide the tolerant strength level of higher strength materials.

The delayed fracture is relate to the toughness of the material to some extent. This characteristic, however, cannot be always estimated by the fracture test for a minute such as ordinary tensile tests. In addition, it is not only changed by mechanical properties of the material, but also by interactions of the material with environments. Despite of the importance of the delayed fracture phenomenon, it has not been widely known.

2. What is the Delayed Failure ?

2. 1 *General conception*

The brittle fracture of materials after a long period of time under static load has been called "Delayed Fracture". Minute delaying time is generally accompanied with fractures even under shock loading and delaying time is longer in fatigue or creep fracture. The delayed fracture, therefore, should not be distinguished by delaying time only, but by following features.

(1) Failures may occur under nominal stress even well below the yield strength.

(2) Failures occur under static loading. For this reason, it is sometimes called "Static Fatigue".

(3) Failures are not attended macroscopically with any plastic deformations, that is to say, they occur in brittle mode.

(4) Failures occur at such low temperature that creep rupture cannot occur.

(5) A period from loading to fracture is comparatively long.

The fracture process from loading to complete failure consists of two periods: incubation period until crack initiation and crack propagation period after crack initiation. Which occupies longer period in whole process depends upon the mechanism of the fracture.

The characteristics of delayed fracture are represented by the relation of applied stress and time to fracture, and time to fracture increases as applied stress decreases.

We describe two important mechanisms of delayed fractures in engineering concern.

2. 2 *Hydrogen Embrittlemen:*

Effects of hydrogen on delayed fractures of steels, from results of many investigators[1], are summarized as follows.

(A) Effects of hydrogen contents

(1) For a given hydrogen content in steel, the longer the time to fracture is, the lower the applied stress is, and a lower critical stress (L. C. S) exists under which failures cannot occur, as shown in Fig. 1. This critical stress and the time to failure decrease as hydrogen content increases.

(2) In the absence of the applied stress, hydrogen produces blisters and cracks in cathodically heavy charged specimens.

(B) Effects of temperature

(1) The maximum embrittlement in ordinary tensile tests occurs at, or just below, room temperature.

(2) The incubation period decreases as the temperature increases.

Activation energy obtained from this relation is in good agreement with the value for the diffusion of hydrogen in alpha-iron. When cracks propagate in a discontinuous manner due to hydrogen diffusion, the period from crack initiation to fracture decreases also as the temperature increases. On the other

* Steels & Alloys Laboratory

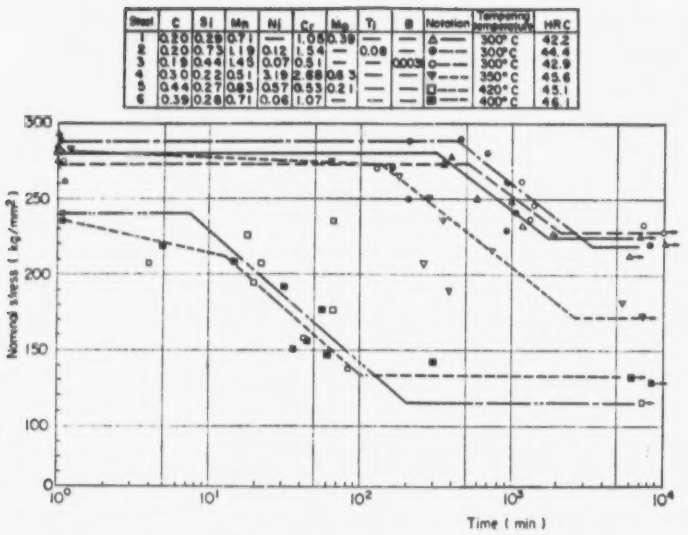

Fig. 1 Results of delayed fracture tests on high strength steels treated to the U.T.S of about 130 kg/mm² and cathodically-charged with hydrogen

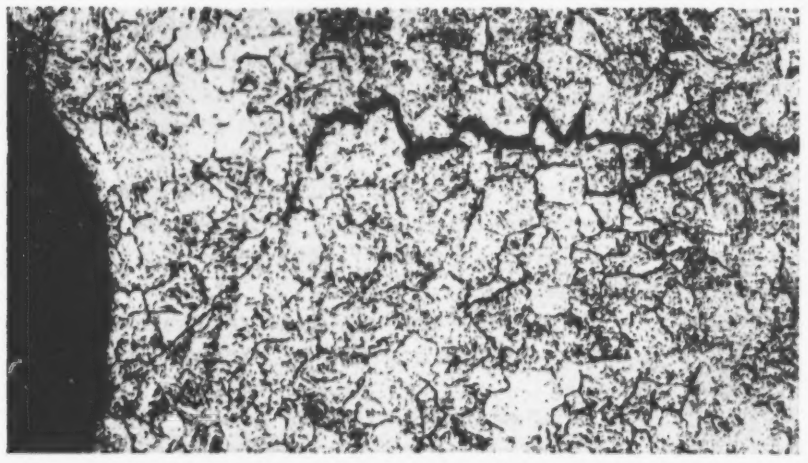

Fig. 2 Delayed fracture crack initiated below a notch root (SCr 4, tempered at 300°C, applied stress: 148 kg/mm², 6 min.)

hand, the specimen may fracture catastrophically as soon as a crack initiates below the transition temperature.

(C) Effects of stress and strain

(1) The crack initiates generally at certain depth below the notch root (where intercrystalline and transcrystalline cracks are joining as shown in Fig. 2). Sharply notched specimens are observed to crack slightly below notch bottom and less sharp notches more deeply. The L.C.S and the time from loading to fracture decreases respectively as the notch severity increases.

(2) There is little dependence of the incubation period upon the applied stress.

(3) The embrittlement is reduced as the rate of straining in ordinary tensile test is increased. The maximum embrittlement, therefore, occurs under static loading.

(4) Cold working decreases the ratio of the L.C.S to the fracture stress before hydrogen charging (L.C.S/F.S).

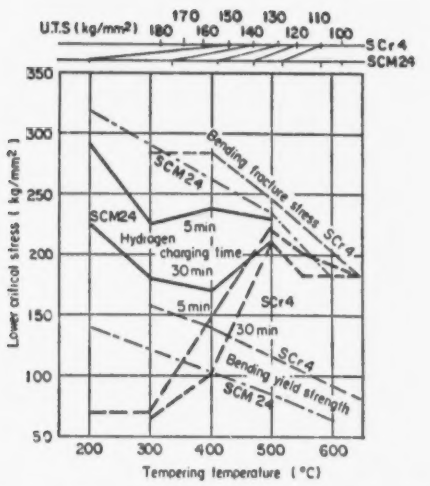

Fig. 3 Effects of tempering temperatures on the lower critical stress

(D) Inherent factors in materials

(1) Chemical compositions affect the sensitivity of materials to delayed fractures. In particular, the higher the carbon contents are, the more sensitive steels become.

(2) L.C.S/F.S decreases as the hardness or the U.T.S increases. Hardened steels with sorbitic structures are less sensitive to fractures than those with tempered-martensitic structures. For low carbon martensitic steels, the L.C.S may become infinitesimal after tempering at about 300°C as shown in Fig. 3.

(3) In ferritic steels, transcrystalline cleavage crack occurs. Grain boundaries, therefore, tend to be a barrier to crack propagation. On the other hand, cracks in tempered martensitic steels have a tendency to pass along prior-austenite grain boundaries as shown in Fig. 2.

(4) Austenitic steels are insensitive to the hydrogen embrittlement.

Although many arguments concerning this problem have been presented, sufficient explanation cannot be obtained yet.

2.3 *Stress corrosion*

It is well known that when two pieces of metals which have different potentials are connected externally and placed in an electrolyte, the anodic metal corrodes preferentially and hydrogen is generated on the surface of cathodic metal. The stress corrosion is caused by the dissolution of anodic regions of a metal with the aid of the stress acting at the extremity of pit.

This corrosion is caused locally since heterogenities in a metal, such as grain boundaries, segregations of element, plastic strains, precipitations, etc., may be a source for the anode formation.

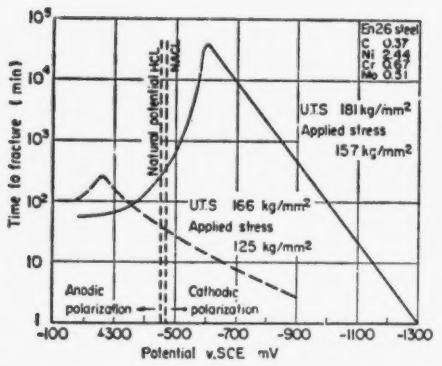

Fig. 4 Effects of applied potentials on time to fracture [2)]

For this reason, it is often observed that cracks initiate along grain boundaries or inclusions. A feature of these cracks is that the crack tip is blunt in contrast with one of the hydrogen induced crack.

Whenever the anodic reaction occurs, the cathodic reaction, in another region, results in introducing of hydrogen into steel. Figure 4[(2)] shows effects of applied potentials on the time to fracture under constant load in 3 % NaCl and 0.1 % HCl. The decrease in failure times resulting from the application of cathodic potentials indicates that hydrogen was causing the embrittlement, while the tendency to the contrary indicates that stress corrosion cracking dominates the fracture process. From these it is inferred that the failure at the natural potential in 3 % NaCl is due to stress corrosion cracking and in 0.1 % HCl to hydrogen embrittlement.

3. Delayed Failures of 11 T Bolts in Service

The low alloy structural steels with the U. T. S in excess of 120 kg/mm² become sensitive to the delayed fracture on whichever mechanism, of hydrogen embrittlement or stress corrosion cracking, the process is dependent, while the materials with the U. T. S of about 110 kg/mm² ought to be less sensitive.

However, delayed failures have occurred in a portion of so-called 11 T bolts. These troubles should be serious matters since 11 T bolts have been employed practically in large quantities. In order to make clear the reason the examination on some failed 11 T bolts was performed. The results were as follows.

3.1 *Case 1: In the Rahmen bridge at Shin-Osaka Station*

Three failed bolts were found out in the lower flange of a friction-type joint, in January, 1968, which had been completed in September, 1964.

These failed bolts and six favorable bolts sampled at random for comparison were used in this examination. The chemical composition and mechanical properties are shown in Table 1.

(1) The environment in service

These bolts have been remarkably corroded with only one exception. Figure 5 shows an example of pitting corrosion in the fillet under bolt head. No waterdrop on the shank of bolt was found when the bolt for comparison were removed, but a rust was recognized all over the inner surface of bolt hole.

Table 1 Chemical composition and mechanical properties of bolt material

Steel	C	Si	Mn	P	S	Cu	Ni	Cr
SCr 4	0.40	0.27	0.73	0.014	0.019	0.14	0.06	1.02

	σ_y (kg/mm²)	σ_B (kg/mm²)	Elongation (%)	R. A (%)	H_{RC}
	112.2	117.9	16.7	49.0	36.9

Heat treatment	850°C oil-quenched, tempered at 500°C

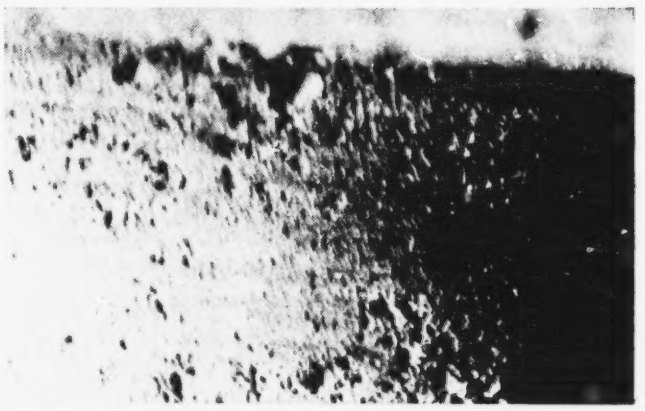

Fig. 5 Corrosion pits in the fillet under bolt head

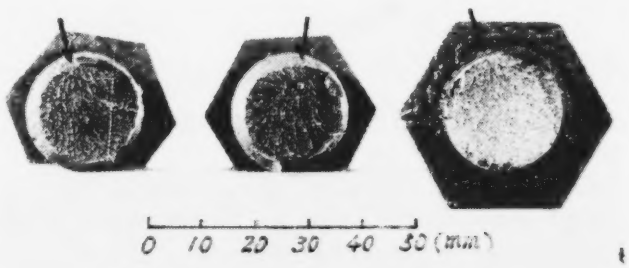

Fig. 6 Fracture surfaces of failed bolts

(2) The characteristic of fracture

Failures are located in an incomplete thread (two bolts) or in a fillet (another). The rust on the fracture surface of only one bolt is formed less considerably than the others, and this suggests the difference of the date on which these failures occurred. On fracture surface, a chevron pattern, that is a characteristic of the brittle fracture, is formed which points toward one origin, as shown in Fig. 6.

(3) The configuration of a fillet and a thread

Rudii of fillets of failed bolts are 2.0 to 2.2 mm, being larger than recommended values.

Radii of thread bottoms of the bolts for comparison range from 0.25 to 0.29 mm. (those of failed bolts cannot be measured)

(4) Hardness

Hardness levels in the transverse section of shank of two failed bolts are considerably high, H_{RC}

43 to 46. The surface hardness, however, was decreased by decarburization, and then the hardness of head sides, being checked usually at inspection, is less than H_{RC} 43 and satisfies the specified hardness range, H_{RC} 33 to 42. The hardness of failed bolts falls after tempering at temperatures above 400°C. From this fact, we conclude that the tempering temperature of these failed bolts were lower than the proper temperature.

(5) Metallographic features

There are some cracks along prior-austenite grain boundaries and non metalic inclusions in the fracture surface. This suggests that these bolts were loaded not only in pure tension but also in torsion and bending.

The grain sizes of these bolts are divided into two groups: grain size number, 9.2 to 9.3 and 7.4 to 7.7. All failed bolts belong to the larger group.

3.2 *Case 2: In the box girder bridge over the 8th belt street at Akabane*

This bridge was completed in October, 1965. In February, 1967, six failed bolts, and then in April, 1968, two failed bolts were respectively found out in the upper and the lower flange of the friction-type joint. In both cases, six favorable bolts for comparison, which had been near each failed one, were respectively used in this examination.

The chemical composition and mechanical properties are shown in Table 3.

(1) The environment in service

The rust on most favorable bolts assumed black immediately after removing, but the color became light brown after a while. From this, it was estimated that oxygen was fed insufficiently in the surroundings of these bolt shanks.

Although there were a few bolts having condensed waterdrops on the surface, a heavy pitting had not been formed.

(2) The characteristic of fracture

Failures were located in a fillet (seven bolts) and in a thread at the end of nut (one bolt).

Small cracks were observed in the fillet of a removed favorable bolt.

On the fracture surfaces, chevron patterns are formed which point toward many origins, as shown in Fig. 8. In one case, bamboo-like fractures developing toward axial direction were observed in the fracture surface.

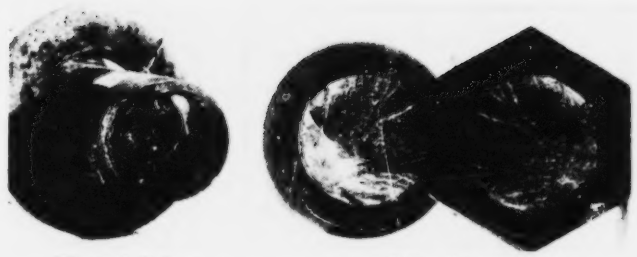

Fig. 7 Fracture surfaces of failed bolts

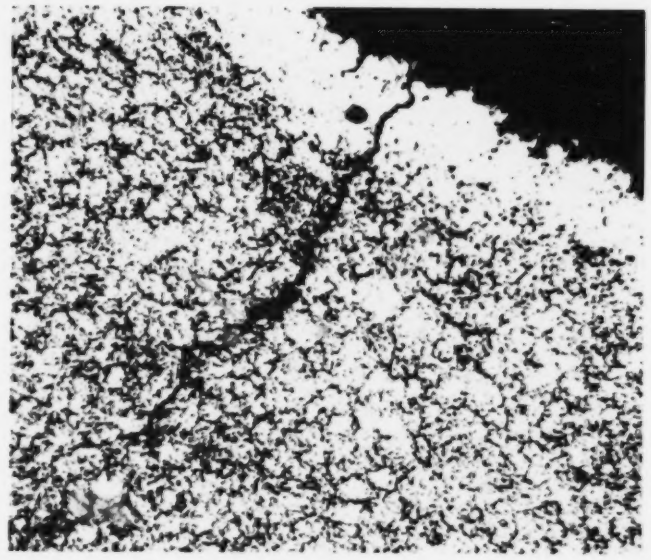

Fig. 8 Micro crack initiated in a bolt for comparison

(3) The configuration of a fillet and a thread

Radii of fillets of failed bolts are 1.53 mm to 1.73 mm, and that of the thread is 0.63 mm, being respectively larger than recommended values.

(4) Hardness

The hardness levels in transverse sections of the shank of failed bolt are in the range of H_{RC} 36 to H_{RC} 39, satisfying the specified range, while they are comparatively lower, H_{RC} 33 to H_{RC} 36, in the case of a thread failure.

On the other hand, these bolts are divided into two groups with respect to the surface layer: carburized layer and decarburized layer.

All failed bolts and the favorable bolt having micro cracks belong to the group with carburized layers.

The furnace in which atmospheres are controled are generally employed for hardening of the high strength bolt, and the operation at lower dew point may result in hardness increasing of the surface layer by carburizing.

The hardness below the surface of these bolts amounts to H_V 500 to 600, and the U.T.S converted from this hardness is more than 170 kg/mm². Such high strength materials are

Table 2 Chemical composition and mechanical properties of bolt material

Steel	C	Si	Mn	P	S	Cu	Ni	Cr	Mo
SCM 3	0.35	0.29	0.69	0.020	0.013	0.18	0.08	0.97	0.16

	σ_y (kg/mm²)	σ_B (kg/mm²)	Elongation (%)	R.A (%)	H_B
	117	123	17	53	362

Heat treatment	860°C oil-quenched, tempered at 610°C

very sensitive to delayed fracture as shown in Fig. 3.

(5) Metallographic features

An example of a micro crack being initiated in a fillet is shown in Fig. 8. This crack propagates along prior-austenite grain boundaries, and its depth is corresponding with that of a hardened layer.

The thread failed bolt has many longitudinal inclusions, along which bamboo-like fractures grow.

4. Conclusion

None of these failed bolts, in above two cases, is a product being normally manufactured.

Conventional structural steels are more sensitive to delayed fracture as the hardness becomes higher above H_{RC} 40. In particular, this tendency are remarkable in medium carbon steels.

Case 1 suggests that when a corrosive attack is severe, the pitting corrosion makes ineffective the advantage that the surface decarburization prevents failures. In this case the crack initiation requires a long period.

On the other hand, in Case 2, the crack propagation dominates the time process to fracture.

It is considered that the fracture mechanism is predominantly stress corrosion cracking in the former, and hydrogen induced cracking in the latter, though some uncertainties are remaining.

The hardness decreasing rate with an increasing of tempering temperature, in the range of 400°C to 600°C, are higher in low alloyed medium carbon steels. Since a small difference of tempering temperture, consequently, sensitively affects hardness, U. T. S, and resistance to delayed fracture, fastener producers must take care of the controling of tempering temperatures.

Furthermore, the temperature and the atmosphere in the furnace for hardening are also important factors, which affect grain size and surface carburizing or decarburizing.

Surface decarburizing makes a bolt insensitive to delayed fractures, but inspectors are afraid that the hardness check in surface could not show the proper value of the material. Therefore, the hardness should be measured after grinding out of decarburized surface layers.

References

(1) P. Cotterill: Progr. in Materials Science, Vol. 9, No. 4, (1961).

(2) P. C. Hughes et al: Jour. Iron & Steel Inst, Vol. 203 Part. 7, p. 728, (1965).

625.122 : 624.137.2

The Investigation of Cutting Slopes — Survey of Slope Soil Structure and Reappraisal of the Point-rationing System Evaluating Slope Failure —

Goji YAMADA *, Sumiji KOBASHI, Dr. Agr. *
Hideo ARAI *, Atsuo IMAI *

The present paper deals with the authors investigations of cutting slope failure, consisting of the following two parts. First, they examined the method of soil stratum surveying of cutting slopes by simplified seismic prospecting. Then they reexamined the point-rationing system for slope failure and proposed an improved system more conforming to the analyses of many failure data.

1. Introduction

Failures of cutting slopes along the railways occur about 300 to 400 times a year, thus occupying a greater part of railway accidents.

The cutting slope is an artificial one, but its strength much depends on the natural environmental conditions. It is, therefore, difficult to understand completely the mechanism of slope failure and to determine site by site the most suitable protective method, but it is essential to judge the degree of slope failure danger to the best of our knowledge.

There is a statistical method introduced on the basis of the analysis of past disaster data. JNR has been collecting the disaster data of all cutting slope for the past several years, and according to the analysis on these data, made the point-rationing system for slope failure danger. By this statistical method, the slope failure danger is judged only from external appearances of the slope (height, gradient, environment conditions, etc), attaining limited precision of judgement. For improvement of point-rationing accuracy, it is necessary to investigate soil stratum, water conditions, etc. in the slope. Besides, the investigation procedure requires higher efficiency, because a few inspectors must take care of many slopes. The present paper consists of the following two parts:

(1) Surveying of the slope stratum by the simplified seismic prospecting: The purpose of this investigation is to explore the possibilities of using this method for surveying slope soil stratum. The authors followed this method on many cutting slopes and compared the data with the data of Swedish-penetrating resistance test.

(2) The reappraisal of the point-rationing system for slope failure danger: The present system was determined from the analyses of a few data. On the basis of more data collected thereafter, the authors reexamined the system and proposed a revised one.

2. Survey of Cutting Slopes by Simplified Seismic Prospecting

The authors had surveyed soil stratum of cutting slopes for three years starting from 1966 along railway lines where many failures of cutting slopes occurred.

It is necessary to understand the mechanism of cutting slope failure in connection with soil strata. Generally, cutting slope consists of two parts; a surface stratum (weathered or deposited soil) on the upper part underlain by a sub-stratum (base rock or hard soil). It is thought that cutting slope failure occurs along a boundary between surface and base (Fig. 1).

The purpose of this investigation is to explore the possibilities to ascertain the extent of the surface stratum by simplified seismic prospecting.

(1) Procedure

The number of slopes surveyed stands at 89. With a handy seismic prospecting apparatus, seismic velocity between two points on slope was measured. Resulting from the analysis of the run-curve plotting the relation between the seismic velocity and the distance between the two points, the thickness of the surface stratum, the seismic velosity in the stratum and the depth of the substratum were determined.

The Swedish-penetration test was made for comparison with the results of seismic surveying.

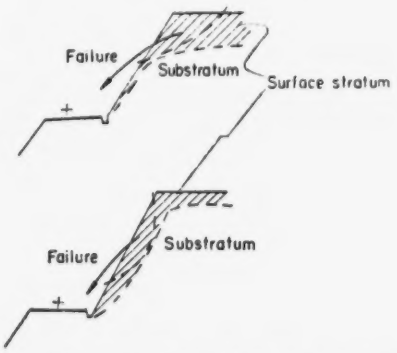

Fig. 1 General conception of cutting slope failure

* Disaster Prevention Laboratory

(2) Results.

The purpose of the investigation is to make clear the relation between the values of the penetration test and of the seismic surveying. The principle of investigation releted with the conception of actual soil stratum is shown in Fig. 2. The A horizon is a soft stratum (humus soil). Its extent evaluated from seismic prospecting agreed to the distance penetrated under weight only (up to 100 kg) by the Swedish-penetration tests. The B horizon is a considerably weathered stratum (weathered soil). Its extent agreed to the distance of penetration under 20 or 40 revolutions by the Swedish-penetration test. The C horizon is a hard soil, a weathered rock stratum or an unweathered base rock. These strate could not be penetrated under 100 or less revolutions.

It was thought that the boundary between the first and the second stratum by the seismic tests was located between the B and the C horizon, corresponding to 100 revolutions by the Swedish-penetration tests. Figure 3 shows the comparison between the depths of the surface stratum evaluated from the seismic tests and the penetration tests, and in spite of scattering of plots, the standerd deviation was 0.65. Large deviations concentrated in some special localities, so that it was thought that the deviations were caused by uncommon factors, for example, inaccuracy of penetration test caused by existence of stones in the soil, difficulty of judging the seismic velocity in the top stratum, or existence of three or more strata.

Figure 4 shows the relation between the seismic velocity (V_1) and the strength by penetration test. The seismic velocity of surface stratum concentrated in the range of 200 to 400 m/sec, so that it was difficult that these velocity values agreed with the strength values from penetration tests.

In the substratum, correlation between the seismic velocity in the substratum (V_2) and the strength shows a certain trend despite of scathering of plots.

The following conclusions were drawn after this investigation:

(a) The measuring lines of the seismic prospecting were established vertically and in parallel to slope or track, and it was verified that parallel lines gave clearer results than vertical ones.

(b) Surveying by simplified seismic prospecting was effective to measure the extent of surface stratum, but it was difficult to show the strength of the stratum from seismic velocity. In the substratum, the relation between seismic velocity and the strength by penetration tends to some result, involving many deviations.

(c) Unstable slopes had largely deep surface strata and showed sharp distinction between surface and base. Surface strata of stable slopes were largely shallow, less than 1 m.

(d) The reason why the extent of surface stratum obtained by seismic prospecting did not agree with the one by penetration tests was that there existed many stones within surface strata or many joints within base rock.

(e) Cutting slope survey by simplified seismic prospecting can practically measure in case of less than 20 m in surveying length and less than 3 to 4 m

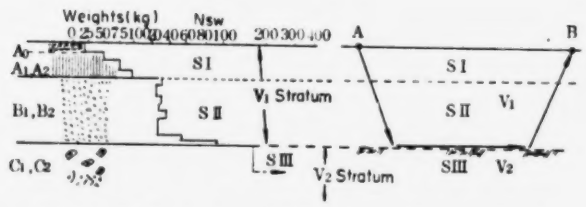

Fig. 2 Soil stratum with penetration test and seismic prospecting

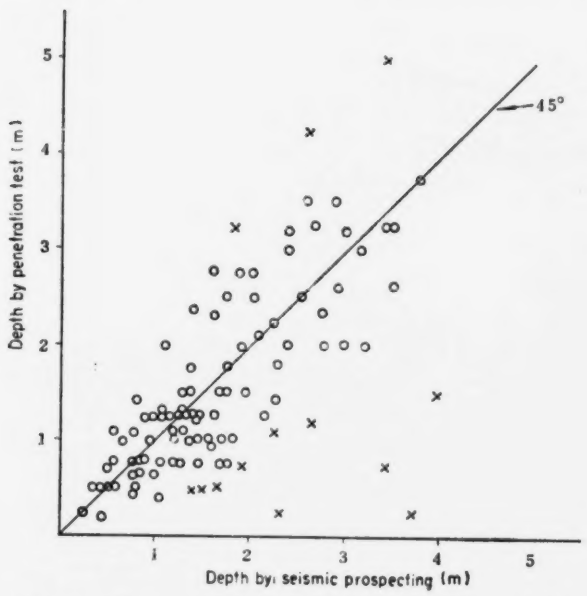

Fig. 3 Depths of surface stratum by penetration test and seismic prospecting

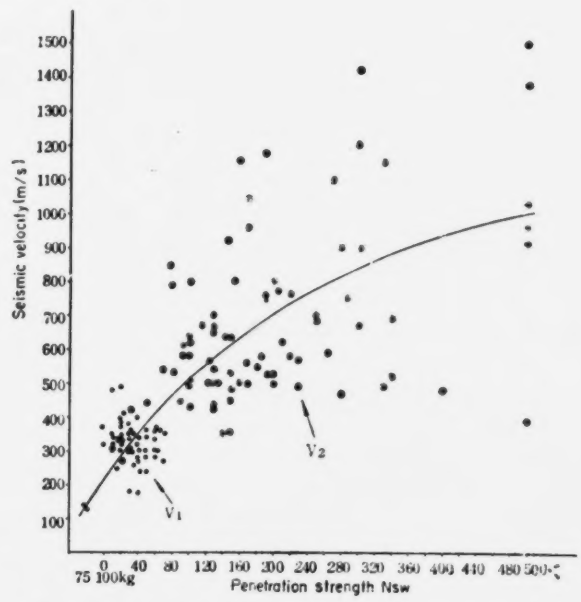

Fig. 4 Seismic velosity and penetration strength of soil stratum

of the extent of surface stratum. In case of more than 20 m, seismic wave damped, annulling seismic prospecting for evaluating the extent of surface strata.

(f) To establish a relation between seismic velocity and soil strength, it is necessary to classify soil conditions geologically. though there are few informations. for this with the authors.

3. Reappraisal of the Point-Rationing System for Slope Failure

The purpose of collecting statistical data of slope failures is to make clear the factors related to slope strength and decide ranking of slope failure danger. This investigation was made mostly on the basis of slope failure records (1, 600 cases from 1964 to 1968).

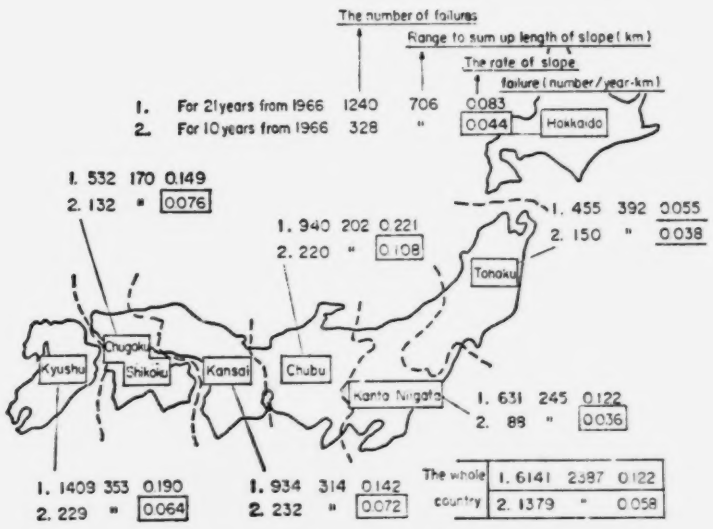

Fig. 5 The number and the rate of slope faiure divided into regional groups

(1) Analysis of slope failure records.

Figure 5 showed the total number and percentage of slope failure occurrence corresponding to each regional group. The rate in the north region was generally lower than the one in the south, the one in the Chubu region being the heighest. This tendency agreed with the tendency of continuous precipitations causing failures; for example, 100 mm in Hokkaido (north), 230 mm in Kyushu (south).

The strength of slope materials in connection with continuous precipitations causing failures varies locally and geologically; small in the region of Tertiarry deposit, volcanic detritus and metamorphic rock, and large in the region of igneous rock and Paleozoic deposit. The strength, naturally, was smaller in higher slopes, but in a region of high precipitation, the difference in strength becomes smaller. Relation of slope gradient to strength of slope materials was so far not clear, since the slope gradient was decided in consideration of slope strength at the time of construction.

Soil types of failed slopes was largely sandy soil (53 %) and SM (30 %) as classified by the Unified Soil Classification System.

The relation between slope strength and the conditions of water in the slope was not so clear. It was thought that judgment of these conditions by field inspectors was difficult and incorrect.

Thirty five percent of failed slopes was equipped with failure prevention works, and 70 % of them were retaining walls. Failures of these structures themseleves were few.

Types of slope failure are shown in Fig. 6,

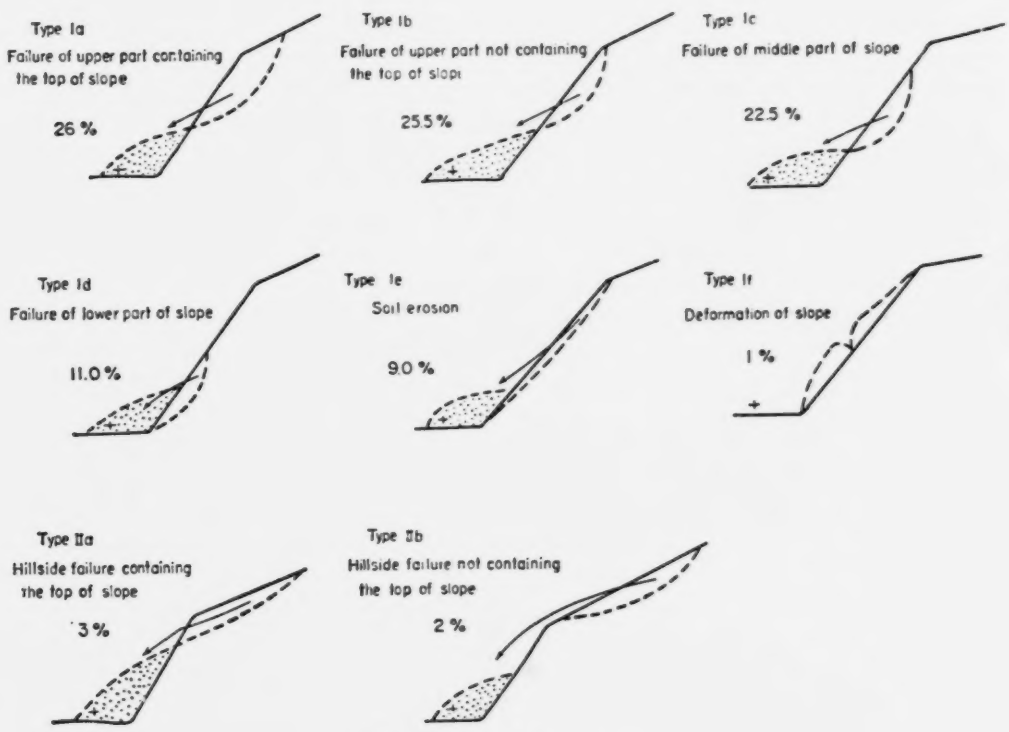

Fig. 6 Slope failure types

failure of the upper part of slope occupying half.

(2) Reappraisal of the point-rationing system

(a) The aim of point-rationing

The aim of point-rationing of slope failure is to judge the necessity for failure prevention works.

In order that a slope have sufficient strength against the estimated precipitation, it is shown:

$$K \geqq P \qquad \cdots\cdots\cdots(1)$$

in which K is the estimated points (or marks) of the slope strength, and P is the points of probable precipitation intensity within the return period corresponding to ranking of the line (for example, for 70 years in the first ranked line).

The magnitude of K shown:

$$K = c + k + f + y \qquad \cdots\cdots\cdots(2)$$

where c is the fundamental points, k the points to be decided by slope conditions, that is the sum of estimated points obtained by slope shapes and conditions, f the points for failure prevention works to be equipped with to be decided by the type of construction and the extent of prevention, and y the points to be given under judgement of local conditions.

At the time of planning, the necessity of prevention works to be equipped with can be estimated by Eq. 1. The system has an object to rank the degree of slope failure danger all over the JNR network and to prevent unbalanced equipment. The system is the standards decided statistically, so that it cannot determine precisely the slope strength of every locality. It is necessary to investigate further by boring into slopes in detail for selection of the failure prevention works to be equiped with.

(3) Revision of the point-rationing system

The present system was determined on the basis of a few slope failure data having been obtained before 1963, so that it did not well explain the results of analysis of many data obtained thereafter. On the basis of the recent data, the system was reexamined and improved.

For revision of the system, the point corresponding to each factor were decided by trial-and-error method, so that the point for slope strength might agree with the point for precipitation having

Table 1 The revised point-rationing system of cutting slope for judgment of failure danger

Points of slope conditions

Conditions		Points			
Fundamental points		+10			
Region		Hokkaido, Tohoku, Niigata	Kanto, Chubu, Kansai, Chugoku	Shikoku, Kyushu	
		0	+10	+60	
Slope conditions	Geological feature	Tertiary deposit, Valcanic detritus, Metamorphic rock	Diluvial deposit, Plutonic rock	Valcanic rock, Mesozoic and palaeozoic system	
		−40	0	+40	
	Soil type	Weathered rock	Sandy soil	Clayey soil	
		−20	−10	0	
	Height of slope	Less than 5 m	5 ~ 10 m	10 ~ 20 m	More than 20 m
		+20	0	−20	−40
	Gradient of slope	Steeper than 1 : 1	1 : 1	gentler than 1 : 1	
		−5	0	+5	
	Water conditions	Dry on the slope	Wet on the slope		
		0	−5		
	Conditions of the top of slope	Mountain side	The lay of water concentration		
		0	−5		
Failure prevention works		1. Spraying of mortar, stone masonry with dry joint + 5 2. Draining of slope, grass seeding +10 3. Covering with concrete, lattice work with concrete +20 4. Lattice work and covering with concrete +70 5. Retaining wall +100			
Special condition		The manager can give points in the extent ±10 by judgment of special conditions			

Points for precipitation

Points	Precipitation (mm/day)
100	450
90	400
80	350
70	300
60	250
50	200
40	150
30	100
20	50

caused slope failure.

With the aboved-mentioned analyses available, factors for the region, the geological feature, the soil types and the height of slope have been correlated closely to precipitation leading to slope failure. Point of each factor was decided that the point for these factors might have as high a correlation as posible between slope strength and precipitation with less deviation.

A few data of failure of prevention works were available, so that point of each failure prevention work could not be examined sufficiently. Since prevention works scarcely failed, point for them was decided as high as the present system.

The system thus improved is shown in Table 1, and according to this improved system, the relation between points of slope conditions and precipitation to cause failure is plotted on the basis of 970 records. As shown in this diagram, the correlation coefficient when points for region were neglected was 0.27, while the one when these were considered was 0.42, though deviation was large (the standard deviation being 49.46).

If fundamental points were decided on the basis of the regression line, half of the judgement by the system might fall in the danger zone. The precipitation to cause slope failure cannot be predicted, but can be probably presumed, even if all plausible factors to correlate the failure might be adopted.

It is necessary to decide the system so that 70 % of slopes along some railway line may fall in the safety zone, or along some important railway line, 99 % of slopes may fall in the safety zone. The fundamental point to decide that 70 % of slopes falls in the safety zone is + 10. The extent of the safety

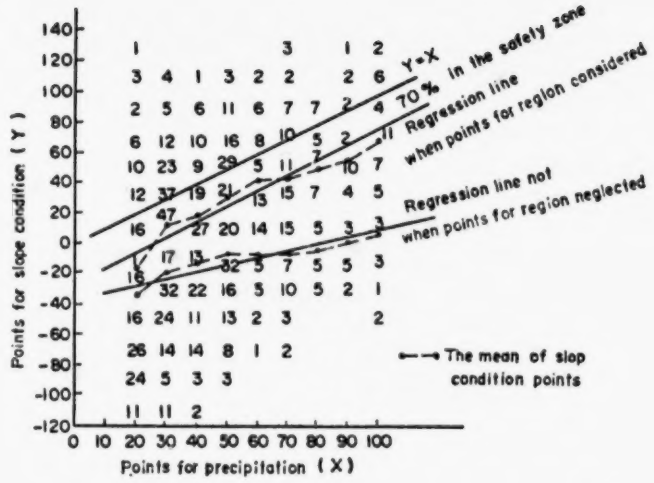
Points for slope condition (Y)
Points for precipitation (X)
Y=X
70 % in the safety zone
Regression line when points for region considered
Regression line not when points for region neglected
The mean of slop condition points

Fig. 7 The relation between points of the slope conditions and of precipitation to cause failure on the basis of 970 recnrds (The numerals in this figure show the distribution when points for region considered)

zone is determined by the change of the fundamental points.

On the basis of many slope failure records, an improved point-rationing system more correct than the present one could be introduced, though the improved system still have large deviations. To make more correct the system, it will be necessary to examine the regional group and else, Rapid progress cannot be hoped. by judging from exterior factor of slope only. It is necessary to use the values of surveying soil structure, water conditions, etc, on which some rapid surveying method will be developed.

(Report No. 699, 1969)

625.143.59 : 624.27.012.46 : 624.58.8

Experiments on Arita River Railway Bridge with the Concrete Bed

Yoshio WARIZAWA *, Iwao IWASAKI *

Experiments on Arita River railway bridge which used 4 kinds of track structures, that is, the two of them using concrete short sleepers or wooden short sleepers on a PC bridge and the other two using steel plates with holes or slabs for fastening rails without sleeper on a RC rigid frame were performed under locomotive passage. It has become clear that care must be taken when the concrete or wooder short sleeper is used on PC bridge.

* Structure Laboratory

1. Introduction

Hitherto the concrete bed has not been used excepting in long tunnel and other particular sites. As a part of track addition between Shirahama and Kainan on the Kisei line, such tracks have been used on Arita River railway bridge since, seemingly, they have many advantages on curtailment of workers and expenses for maintenance of railway and on reduction of dead load. The concrete short sleepers and wooden short sleepers were used on a PC bridge having three continuus spans. The steel plates with

holes and slabs for fastening rail without sleeper were used on a RC rigid frame double-track bridge with three continuus spans. To investigate the effects of locomotive testrun on such tracks, the experiment was performed.

2. Method of Experiment

The strain and deflection of the main beam, the strain near the sleeper and the vibration of the structure were measured under the loading of passing two locomotives (D 51 type) at four stepped velocities; 5, 20, 40, 65 km/h.

3. Results

3.1 *On PC beam*

(1) Strain in the beam. There was no distinction on the strain in the case of using wooden short sleeper on the up bound line and the case using concrete short sleeper on the down bound line. The values converted into stress were considered satisfactory.

(2) Deflection in the beam. There was a little difference, if any, in the deflection that occurred at up bound and down bound line. As the greater part of such difference occurred at a speed of 5 km/h, it was considered that such difference was caused by the difference in stiffness of beam. Since the deflections were about 10 mm, stiffness of such beam might be considered smaller than the one of general PC beam.

(3) Strain near the face of sleeper. The compressive strains on up bound line were affected by velocity, being larger than the strains on down bound line. The vertical tensile strains under sleeper at both lines were measured to exist, which hitherto had not been found at the track with concrete short sleeper in tunnel. It was considered that this phenomenon was characteristic of the track with short sleeper on PC beam and was affected by vertical deformation (because of Poisson's ratio) of concrete bed and difference between prestressed and nonprestressed ports.

Under loading of freight cars having flat tyres, the compressive strain that occurred under sleeper on down bound line increased with velocity. Three types of rail pad of 100, 50, 30 t/cm were used. If the strain occurred by using a 100 t/cm rail pad was assumed unity, the strains for the other two were 0.8 and 0.25 respectively. Therefore, they strongly depend on the spring coefficient of rail pad.

(4) Vibration of the structure. As for the vibration of structure in axial direction of bridge, there was little difference in amplitude that occurred on up bound line and down bound line. As for the lateral vibration of structure, the amplitude that occurred on down bound line was about 50 % larger than that of the up bound line. As for the vertical vibration of structure the amplitude that occurred on down bound line was about 5 times as large as that on the up bound line, but the amplitudes were small. The difference must have been caused by respective stiffness of structure, since the deflection of the structure on down bound line was a little larger than that on the up bound line.

3.2 *On RC rigid frame*

3.2.1 On the No. 14 rigid fram (Fig. 2)

(1) Strain in main beam. Both the strains in main beam on the up bound line, using ballast bed with natural sleeper, and those on the down bound line, using steel plates with holes for fastening rail without sleeper, were not affected so much by velocity in case of locomotive passage. The strains were small and it was considered that the tensile stress of that concrete effectively acted on the beam. The strain under passage through down bound line was a little larger than that of the up bound line.

(2) Deflection in main beam. The deflection in main beam in case of locomotive passage through up bound line and down bound line were not affected so much by velocity. The deflection were about 1.3 mm and the difference was small.

(3) Strain near the face of steel plates with holes. The compressive strains were measured under the steel plates with holes and the tensile strains were measured above the top of beam slab, but the strains were small. The phenomena were considered that the re-deposited concrete acted as lapped beam.

(4) Vibration. Comparing the amplitudes of vibration that occurred in case of locomotive passing through up bound line and down bound line: As for the horizontal vibration, the former was

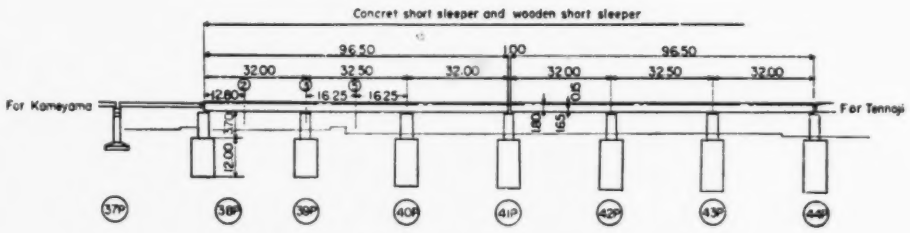

Fig. 1 Arita river PC railway bridge

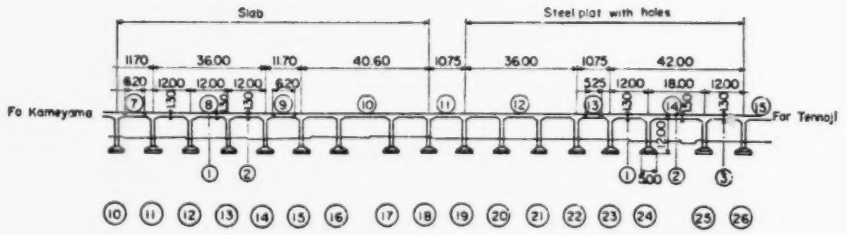

Fig. 2 Arita river elevated RC rigid frame bridge

generally larger than the latter, while as for the vertical vibration, the former was three times as large as the latter. As for the vibration in axial direction of bridge, thefo rmer was less than half of the latter. As for the latered vibration of the former, the ratio of amplitude under part of pillar to the amplitude on the slab was 1 : 5, and it was not clear if the difference was affected by such track structure.

3.2.2 On the No. 8 rigid fram (Fig. 2)

(1) Strain in main beam. The strains in main beam in case of locomotive passage through up bound line, using ballast bed with natural sleeper, and through down bound line, using slab bed without sleeper, were not affected so much by velocity. The strains were small and it was considered that the tensile stress of concrete effectively acted on beam. The strain under passage through up bound line was a little larger than that on the down bound line.

(2) Deflection in main beam. On the deflection in main beam, the difference that occurred in case of locomotive passing through up bound line were small and not so affected by velocity. The deflections were about 0.7 mm.

(3) Vibration. Comparing the amplitude of vibration occurred when locomotive passed through up bound line and down bound line: As for the lateral vibration, the amplitude at one portion was 20 % larger than that at another, to be and it was considered that the twist vibration occurred, while as for the vertical vibration, these were much the same. As for the vibration along the axis of bridge, the former was a little larger than the latter. As for the lateral vibration of the former, the ratio of amplitude under part of pillar to the amplitude on the slab was 1 : 5, and this case was the same as the one in the No. 14 rigid frame.

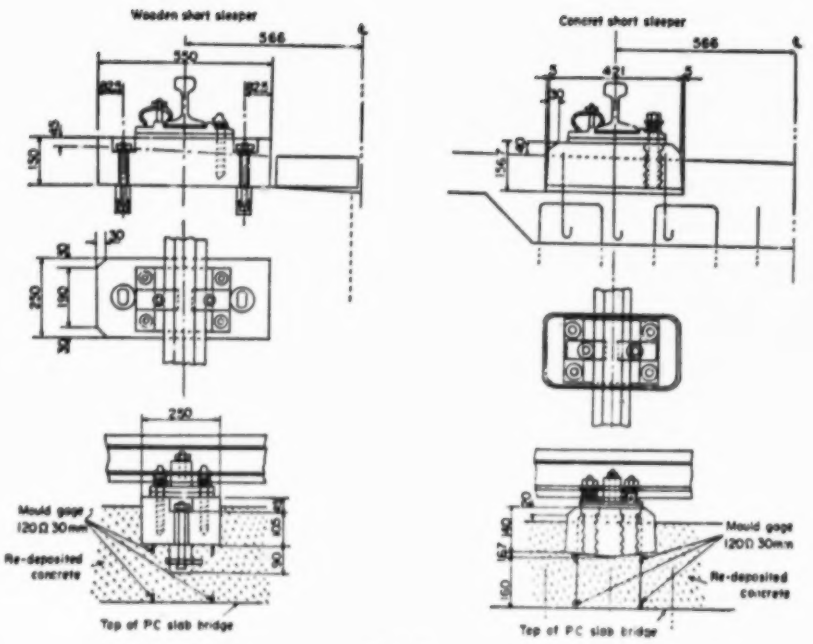

Fig. 3

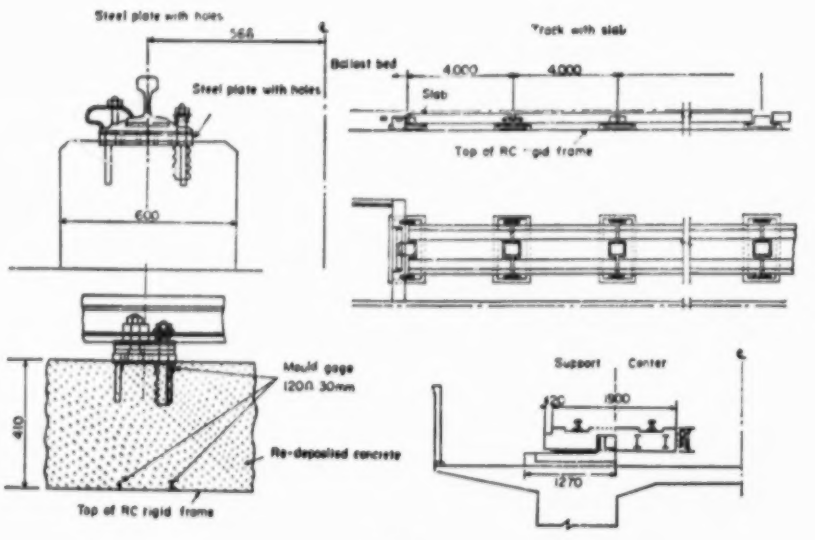

Fig. 4

4. Conclusion

Within the limits of the above results, there were no results which were specifically affected by the structure of railway bed excepting the one using wooden short sleepers and concrete short sleepers on a PC bridge. Therefore, care must be taken when concrete or wcoden short sleepers are used on a PC bridge.

(Pre. Report No. 231, 1969)

625.2—592.356 : 656.2.022.81

Standing Test of Eddy Current Rail Brake Set to a New Test Electric Car

Hisakazu SOOKAWA *, Yoshihiko SATO, Dr. Eng. †
Eiji ITAKURA ‡, Miyato MIYAIRI, Dr. Eng. §

To strengthen the braking force of the car at higher speed on the Shin Kansen, newly developed eddy current rail brakes (ECB) were tested in standing conditions with use of a new test electric car. Following items were studied in the test. (a) Flux intencity of pole. (b) Vertical displacement of exciting ECB. (c) Displacement and strain of track and turnout. (d) Distribution and effect of flux near ECB. (e) Magnetization of rail.

1. Introduction

The electric car on the Shin Kansen is expected to be model-changed when the Sanyo Shin Kansen is completed. At that time it is also hoped that the maximum speed which is now 210 km/h should be raised up to 250 km/h. At such a high speed braking distance will be elongated not only by the increased speed but also by the decrease of the frictional coefficient between wheel and rail if the car is braked depending only on the conventional rail/wheel friction. To strengthen the braking force of the car at a higher speed, newly developed eddy current rail brakes (ECB) were tested with use of the new test electric car which was made in 1969 for the test proceeding the model-change of electric cars on the Shin Kansen.

ECB's were set under two bogies of the test train composed by test electric cars and a locomotive, facing to the rail surface. When ECB is excited by supplying DC, the car is braked directly by the rail electromagnetically. As the braking characteristics of ECB had already been investigated precisely by the experiment made in the laboratory, it was considered necessary as the next step to make clear the following effects of ECB to the track and signalling equipment which had not been studied so far.

(1) Increase of track deformation due to electromagnetic force of ECB

(2) Rise of rail temperature due to eddy current caused in the rail

(3) Flux intensity near ECB and attraction and drop of iron pieces

(4) Increase of unsprung mass due to the weight of ECB itself and connecting mechanism of ECB and increase of track deterioration due to the increased unsprung mass

(5) Magnetization of rail

(6) Effect of the difference of both electric conductivity and magnetic permeability between manganese crossing and ordinary rail to the running of rolling stock.

The braking force caused by ECB is small at low speed in principle. As ECB's equipped under the test car are excited with the electricity generated in the dynamic brake and the power generated in the dynamic brake itself decreases rapidly as the running speed of the car becomes lower, the braking force and also the attraction become so small at a low speed. Of course, there are neither braking force nor attraction under the standing car. Further, as for the action of ECB set to the running car, the intensity and the distribution of the flux vary with the eddy current generated in the rail. Thus, it is very sure that the effect of ECB must be investigated in running condition, but as there are too many unknown phenomena about ECB, a series of tests with ECB's set to the standing car were performed as a prerequisite of the running test, especially so as to make clear the effect of ECB both on the track and on the signalling equipment as much as possible.

2. Experimental Procedure

The test was performed in the yard of the Osaka operating depot of the Tokaido Shin Kansen branch office of JNR for three days from May 21st to 23rd in 1969. The test cars were mainly in standing condition and partly in running condition at a low speed. The composition of the train for the test is as shown in Fig. 1. Four ECB's were set under the front and rear bogie of the car 951—1, facing to the rail. The gap between ECB and rail surface was taken to be 9.5 mm on sea-side and 11.5 mm on hill-side though its design value was 6.5 mm.

Three different sections of tracks were offered for the test. These were an ordinary section, a jointed section of the track and a turnout section. Fishplates of the joint were removed so that this section could resemble that of the broken rail.

As ECB's of the test car could not be excited

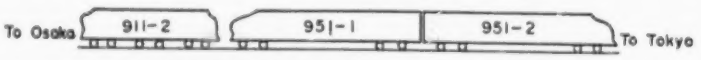

Fig. 1 Composition of test train

* Car Performance Laboratory, † Track Laboratory
‡ Signalling Laboratory, § Physical Testing Laboratory

with existing circuit when the train was standing, ECB's tested were connected to the powering circuit by disconnecting main motors of the car from the circuit. Thus, ECB's were excited with the electricity supplied through the trolley. As a consequence, the current supplied to ECB's was DC with some ripple of 120 Hz, which was made by rectifying AC of 60 Hz. The ripple ratio corresponding to the measured value of current was shown in Table 1.

Table 1 Ripple ratio

ECB current	Ripple ratio
80 A	2.94 %
160 A	3.89 %
240 A	5.68 %
315 A	6.32 %

3. Results

3.1 *Flux intensity*

The flux intensity of the pole was measured with a flux meter, using a search coil. Fig. 2 is an example of the flux intensity measured on the ordinary section of the track. The flux intensities measured also on the curved section and on the joint were nearly the same as that on the ordinary section. The maximum mean magnetic flux intensity were from 1.37 to 1.4 Wb/m². These values were mean. Thus, the flux intensity at the center part of the rail is higher than these, because the rail surface is rounded up.

3.2 *Vertical displacement of ECB*

The vertical displacement ECB was measured from both the wheel level and the ballast level when ECB was excited. Fig. 3 shows an example of measured displacement values of ECB with the gap of 11.5 mm. The displacement measured from the wheel level is 1.3 mm at the ECB current of 315 A. The value is near to the aimed value 1.6 mm which is considered for the gap 6.5 mm. As the rail at the resembled broken rail section was sticked to ECB when ECB was excited, the displacement was not measured.

3.3 *Effect of ECB to ordinary track*

As for the ordinary section of the track, variations of the wheel load, the rail stress and the rail displacement were measured.

The measurement of the wheel load was performed, aiming not only the measurement of the increase of wheel load due to the attraction between ECB and the rail but also the measurement of the attraction itself caused by ECB, because ECB was suspended under an axle box beam which is directly supported through fairly hard rubber bush by wheels. Figure 4 shows the increase of wheel load due to ECB current. The wheel load increases in proportion to the 0.75th power of ECB current. The calculated increase of wheel load based on the measred data was 1.72 t on sea-side and 1.35 t on hill-side when ECB current was 320 A. The value of ECB current used for calculation is nearly as same as the maximum value 315 A in the test. Then the attraction acting between ECB and the rail was 3.4 t on sea-side and 2.7 t on hill-side. The difference of the force is due to the difference of the gap between ECB and the rail.

The bending stress of the rail also increased in proportion to the power of ECB current. The maximum vertical bending stress of 580 kg/cm² compression under the wheel and 300 kg/cm² tension under the center of ECB which were caused by the weight of the test car increased to 720 kg/cm² compression on sea-side by increase of 140 kg/cm² under the wheel and also to 440 kg/cm² tension by increase of 140 kg/cm² below the center of ECB by exciting ECB. On hill-side the maximum bending stress increased by 100 kg/cm² to 680 kg/cm² compression under the wheel and by 90 kg/cm² to 390 kg/cm² tension below the center of ECB.

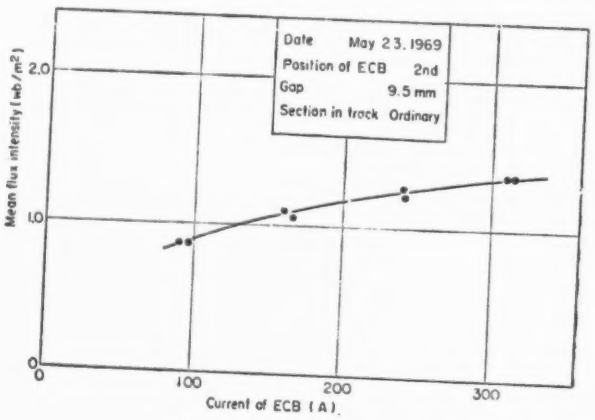

Fig. 2 Flux intensity

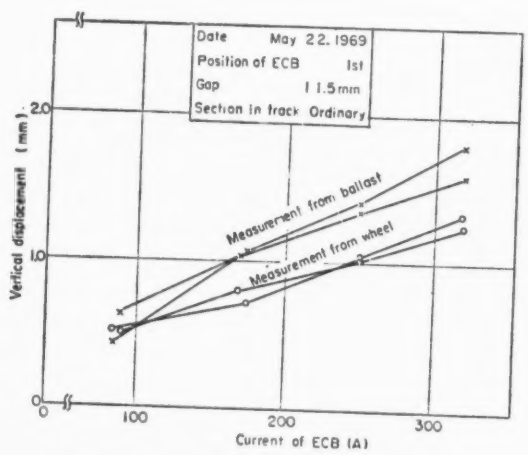

Fig. 3 Vertical displacement of ECB

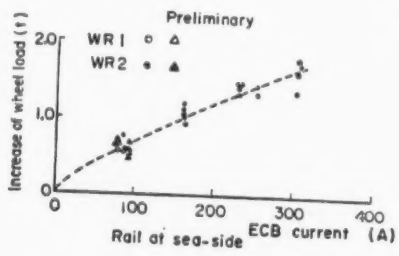

Fig. 4 Increase of weel load due to excitation of ECB

The displacement of rail also varies in proportion to the power of ECB current. The rail displacements due to car weight of 1.7 mm under the wheel and 1.4 mm below the center of ECB increased under the wheel by 0.1 mm and decreased by 0.21 mm at sea-side and 0.18 mm on hill-side below the center of ECB by exciting ECB.

Such measured values of the rail stress and displacement are nearly the same as calculated values with some assumptions.

3.4 *Effect of ECB to resembled broken rail track*

To make clear the effect of ECB to the broken section of the track, the joint section of the rail resembled the broken rail track by removing fishplates and a rubber pad under the rail. The test car was stopped as an end of ECB of the front bogie came to the 10 cm for Tokyo from the joint.

When ECB was excited with the current of 80 A as a preliminary test, the rail was sticked to ECB. Through the whole tests in this section such phenomena were common. Thus, the rail displacement caused by ECB current beyond 160 A was saturated with a constant value which was different corresponding to the relative horizontal position between ECB and the rail.

The maximum rail stress was caused at rail surface under the wheel. The value was 510 kg/cm² compression due to the weight of test car plus 580 kg/cm² compression due to excited ECB. The total was 1090 kg/cm² compression. This value is not so small as the bending stress, but as the longitudinal force does not act at such a broken part of rail, there will be no problem.

3.5 *Effect of ECB to turnout*

The tongue rail of the turnout was held upward just by lateral compressing force of switch-bar with aid of wedge action of the tongue as shown in Fig. 5. Thus, the resistance to the upward is far smaller than to the downward.

The deformation of turnout was investigated under two conditions. The first was that ECB was over the tongue, an end of ECB coincided with the tip of the tongue and the wheel did not constrain the upward movement of the tongue. The second was that the center of ECB coincided at the bent point of the tongue. The fixing of the tongue is the poorest near the bent point.

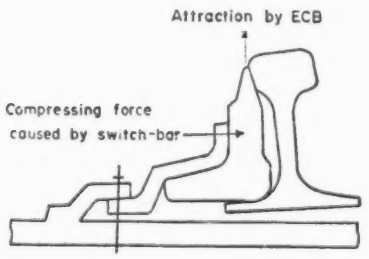

Fig. 5 Fixing of tongue

The measurement showed that the stress of the tongue and switch-bar did not vary exceeding 50 kg/cm² under the first condition, and that, though there was 50 ~ 100 kg/cm² stress variation at the bent point of the tongue and in the main rail under the second condition, these values were small enough to make the further discussion unnecessary.

The displacement of the tip of the tongue increased under the first condition as ECB current increased. However, as its value was 0.26 mm at ECB current of 320 A, there is no problem. Also, the tongue which was on detached side and was free upward before the switch-bar touched to the bottom of the main rail did not show any definite variation of the displacement.

3.6 *Attraction of iron pieces*

To investigate the attraction of iron pieces from the neighborhood of rail, the plate which was made of bakelite and had 60 grooves was set on the side of ECB under the rear bogie as shown in Fig. 6. The plate was set as an edge of the plate was at the rail head surface, going down outside with a slope of 1/20. In a groove a steel ball with the diameter of 5 mm was put with a predetermined distance from the side surface of the rail head.

Sea-side balls were attracted within 92 mm at ECB current of 80 A. The extent of ball attraction increased to 112 mm at ECB current of 315 A. On hill-side the extent of 87 mm at 80 A was increased to 98 mm at 315 A.

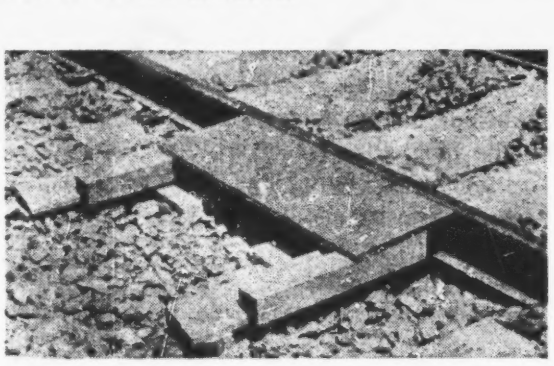

Fig. 6 Steel table set contacting to rail head

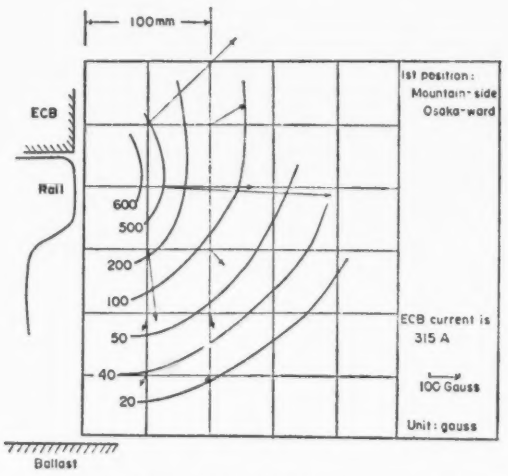

Fig. 7 Distribution of flux near rail

3.7 *Distribution of flux near ECB*

Figure 7 shows the distribution of the flux when ECB was excited with the current of 315 A. As the center position of the switch machine is apart from the rail by 1,050 mm and the flux at the machine only several gauss, the polar relay will not be affected by excited ECB.

3.8 *Magnetization of rail*

The bellow curve in Fig. 8 shows the magnetization of the rail after ECB set to the test car was excited in short time in the standing condition and then the car with ECB was removed. The upper curve in the figure shows the flux distribution of excited ECB. By comparing these two curves in Fig. 8, it is made clear that the polarity of the rail is opposite to that of ECB and the magnetization is under 20 gauss.

When ECB in excited condition was moved above an insulated joint, the rail head aparted from the joint by 10 mm was magnetized as shown in Fig. 9. The one section of the abscissa corresponds to one passage of the test car. The direction of the running and the supplied current were as shown in the upper table in the figure. This figure shows that the first passage of ECB magnetized the joint up to 30 ~ 40 gauss, but there was not any distinct growth by further passages of the test car. However, even in this degree of magnetization of the insulated joint the short circuit can be made by sticking iron filings. As the further bad state can be imagined by the combination of conditions, some countermeasures must be considered. One of the simplest measure is to set the orders of the polarities of 2 ECB's in one car upon one rail opposite. Figure 10 shows the magnetization of an insulated joint which was caused by changing the running direction of the test car one by one.

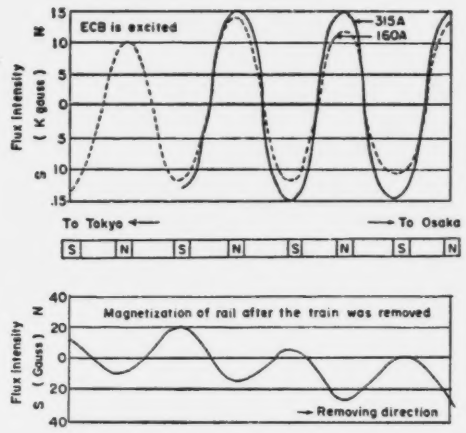

Fig. 8 Magntization of rail under ECB (standing)

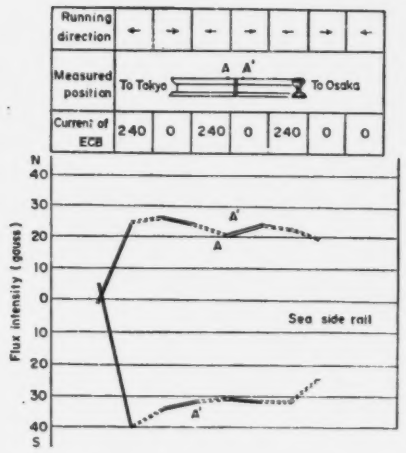

Fig. 9 Magnetization of insulated rail joint (double line operation)

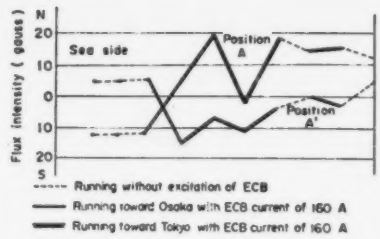
Flux intensity (gauss)
Sea side
Position A
Position A'
Running without excitation of ECB
Running toward Osaka with ECB current of 160 A
Running toward Tokyo with ECB current of 160 A

Fig. 10 Maganetization of insulated rail joint (single line operation)

4. Concluding Remarks

Above-mentioned tests made clear considerably many effects of ECB on both the track and signalling equipment, though the braking characteristics, the temperature rise of the rail and the increase of track deformation due to the braking remain untouched. As already shown in the introduction, ECB does not work in principle when the car is standing. The phenomenon that takes place in running may be a little different from that in the standing car. Especially, both the flux intensity and the distribution of the flux vary in running condition. The characteristics of ECB including these points are expected to be discussed in the report of running test.

(Pre. Report No. 1024, 1969)

621.332.23 : 621.314.223 : 681.32.06

Computer Program for Analysis of the Feeder Circuit with Auto-Transformers on AC Electrified Railway

Jiro MIZUNO*, Shoichiro HAMAYOSE†, Kazunori ISHIKAWA‡

As the network of the feeder system with auto-transformers is more complex compared with that of the feeder system with booster transformers, it is hardly possible to calculate the distribution of voltage and current in the network with figure.

The computer program for the numerical analysis of the network was developed at the same time when the investigation began in Oct. 1965 and was completed at the beginning of 1968.

This paper shows the theoretical formulas and numerical solutions on which this program was based.

1. Introduction

The theoretical research for "the feeder system with auto-transformers" (so-called, AT-system) was begun Oct. 1965,

First of all, we investigated the equivalent circuit for the feeder circuit, and completed the Fortran-program for calculation of the single line composed of 3 conductors at the beginning of 1966. Consequently, we could clarify the fundamental characteristics of the AT-system. On the other hand, we testified the justice of the method of forecast-calculation through the experimental results on the Nippo line (Jul. 1966) and the Mito line (Dec. 1966), thus, we confirmed that this system might be useful for the feeder system of the Sanyo Shin Kansen.

On the ground of above fruits, we developed the program for calculation on the Sanyo Shin Kansen, which made it possible to analyse the characteristics of the system with double track, ground wire, track circuit, etc.

Based on this project, the generalized program on AT-system with 12 conductors was completed by cooperation of 3 laboratories, electric power, communication and signaling. Using this program, following characteristics can be analized.

(1) The inductive characteristics of communication lines.

(2) The characteristics of voltage drop.

(3) Voltage and current distribution in case of fault.

(4) The influences on the track circuit.

These results are adopted on planning of the electrification by AT-system on the Kagoshima Line, and the Sanyo Shin Kansen.

The following descriptions are concerned with those of theoretical formulas and numerical solutions for the above program, and explanation of the program itself.

2. How to Calculate the AT-System

2.1 *Fundamental formulas*

In order to calculate the feeder circuit, we convert such conductors as rails or shield wires with distributed parameters in itself into those with concentrated ones, express relations between voltages and currents in each-section by circuit admittance, and can get the solutions of voltages and currents of whole system by solving the simultaneous equations. As shown in Fig. 1, the fundamental equations are derived from the relation between voltages and currents at the point where the equivalent circuit composed of parallel conductors are cut at an arbitrary position (i.e. $K-1$, K, $K+1$, etc.). The subscript m refers to the kind of a conductor.

When the current I and the voltage V are defined by the matrices as follows,

$$\begin{bmatrix} i_k^1 \\ i_k^2 \\ \vdots \\ i_k^m \end{bmatrix} = [I]_k^m \qquad \begin{bmatrix} V_k^1 \\ V_k^2 \\ \vdots \\ V_k^m \end{bmatrix} = [V]_k^m$$

thus, the next relations are gained

$$[I]_{k+1} - [I]_k + [Y]_k [V]_k = [G]_k \quad \cdots\cdots(1)$$

$$[V]_k - [V]_{k-1} + [Z][I]_k = 0 \quad \cdots\cdots(2)$$

By combining Eq. (1) with (2), we gain the following form

$$-[Z]_k^{-1}[V]_{k-1} + \{[Y]_k + [Z]_{k+1}^{-1} + [Z]_k^{-1}\} V_k - [Z]_{k+1}^{-1}[V]_{k+1} = [G]_k \quad \cdots(3)$$

Indicating above equations in matrix form with q sections,

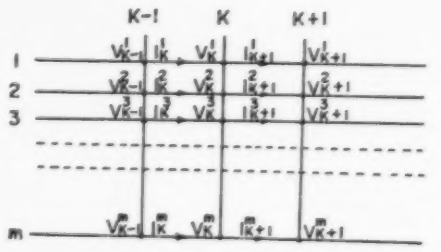

Fig. 1 Construction of lines

* Electric Power Laboratory, † Communication Laboratory
‡ Signalling Laboratory

$$\begin{bmatrix} M_1 & E_1 & 0 & & & \\ D_2 & M_2 & E_2 & 0 & & \\ 0 & D_3 & M_3 & E_3 & 0 & \\ & \ddots & \ddots & \ddots & \ddots & \ddots \\ & & 0 & D_{q-1} & M_{q-1} & E_{q-1} \\ & & & & D_q & M_q \end{bmatrix} \begin{bmatrix} V_1 \\ V_2 \\ V_3 \\ \vdots \\ V_{q-1} \\ V_q \end{bmatrix} = \begin{bmatrix} G_1 \\ G_2 \\ G_3 \\ \vdots \\ G_{q-1} \\ G_q \end{bmatrix} \quad \cdots\cdots(4)$$

where, $D_k = -[Z]_k^{-1}$, $M_k = [Y]_k + [Z]_k^{-1} + [Z]_{k+1}^{-1}$, $E_k = -[Z]_{k+1}^{-1}$

This is the complex equations with unknown voltage matrix, and solving these equations, we gain the values of voltage $[V]$ and current $[I]$. As a condition for solution, the coefficients in each section, i.e.,

$[Z]_k$: Impedance matrix in a interval of a section k

$[Y]_k$: Admittance matrix in a section k

are required. Namely, line constants, load impedance of AT, must be represented in the matrix form.

2.2 *Numerical solution*

Eq. (4) is the same form as that of the boundary problem on Laplace's partial differential equation, so-called Block Tridiagonal Matrix. The way to solve this equation directly is studied variously. As one of the solutions there is the S. Schechter's L—U process. We use this method here.

It follows from Eq. (4) that

$$Q = [D_n,\ M_n,\ E_n]_1^q$$

where $Q \cdot V = g$.

Now, according to S. Schechter's method Q is divided into two matrices, the Upper Matrix (U) and the Lower one (L) as follows

$$Q = L \cdot U \quad \cdots\cdots(5)$$

where $L = [C_n,\ I_n,\ O]_1^q$ $\cdots\cdots(6)$

$$U = [O,\ A_n,\ E_n]_1^q \quad \cdots\cdots(7)$$

Thus, these variables are defined as

$$\left.\begin{aligned} A_1 &= M_1 \\ C_n &= D_n \cdot A_{n-1}^{-1} \\ A_n &= M_n - D_n \cdot A_{n-1}^{-1} \cdot E_{n-1} \end{aligned}\right\} \quad \cdots\cdots(8)$$

where $1 < n \leqq q$

After having divided Q into L and U, by combining Eq. (6) and Eq. (7) with Eq. (8), the unknowns V are calculated easily.

That is

$$L \cdot U \cdot V = g$$

By writing

$$U \cdot V = y$$

It follows that

$$L \cdot y = g$$

Hence, the following formulas are gained

$$\left.\begin{aligned} y_1 &= g_1 \\ y_n &= g_n - C_n \cdot y_{n-1} \\ V_n &= A_n^{-1} \cdot (y_n - E_n \cdot V_{n+1}) \\ v_q &= A_q^{-1} y_q \end{aligned}\right\} \quad \cdots\cdots(9)$$

where $1 < n \leqq q$

From the above expressions, we can determine the values of V ($V_1 \cdots\cdots V_n$) one after antoher.

3. Programs for Calculation

As the program is made for the Sanyo Shin Kansen, the 8 conductors, that is, (trolley, feeder, rail and protecting wire) × 2(double track) = 8, and 4 conductors of usual Sanyo Line or other private lines which run parallel to the Sanyo Shin Kansen, after all, 12 conductors were assumed.

The number of devided sections, when the length of feeding distance is 60 km and the leakage conductances are concentrated on each 0.5 km, 120 is needed, but we used 100 sections because of the limitation of the memory capacity of the computer (IBM—360—75 I).

This program is divided into 3 kinds according to how to use the shield lines except the fundamental 8 conductors. They are;

(1) <KIDEC>

Calculating the induced current in the shield lines near the AT-feeder circuit.

(2) <KIDOC>

Calculating the characteristics of a track circuit, single rail or double rails track circuit, when the track circuit is normal or failed, (containing break down of rail).

(3) <KIDEC-R>

Calculating the feeder circuit with the conductors (sub-feeder lines) laid in parallel to a trolly and feeder.

In every program, to make it easy to use, after such fundamental constants as geometric dimensions and self-impedances are given, the positions of AT, load, sub-station, short point, etc. can be put into a computer in the form of data cards, and output of voluntary position and characteristic can be designated.

Further more, calculations of movement of load and those of harmonics are easily performed to required extent.

The results of calculation are printed in the form of voltages and currents, sum of currents of each conductors in every section and total Amp·Km. As for the impedance-bond, the voltages on both sending and receiving terminals are calculated.

4. Concluding Remarks

As described above, by making use of this program, the calculation on a feeder-circuit, which has hitherto been performed by calculation with figure for a very simple equivalent circuit, has come to be able to calculate as a precise circuit with quasi-distributed parameters.

Especially, in case of such a complex circuit composed of many meshes and branches as the AT-feeder circuit, it is hardly possible to calculate the Amp·Km and analyze the characteristics of a track circuit with figure; this program made it possible

initially.

Nevertheless, as there are some incovenience in this program for application to actual problems, we are making a new program which makes it possible to calculate 16 conductors and to investigate sending lines as well as the feeder-circuit and that, comprises the function of 3 programs. It is to be improved basing on the fundamental formulas and method described above.

(Pre. Report No. 1, 1970)

621.335.42 : 625.2.066.013 : 3 : 620.179.1

Nondestructive Snapping Inspection of Stranded Wire in Jumper Cable of Railway Car

Takushi MATSUNAGA*, Masaharu NAKANO†, Miyato MIYAIRI, Dr. Sc.‡

As a method of nondestructive inspection for stranded wires in a jumper cable of a railway car, the electric resistance of stranded wire of a cable was measured under swinging (rocking) condition of the cable. When some wire elements in a strand were snapped anywhere, the electric resistance of the strand shows a very unstable value according to the swinging of jumper cable. This instability of the electric resistance seems to be related to the number of snapped wire elements. To detect this unstable change of electric resistance (variation of resistance) is the principle of the nondestructive testing method of jumper cables. A new automatic nondestructive testing apparatus using this principle has been developed to inspect jumper cables of railway cars in Japanese National Railways. Following faults in jumper coupler have been detected with this apparatus.

(1) Even a snapped wire element in a strand of 21 wire elements.

(2) Failures of soldering between terminal tip and strand in jumper plugs.

(3) Kink and fatigue in stranded wire.

1. Introduction

It is a very important and difficult problem to detect, at the earlier stage, the fatigue failure of wire elements of a stranded wire in a cable. An electro-magnetic induction method (eddy current method) was tentatively applied to a stranded steel rope, but the eddy current method is not so suitable one for a stranded wire in a cable because the ratio of the cross section of the wire to that of the searching coil of the apparatus is small. It is also unsuitable for the problem to apply a radiographic method because of the reason that the jumper cables are made from multicore strand cable. The electric resistance of strands in a cable is scattering on a very wide range, therefore the resistance measuring method is not suitable to the problem either.

Thus, for the purpose, the method of measuring the variation of electric resistance of stranded wire under swinging (vibrating) condition was devised.

2. Potentially Occurring Position of Snapping

In operating a railway car, jumper cables are subjected to bending and torsional vibration. By repetition of vibrations, stranded wires in cables may be failed by fatigue of wire elements. These failures occur possibly in following positions.

A. Tip soldered position.
B. Insulator bared part.
C. Somewhere in insulated part.

In these positions, A and C cannot be detected by using the conventional methods of nondestructive testing.

3. principle of the Method

The values of electric resistance of sound stranded wires in a jumper cable are sometimes scattering within the range of 6—8 mΩ.

The amount of resistance increase of a stranded wire by a snapping of wire element is only about 0.1 mΩ. Thus the scattering range of resistance of strands in a cable shows rather larger value in comparison to the resistance by a wire element snapping. This is the reason why the statical resistance measuring method cannot be used for the purpose.

The electric resistance of a stranded wire with one snapped element can be represented by the following formula.

$$R = R_m + R_f + \frac{\rho\,\delta}{S}\,\frac{1}{N(N-1)} \quad \left(R_m = \frac{l}{NS}\right) \qquad \cdots\cdots(1)$$

* Rolling Stock Investigation Laboratory, † Hatabu Work Shop, ‡ Physical Testing Laboratory

where δ is, as shown in Fig. 1, a detached length of snapped wire element from the main part of the stranded wire, R_f is the deviation from the mean value of resistance of strands in a cable, Rm. S is the crossectional area of a wire element, l is the length of the wire element, N is the number of wire elements in a strand, and ρ is the electrical resistivity of copper.

When $n(n \geq 2)$ snaps are occurred in a strand, the expression of the resistance has to be divided into two forms according to following cases, (considering most extreme cases.)

A. All snappings are concentrated at a point.

B. All snappings are scattered all over the length of a strand.

$$R_a = R_m + R_f + \frac{n\rho\delta}{S}\frac{1}{N(N-n)} \quad \text{Case A} \qquad \cdots\cdots(2)$$

$$R_b = R_m + R_f + \frac{n\rho\delta}{S}\frac{1}{N(N-1)} \quad \text{Case B} \qquad \cdots\cdots(3)$$

In these expressions, R_f takes different value for each strand in a cable, and the value of the term containing δ varies with time by swinging the the jumper cable. Thus, the time dependent value of this term (related to the number of snappings) can be used as a signal of existence of snappings of wire elements, and the value, as seen in formula (2), depends upon the number of snappings.

The principle of the method is based on the electrical detection of the signal.

4. Fundamental Experiments

At the start of the experiments, the conditions of swinging to be given to the test jumper coupler have to be determined, and they were selected among the values obtained from actual operation of railway cars in JNR.

There are three typical movements (swinging conditions) in jumper cable motion in actual operation of railway cars, namely;

A. Longitudinal movement of jumper plug.
B. Mutually opposite transverse movement of jumper plug.
C. Torsional vibration of jumper cable.

In these movements, the transverse movement is naturally followed by the torsional vibration.

The variation of electric resistance of stranded wires with some artificial snappings were measured with a simple bridge under swinging condition of longitudinal and transverse movement of jumper plug, and the results are shown in Fig. 2. In the figure, the variation of electric resistance measured under torsional vibration is also shown. In the specimen of this experiment, all snappings were made at a single point in a stranded wire.

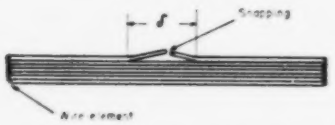

Fig. 1 Schematic illustration of a snapping

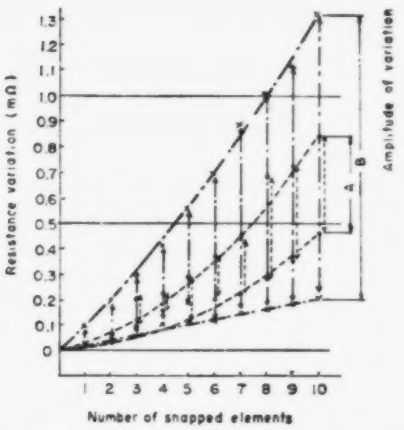

A; Torsional vibration only
B; Longitudinal and transverse movements

Fig. 2 Resistance variation of stranded wires with snapped elements

5. A Newly Developed Testing Apparatus

A new model of the inspection apparatus was tentatively arranged by using the principle. This apparatus was designed to detect snapped wire elements and to examine the fatigue properties of jumper cable for railway cars in JNR. The block diagram of the apparatus is shown in Fig. 3, and photograph of the apparatus is shown in Fig. 4.

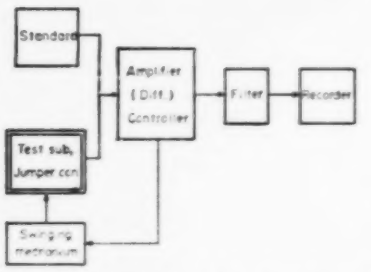

Fig. 3 Block diagram of a newly developed apparatus

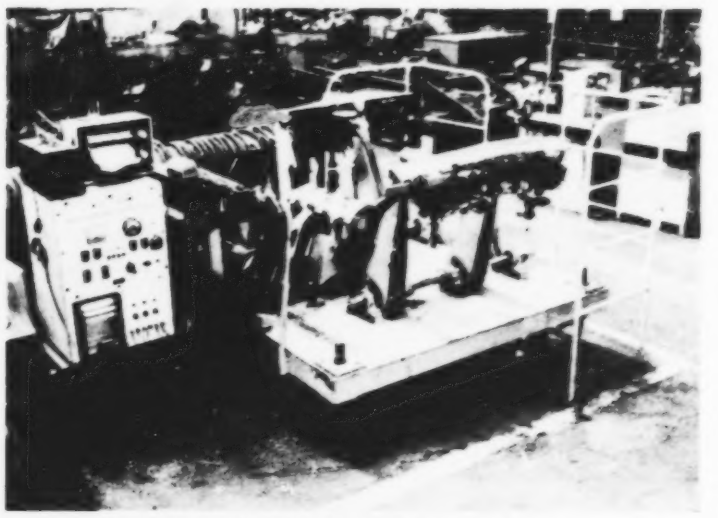

Fig. 4 General view of the apparatus

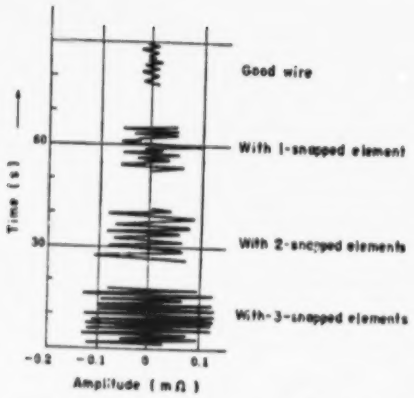

Fig. 5 Examples of record obtained by the apparatus

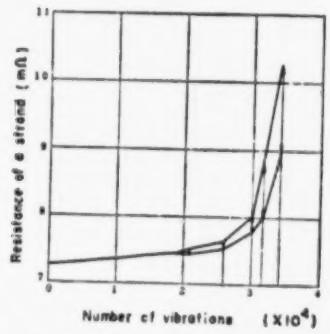

Fig. 6 Electric resistance increase of a stranded wire in a jumper cable by fatigue and snappings of wire elements

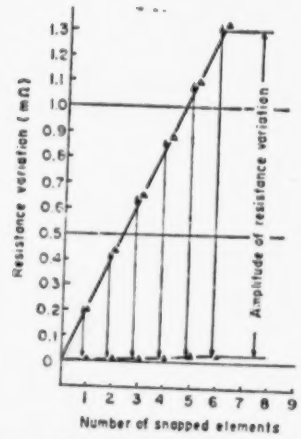

Fig. 7 Electric resistance variation of a stranded wire with a number of snapped elements by fatigue

The longitudinal movement of jumper plug was made through two rocking arms, and the adjustable range of the amplitude of the motion was 0—300 mm, the period of the motion being 5 sec.

The mutually opposite transverse movement of plugs was also made through the same rocker arms, the adjustable range of the motion was 0—300 mm, and the period was 3 sec. This transverse motion is followed by the torsional vibration of the cable, with an amplitude range of 0—50°.

These values of adjustable ranges were almost the same as those obtained from the actual operating test of railway cars in JNR.

Examples of results obtained by the apparatus for a jumper cable containing strands with some snappings or other failures are shown in Fig. 5.

The process to a fatigue snapping of a wire element was studied by using the apparatus as a fatigue testing machine for a jumper cable (coupler).

The results, relations between the electric resistance and the number of repetitions of transverse motion, are shown in Fig. 6. A relation, obtained from these results, between electric resistance variation and the number of fatigue snappings of wire elements is shown in Fig. 7.

6. Another Application of the Method

An application of the method has been tried in the nondestructive testing for a lead conductor (stranded wire) of a main motor of an electric car. The cross sectional area of the lead is 80 mm², and the number of wire elements is 513.

The results are shown in Fig. 8, and the figure shows that 20 snappings of wire elements in 513 can be surely detected.

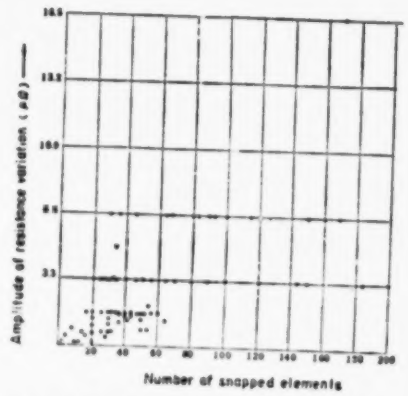

Fig. 8 Relation between amplitude of resistance variation and number of snapped elements in motor lead

7. Conclusions

For a jumper cable of a railway car, multi-core cable is used. Sometimes wire elements in the stranded wire have been damaged and snapped by fatigue. To detect these snappings nondestructively in the earlier stage is a very difficult and important problem for railway car maintenance.

The authors studied the problem, and following results were obtained.

(1) The conventional nondestructive testing methods such as radio-graphy, thermography, ultrasonic test, eddy current method, or acoustic method are not so suitable for the purpose.

(2) Statical measuring method of electric resistance cannot be used to detect 2—3 snappings (earlier stage of fatigue failure) of wire element since the electric resistance of each strand in a jumper cable is scattering on a rather wide range in comparison to the resistance increase of a strand by a snapping.

(3) The electric resistance of a strand with some snapped elements, measured under swinging condition of the jumper cable, changes unstably. This unstable resistance variation can be used as a signal of existence of some snapped wire elements.

(4) As an application of the method, the lead conductor of a main motor of electric car was tested By the method, 20—snappings in a strand of 513 wire elements were surely detected.

(Report No. 692, 1969)

539.43 : 621.791.052

Fatigue Strength of Side Fillet Welded Joint

Shozabura OHTA, Dr. Eng.*, Shigemichi TERADA*
Yasuhira EGUCHI†, Seiichi DEGUCHI†

Pulsating tension fatigue test of double-strapped side fillet welded joint on 80 kg/mm² high tensile strength steel was performed. As the result it is found that the fatigue strength, unlike the static strength, is stabilized the more over a wide range of the number of cycles to failure, the longer the fillet weld, i.e., the closer the throat area to the cross section of plate——this is favourable for designing. On the contrary, in the case of the fillet weld being extremely short, i.e., the throat area being very small as compared with the cross section of plate, the base metal in extremely low stress comes to a failure. Thus, even though it may look like a waste from a standpoint of strength, it is desirable to make the throat area commensurate with the cross section of plate, otherwise no guarantee for strength can be given even if the nominal stress is low.

1. Introduction

JNR specifications permit use of mild steel and high tensile strength steels of up to 55 kg/mm² class, except in special cases, as structural steels (rolled steels) for railway bridges.

In designing a long-span railway bridge like a channel-crossing one, the bridge structure necessarily dictates a reduction of its own weight (dead load). In addition to this, an increase in train load or in train speed must be considered and accordingly adoption of the conventional grades of steel alone is likely to result in an uneconomical design of the bridge.

Thus use of high tensile strength steels of higher classes comes up as a solution to the difficulty and thereby the most controversial from a standpoint of structural strength is the fatigue strength of welded joint in the bridge structure, because the fatigue strength of stress concentration or welded joint does not increase at the same rate as the tensile strength or yield strength; in the high cycle range it occasionally remains at the same level as the fatigue strength of a mild steel welded joint. Therefore, in designing a welded structure of high tensile strength steel, full research and investigation must come before determining the allowable stresses for different constructional details.

Concerning a domestic 80 kg/mm² class high tensile strength steel which is expected to constitute a structural part of a channel-crossing bridge, a fatigue strength test of the side fillet welded joint, whose fatigue strength in large-size specimens is practically unknown, has been performed and some basic data useful for reasonable design of welded joint have been collected. Side fillet welded joint is applied, for instance, for attaching an angle to the gusset plate in the construction of a railway bridge (see Fig. 1).

The static strength of a side fillet welded joint is affected by the cross-section of plate (A_p), the throat area of fillet weld (A_w), the strength of plate (σ_p), and the shear strength of fillet weld (τ_w). Depending on the magnitudes of the load carrying capacity on the plate ($A_p\sigma_p$) and the load carrying capacity on the side fillet weld ($A_w\tau_w$), a failure of fillet weld ($A_p\sigma_p > A_w\tau_w$) or one of plate ($A_p\sigma_p < A_w\tau_w$) occurs (under static load the influence of stress concentration is small). Thus, under $A_w = \sum a \cdot l$ (a = throat depth, l = weld length) at $A_p\sigma_p = A_w\tau_w$, the failure occurs at the plate if the weld length is larger than l; and at the fillet weld, if the weld length is smaller than l. Under fatigue load, however, the fatigue strength is remarkably influenced by stress concentration and it is probable that the behavior of failure becomes considerably different from that under static load.

In the present test the pulsating tension fatigue strengths were measured of various specimens with the weld length varied in four values, but the cross section of main plate set nearly equal to those of strapped plates (sum for two strapped plates) and the leg length of fillet weld ($h \fallingdotseq 1.4\,a$) kept constant; and thereby the effect of weld length on the fatigue strength of a side fillet welded joint was examined.

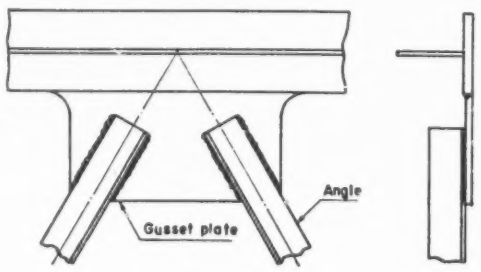

Fig. 1 Fillet weld of angle to gusset plate

* Welding Laboratory, † Physical Testing Laboratory

2. Test Procedure

Test material was a 32 mm thick plate of 80 kg/mm² class high tensile strength steel, the electrode employed being ASTM E 11016 (low hydrogen type), 4 mm ϕ.

Chemical compositions and mechanical properties of test steel and deposited metal are listed in Table 1. Fatigue test specimens of base metal and side fillet welded joint are illustrated in Fig. 2. Welding conditions: welding current 170 A, voltage 24 V; welding speed 15 cm/min, preheat temperature 100°C; single layer bead, leg length 7 mm. Corresponding to l = 80, 60, 40 and 20 mm, the symbols for side fillet welded joint specimens are taken as L 8, L 6, L 4 and L 2.

Using a Losenhausen type fatigue testing machine of 100 t maximum dynamic load, a pulsating tension test with the lower limit load 0.8—3.3 t (plate stress less than 2 kg/mm², weld throat stress about 2.0 kg/mm²) was performed at a rate of 400 cycles per minute.

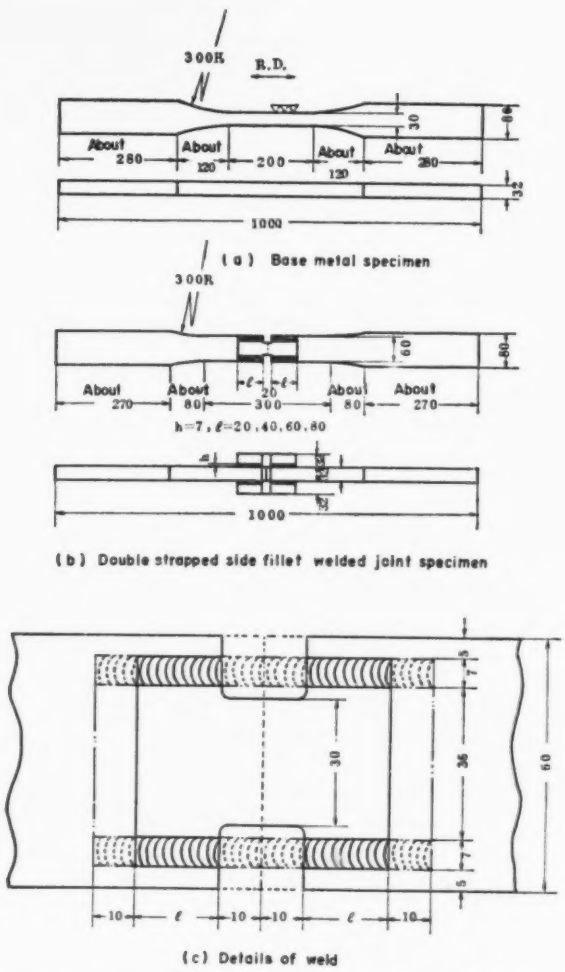

Fig. 2 Fatigue test specimens of base metal and double strapped side fillet welded joint

3. Test Results

In the range of the present test (l = 80 − 20 mm, l/a = 16 − 4), two failure modes of side fillet welded joint were distinguishable: fillet weld failure and plate failure.

In the former, the throat stress was high and the number of cycles to failure was relatively small, whereas in the latter the plate stress was low and the number of cycles to failure was large. When both are plotted together on the same S—N diagram (Fig. 3), it is seen that a sudden change happens in transition from side fillet failure to plate failure; the transition is the more abrupt, the smaller the value of l or the smaller the throat area as compared with the plate cross section, the transition being the least sudden for L 8.

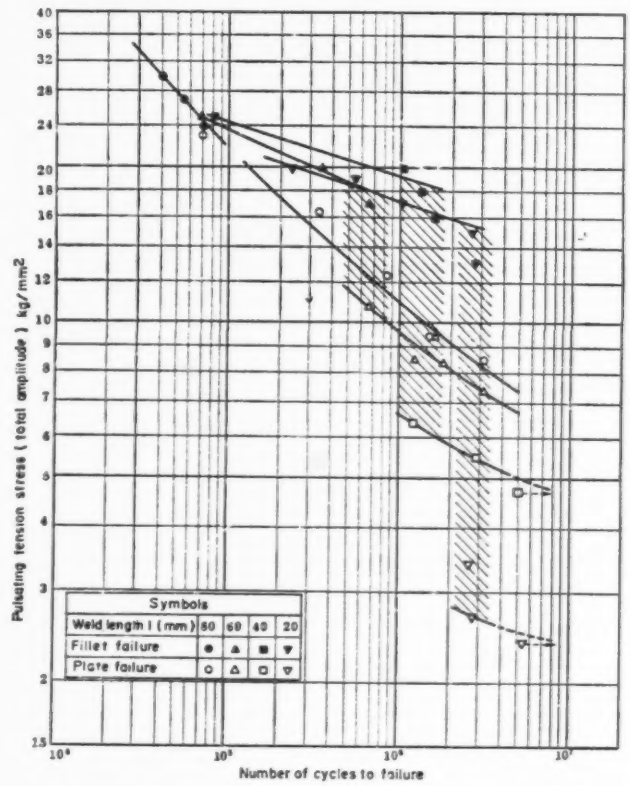
Pulsating tension stress (total amplitude) kg/mm²
Number of cycles to failure
Symbols
Weld length l (mm) 80 60 40 20
Fillet failure
Plate failure

Fig. 3 S—N diagram for double strapped side fillat welded joint

Table 1 Chemical compositions and mechanical properties of test steel and deposited metal

Materials	Chemical compositions (%)										Mechanical properties *			
	C	Si	Mn	P	S	Cu	Ni	Mo	Nb	B	Yield point (kg/mm²)	Tensile strength (kg/mm₂)	Elongation (%)	Charpy impact value (2 mm V-notch) kg-m
Test steel	0.13	0.33	1.40	0.016	0.002	0.09		0.56	0.044	0.002	82.4(L)	85.0(L)	40(L)	21.5(L), 13.8(C), (15°C)
Deposited metal	0.06	0.50	1.50				1.74	0.53			72	83	24	13 (0°C)

* L: rolled direction C: normal to rolled direction Tensile test specimen conforms to JIS No. 5

The critical throat stress and the critical plate stress tend to be lower with a decreasing value of l, while the critical number of cycles to failure tends to be larger with a decreasing value of l.

It has been confirmed that fatigue cracks are initiated by shearing at the root of side fillet weld end. Thus four broad modes of failure have been distinguised.

4. Conclusions

The fatigue strength of side fillet welded joint shows a transition at the critical number of cycles to failure, N_c, which increases with a decrease in the weld length l: below N_c, high stress causes a fillet weld failure, and over N_c, low stress causes a plate failure. In all cases, the initial crack is represented by a shear crack at the root of side fillet weld end. The rate of decrease in fatigue strength at N_c is the more conspicuous, the smaller the value of l, or the smaller the throat area as compared with the plate cross-section.

It can be concluded that the fatigue strength of side fillet welded joint makes a different behavior from the static strength of it. Thus, the fatigue strength of it is stable over a wider range of N for an increasingly larger l than 80 mm ($l/a = 16$, $A_w/A_p = 0.83$), or in other words as the throat area is closer to the plate cross-section; and this would be favourable for designing.

By contrast, in the case of fillet weld being very short, that is, the throat area being extremely smaller than the plate cross-section, the fatigue strength is very low and precaution must be taken against a possible failure of base metal. To put it otherwise, it would be desirable, though it may at first sight look wasteful from standpoint of strength, that the throat area is commensurate with the plate cross-section; if not, no safety can be guaranteed even though the nominal stress may be low.

It should be noted that the fatigue behavior of side fillet welded joint exhibits a considerable variation depending on the specimen dimensions, that is, the combination of plate thickness and fillet weld leg length; meanwhile, a welded joint of mild steel is not expected to show so remarkable a phenomenon of transition as in the present experiment.

(Report No. 697, 1969)

625.2.012.3 : 625.2—597.2 : 678.6/8

On the Thermal Effect of Tread Braking upon Car Wheels

Toshio HIROOKA *, Hideo TERAMURA *, Takayoshi SAITO *
Takehiko KIKAWA *, Kentaro ISHII †

Some effects of tread braking with composite brake shoe upon solid wheels were studied by a full-size brake testing machine. The temperature rise, the temperature distribution in the wheel, and the friction coefficient of brake shoe were measured during drag or stop brakes. The residual stresses set up in wheels after the brake applications in different conditions were also studied, and some clear differences were observed between the states of residual stress in the wheel drag braked and the one repeatedly stop braked.

1. General

Owing to the speed up of the rolling stocks and to the introduction of the composite brake shoes with poor heat conductivity, the thermal load to a car wheel tends to increase recently. As a result, small thermal cracks and extended cracks which presumably advanced from the former, can be observed in some wheels suffering brakes with composite shoe. In this situation, it seems necessary to find out the limit of thermal input permissible for the present wheels, and to extend the limit by improving the shape or the material of them.

We studied experimentally by a full size brake testing machine, the temperature distribution and the state of internal stress in wheels, during or after the brake application in several conditions-stop and drag brakes, with the solid wheels and the composite brake shoes currently used in JNR.

2. The Procedures and the Results of Experiment

(1) The temperature rise at several points of a wheel (points A—E in Fig. 1), was measured during the period of drag brakes with different brake powers.

The results are shown in Fig. 1, where two

* Steels and Alloys Laboratory
† Vice-director of Suita Works

groups of curves show respectively the temperature rise at 10 and 20 minutes after the beginning of a drag brake. In this experiment, the cooling effect due to running and the conduction heat loss from wheel to rail are lacking, so the results in the figure would somewhat overestimate the temperature rise of a wheel in service condition.

When a car with load of 6 tons per each wheel, descends a slope, with 33‰ gradient and extending 10 km, in a equilibrated speed of 60 km/h without any other brake devices, the necessary tread brake power is about 33 kW per each wheel. Then from the figure, the temperature rise at points A and C in the wheel, can be estimated as about 300°C and 150°C respectively at the highest.

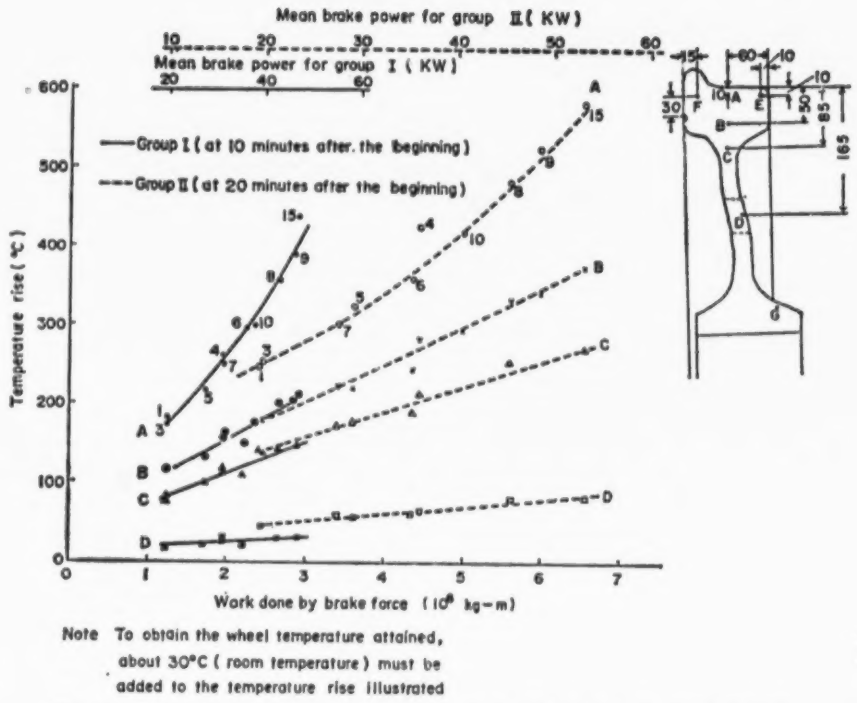
Mean brake power for group II (KW)
Mean brake power for group I (KW)
Group I (at 10 minutes after the beginning)
Group II (at 20 minutes after the beginning)
Temperature rise (°C)
Work done by brake force (10⁵ kg-m)
A
B
C
D
Note To obtain the wheel temperature attained, about 30°C (room temperature) must be added to the temperature rise illustrated

Fig. 1 The temperature rise of a wheel drag braked with different brake powers

Figure 2 shows some examples of the temperature distribution along radial direction of a wheel at 10 and 20 minutes after the beginning of drag brakes. Naturally, the greater is the brake power, the steeper is the temperature gradient. The mean temperature gradient in the wheel rim is more than twice as steep as that in the wheel plate, even after 20 minutes from the beginning. As to the temperature distribution in the axial direction at the layer 10 mm under the tread, the temperature at the center portion of tread (point A Fig. 1) is the highest, and that at the flange side (point F Fig. 1) is about 80—200°C lower than the former.

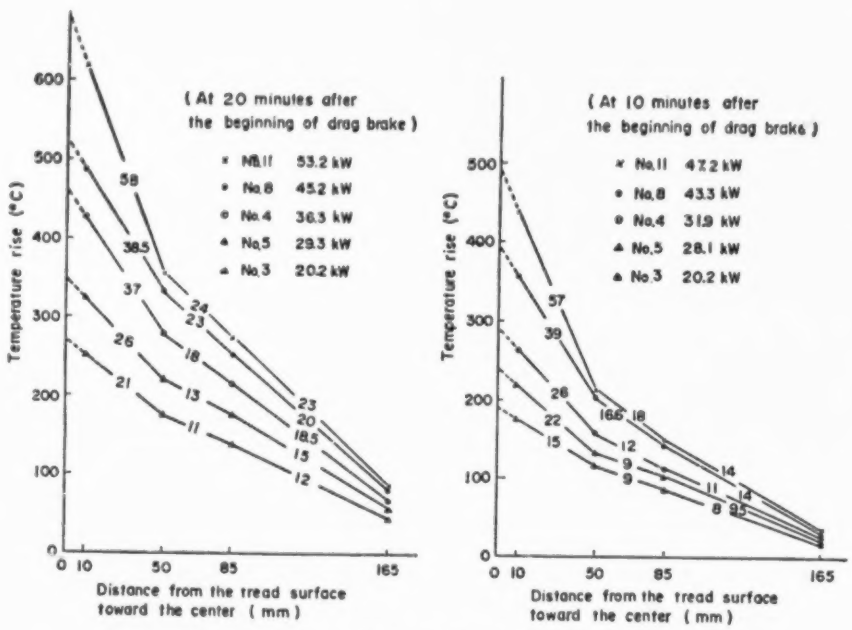
(At 20 minutes after the beginning of drag brake)
No.11 53.2 kW
No.8 45.2 kW
No.4 36.5 kW
No.5 29.3 kW
No.3 20.2 kW
(At 10 minutes after the beginning of drag brake)
No.11 47.2 kW
No.8 43.3 kW
No.4 31.9 kW
No.5 28.1 kW
No.3 20.2 kW
Temperature rise (°C)
Distance from the tread surface toward the center (mm)
Note The figures in the curves indicate the mean gradient of temperature in(°C/cm)

Fig. 2 The temperature distributions along the radial direction of a wheel during a drag brake

(2) During every stop brake, prominently higher temperature band or bands were observed on the tread with a radiation thermometer. The maximum temperature rise in every stop brake from the initial rim velocity of 120 km/h, was measured at a point 5 mm under the surface of the tread. It scattered within the range between 90°C and 350°C, and this also indicated that the location of the prominently higher temperature band varied from a brake to a brake.

(3) After repeating over ten times the drag brake which prolonged for twenty minutes (the maximum temperature at point A was 630°C), the residual stress in the wheel was studied by the layer by layer boring method. Throughout almost entire section of the rim, the tangential residual stress was tensile. Its value was about 50 kg/mm² at the tread surface, and could be assumed to decrease as the distance from the tread surface increased.

At the plate part of the wheel, radial residual stresses at the inner (flange side) and the outer faces were of opposite sign with each other, —the former was tensile and the latter compressive. That is, the plate part suffers bending effect along its periphery from the rim.

(4) A wheel which was subjected to severe stop brakes repeatedly, was examined for its internal stresses. At the tread surface, intense tensile stress as high as about 60 kg/mm² in tangential direction

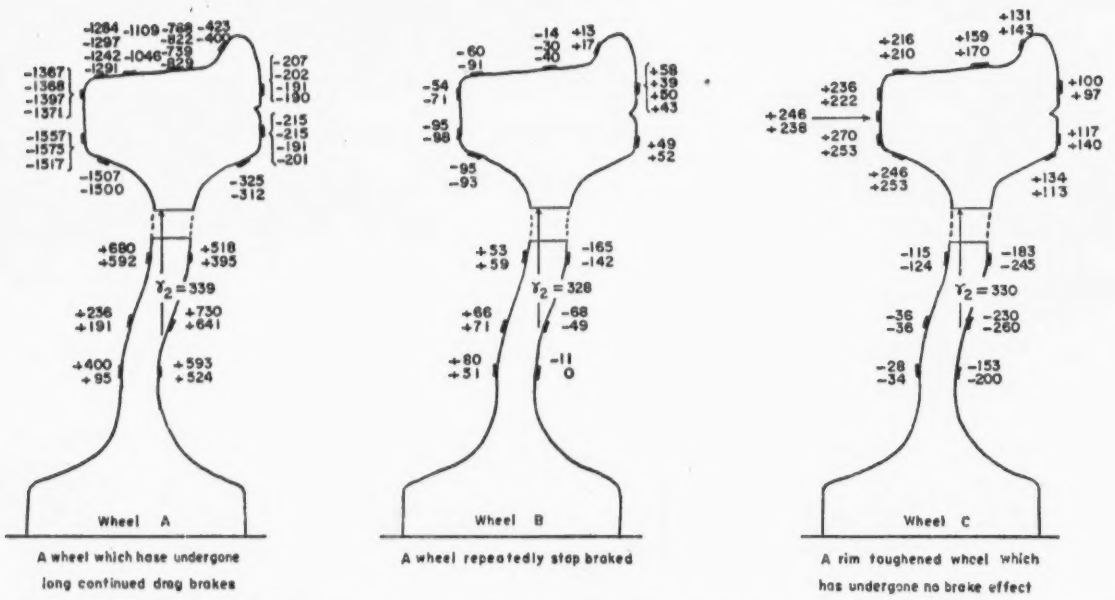
Wheel A
A wheel which hase undergone long continued drag brakes
Wheel B
A wheel repeatedly stop braked
Wheel C
A rim toughened whcel which has undergone no brake effect

Fig. 3 Tangential strains measured when the wheel rim is detached from the center portion as a ring (unit, 10^{-6})

was revealed. Its existence, however, could be assumed to be restricted only within the outer layer not so distant from the tread surface, and at the inner portion of the rim, the tangential residual stress was compressive.

The residual stress along the axial direction was fairly tensile at the center portion of the tread surface, and the fact could not be observed by the wheel which had undergone only drag brakes.

By the way, as to a new wheel which was rim quenched and tempered, the tangential residual stress was compressive about the entire surface of the rim.

(5) Some examples of strains at several portions of a wheel observed when the wheel rim was detached as a ring, from the center portion of a wheel, are shown in Fig. 3. As to wheel A which suffered the drag brakes and consequently heated up for long time, the rim portion contracted considerably by the detachment. The rim contraction was only slight as to wheel B, which suffered repeatedly stop brakes, and as to wheel C, a new wheel which recieved no any effect of brake, showed a slight expansion.

The tangential strains of the wheel rim thus revealed would be considered as a characteristic value resembled to the integral of tangential residual stress throughout the section of the wheel rim.

It may be appreciated as a measure of the over heating which the wheel rim has ever undergone, and by the measure, the abnormally heated wheels may be clearly distinguished from the normal ones.

(6) A wheel which was excluded from service on account of excessive thermal crack damage, was fitted to the test machine and drag braked for half an hour. The rim temperature got to about 430°C, and after natural cooling, considerable advance of the initial crack through the wheel rim into the wheel plate was found.

(7) A rim-toughened new wheel was subjected to severe stop brake tests repeatedly (initial rim velocity 120 km/h, brake pressure upon each shoe 2.5 ton, clasp).

In this experiment, the brake shoes were fitted to the machine consciously so as to hang over the corner edge of the wheel rim. At the corner edge of the wheel rim opposite to the flange, numerous fine thermal cracks, 1.3—1.5 mm long, were observed, but they seemed difficult to grow up larger within our limitted number of brake tests (about 500 times). However, if there were some defects like a drill or punch hole at the wheel corner, cracks initiated from these defects and grew up somewhat easily to larger ones.

(8) The friction coefficient of the composite brake shoe against a wheel was measured during the prolonged drag brake tests. Generally speaking, the coefficient attained a maximum value when the wheel temperature at point A (Fig. 1) was elevated as high as 60—100°C, and fell to a considerably lower level at higher temperature over 300°C. At these higher wheel temperatures, the friction was somewhat unstable, and in some cases it suddenly rised up to a rather abnormally high value. The phenomenon perhaps concerns to the softening of the wheel and the shoe surfaces, or to the material transfer between shoe and wheel faces.

(9) The hardness of the wheel tread which was heat-treated to a level as hard as Hs 42—45, softened about 6—8 degrees in shore hardness after repeated stop or drag brakes without rolling contact of wheel to rail.

After stop brakes, a white, hard and extremely thin phase, which showed no distinct microscopic structure even after etching, was observed on the tread surface. (Pre. Report No. 222, 1969)

678.61.8 : 620.178.30

A New Method of Measuring Fatigue and Fatigue Behaviors of Plastics

Fujio OHISHI*

In this paper, a new method of measuring fatigue behavior continuously for plastics is proposed. By this method the fatigue behaviors of the ten kinds of plastics were experimented and classified into several types, besides tried to relate to fatigue process.

The fatigue testing machine is based on ASTM D 671-63 T-B, and was equipped with differential transformer to catch dynamic deflection (d_0) of a specimen end and with thermocouple to catch temperature rise ($t°$) of specimen surface. The relation between d_0 and absolute dynamic modulus ($|E^*|$) was derived.

1. Introduction

Recently, plastics are increasingly used as structural materials. In our railways, various plastics are used for track and rolling stock. Therefore dynamic durability of plastics has become important. Here, dynamic durability indicates resistance of materials against repeated stress or deformation under various service conditions; temperature, humidity, ultraviolet rays, oxygen, reagents. As plastics is a new material and experience for dynamic usage is less than in rubbers, informations on research and techniques for dynamic durability are wanted in the world.

Therefore, a new method is developed for measuring fatigue, by introducing differential transformer (DTF). Dynamic deflection (amplitude of deflection at the free end of specimen) can be measured continuously during fatigue test with some modification of ASTM D—671—63 T—B, and apparent value of absolute Young's modulus from dynamic deflection can be obtained. Temperature rises of specimen are measured with thermocouple.

From the experimental results of ten kinds of plastics, dynamic deflection change and temperature rise of specimen were characteristics of the material and fatigue condition, so these show fatigue behaviors. These behaviors, therefore, are classified into several types and related with types of fatigue process.

2. Conversion of Dynamic Deflection to Modulus of Specimen

As plastic are rheological materials, absolute dynamic modulus $|E^*|$, under sinusoidal vibration of stress, is expressed as the ratio of amplitude of stress σ_0 to amplitude of strain ε_0.

In this case of cantilever bending by constant amplitude of load, σ_0 is convertible to amplitude of load P_0 and ε_0 is to dynamic deflection d_0 as follows,

$$|E^*| = \sigma_0/\varepsilon_0 = K P_0/d_0 \qquad \cdots\cdots(1)$$

here, K is specimen size constant.

In the case of rectangular specimen,

$$K = 4L^3/b\,h^3 \qquad \cdots\cdots\cdots(2)$$

and triangular specimen, used here,

$$K \fallingdotseq 3L^2/\tan\theta \cdot h^3 \qquad (3)$$

where L, b, h, υ is distance between grips, width of rectangular specimen, thickness of both specimens, inclination angle of triangular specimen, respectively. The change of $|E^*|$ can be traced continuously during fatigue test from these relations. Further, tangent δ may be obtained by measuring phase difference between dynamic load and deflection, and dynamic modulus E' and loss modulus E'' from $|E^*|$ and δ.

3. Experimental Method

(1) Fatigue testing machine

Fatigue machine used here is based on ASTM D 671-63 T-B, constant load type cantilever bending.

Table 1 shows its specifications. General view including measuring apparatus is shown in Fig. 1.

Table 1 Specification of the fatigue testing machine

Type of vibration	Rotating unbalance mass
Alternating load	Maximum 25 kg
Test speed	1,500 rpm
Limit of deflection	10 mm (displacement meter: 5 mm)

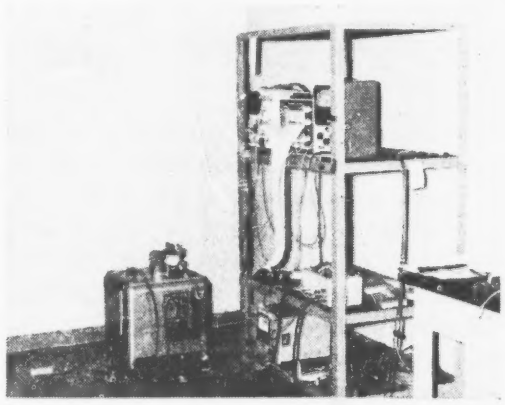

Fig. 1 General view of the apparatus

* Chemistry Laboratory

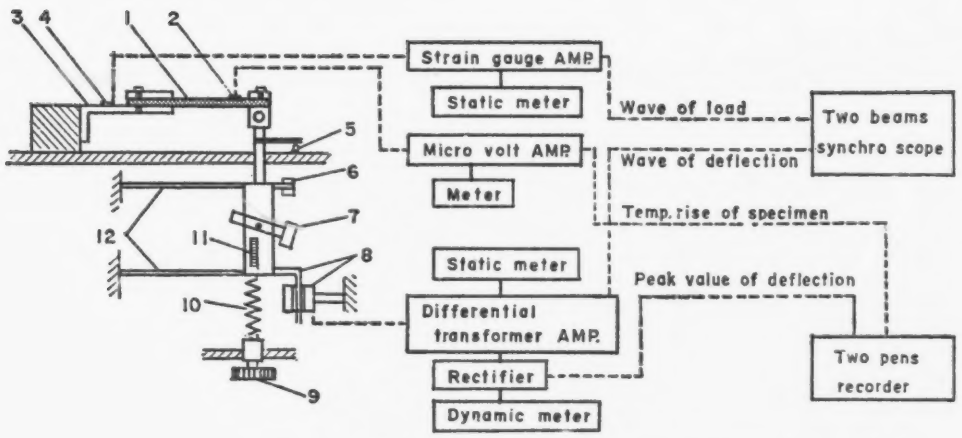

1 Specimen
2 Thermocouple
3 Moment bar
4 Strain gauge
5 Auto stopper
6 Control weight
7 Rotating eccentric mass
8 Differential transformer
9 Preload handle
10 Compensator spring
11 Vibratory force scale
12 Transverse fixing springs

Fig. 2 The schematic view of measuring method

Table 2 Materials of fatigue specimen

Symbol	Materials	Class*	Molding method
PS	High impact polystyrene	TP	Extrusion
ACC	Acetal copolymer	TP	Injection
MMA	Poly methyl methacrylate	TP	Casting
4FE	Polytetrafluoroethylene	TP	Compression and baking
ES	Unsaturated polyester	TS	Casting
EP	Epoxide resin	TS	Compression
PH	Phenol resin	TS	Compression
	Materials below are sample of the previous paper.		
PC	Polycarbonate	TP	Extrusion and press
PVC	Polyvinyl chloride	TP	Calendering and press
PAm	Polyamide (Nylon 6)	TP	Injection

* TP: Thermo-plastics TS: Thermo-setting plastics

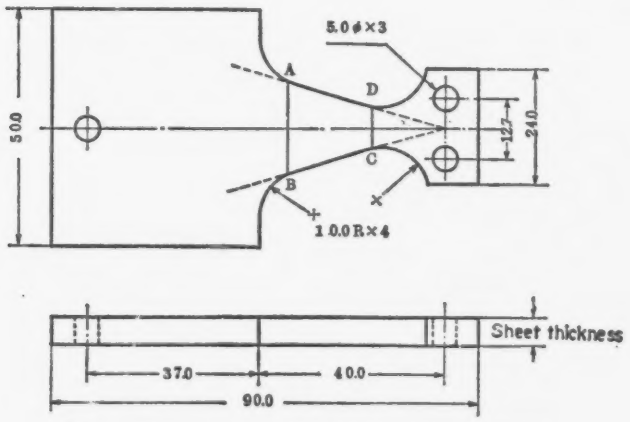

Fig. 3 Test specimen (ASTM modified type)

(2) Measuring method of fatigue behavior

Dynamic deflection can be measured by rectifying the vibrating displacement measured with a differential transformer (DTF) at the free end of specimen. On the other hand, temperature rise of specimen during fatigue test can be followed with thermocouple attached on the specimen surface by adhesives. Fatigue behaviors are determined by following the change of dynamic deflection and temperature rise of specimen.

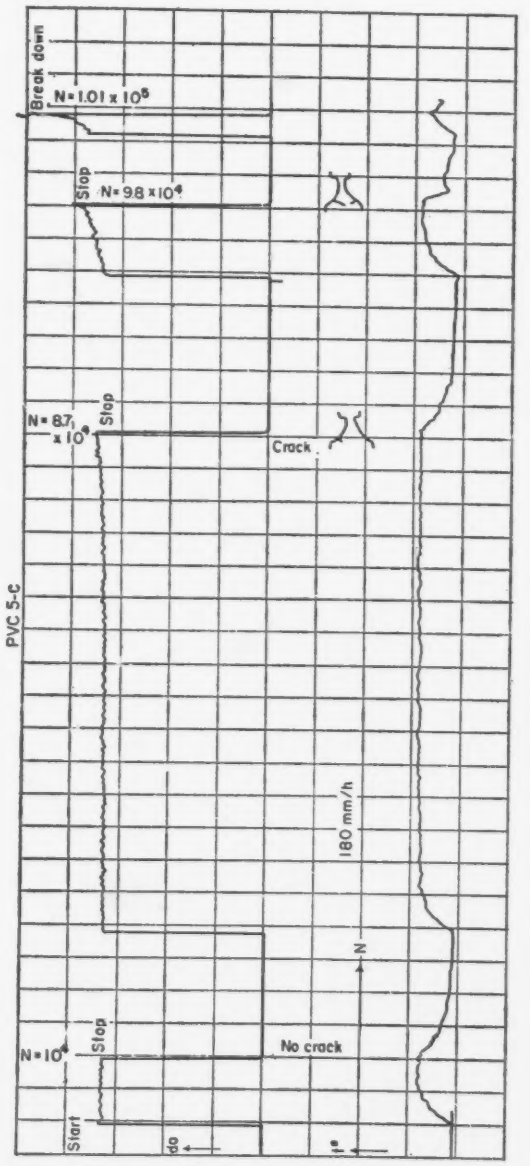

Fig. 4 Typical data on analysis of dynamic deflection change — Polyvinyl chloride ±5kg — (d_0: dynamic deflection, t°: temperature rise, N: number of cycle)

(3) Specimen size and sample materials

Specimens used here are the modified type of ASTM, as shown in Fig. 3, with the area ABCD of specimen, bending stress being uniform. Sample

materials are listed up in Table 2. Specimens used here are provided by machining commercial sheets.

4. Changes of Dynamic Deflection and Temperature Rise During Fatigue Test

Typical example is shown in Fig. 4. From these data, it is clear that the change of dynamics deflection and temperature rise were characteristics of sample material and stress condition, so these show fatigue behavior for plastics.

Conversion of dynamic deflection to absolute modulus was not significant in the case of crack development and softening by temperature rise.

S—N curves for polyvinyl chloride and poiycarbonate are shown in Fig. 5.

5. Fatigue Behaviors of Various Plastics

By the results of the ten kinds of plastics, fatigue behaviors were tried to classify into several types.

Further, fatigue behavior was tried to correlate with fatigue process by the help of the experiments for analizing the cause of deflection change.

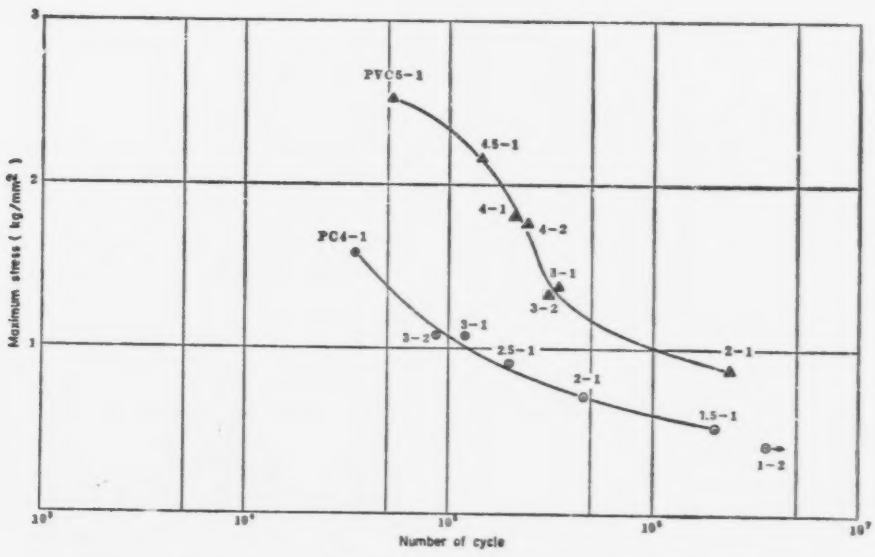

Fig. 5 S—N curves for polyvinyl chloride and polycarbnnate

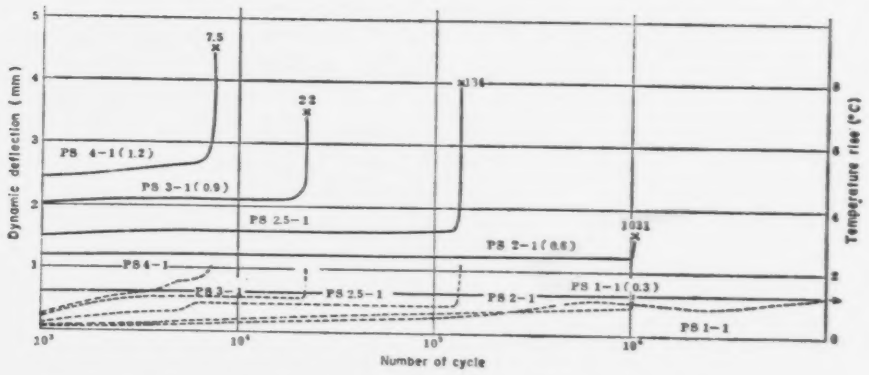

Fig. 6 Typical data on fatigue behavior — High impact polystyrene — (full line: dynamic deflection, broken line: temperature rise.) Symbol PS 4-1 (1·2) indicates that alternating load is ± 4 kg (bending stress is 1.2 kg/mm²)

Figure 6 shows one of the fatigue behaviors, in the case of high impact polystyrene.

Analysis of dynamic deflection change

The causes of deflection change during fatigue test are considered as follows; softening by heat evolution, crack development, and material change. To separate the cause, the following complemental experiments were conducted.

(1) The change of dynamic deflection in the case of cool or warm wind by hand drier is watched during fatigue test. From this result, the effect of temperature on dynamic deflection can be known.

(2) Crack initiation and development is watched, when the fatigue machine is stopped on the way of test. When the machine is driven again, deflection before stopping and after driving again is compared. Then the cause for this change of deflection can be known. Though these data are not shown here, some examples are as follows:

In the case of MMA ± 6.5 kg, dynamic deflection increased according to temperature rise during fatigue test, and when cool wind blew the specimen, deflection decreased according to temperature fall, to the starting value. When warm wind blew the specimen, deflection increased according to remarkable temperature rise.

Therefore, in the case of this, the cause of deflection change is considered to be thermal softening.

In the case of PC ± 3 kg, temperature rise was negligible and deflection increase by hot blowing was less than in MMA. While deflection was constant, no crack was found. But when deflection increased gradually, several small cracks were found by watching during the test, refered to Fig. 4. Therefore, in this case, the cause of deflection change is considered to be crack development.

From the results of these experiment, the following characters were found: for EP, PS, ES, temperature rise was not remarkable and quality change of material happened, and for PAm, 4 FE, MMA, temperature rise was remarkable, then thermal softening happened, for PC, PVC, crack developped slowly, deflection change was caused by local change of specimen thickness.

Consideration on heat evolution

Inner heat evolution of specimen under sinusoidal deformation

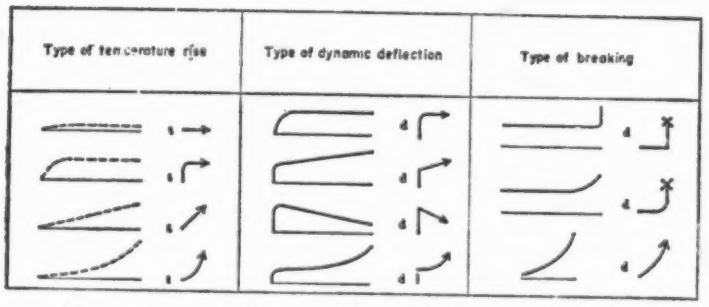

Fig. 7 Classification of fatigue behaviors of plastics

for rheological materials is expressed as follows,

$$H = \pi \varepsilon_0^2 G'' = \pi \varepsilon_0^2 G' \tan \delta \qquad \cdots\cdots(4)$$

here H: heat evolution of specimen per 1 cycle of deformation, ε_0: amplitude of strain, G'': loss modulus, G': dynamic modulus, δ: phase difference between stress and strain.

In this case of fatigue, stress distribution is uniform on the plane of specimen, so ε_0 is uniform and then distribution of heat evolution must be uniform on the plane.

Translating ε_0 by d_0 (dynamic deflection), H is expressed as follows.

$$H = \pi h^2 d_0^2 G''/L^4 \qquad \cdots\cdots(5)$$

Therefore, increase of d_0 according to softening caused by heat evolution causes heat evolution again cyclically.

Though relation between H and surface temperature is not simple, surface temperature can be a measure for H in the case of the same specimen size and heat conductivity.

6. Conclusions

(1) By introducing a differential transformer, dynamic deflection change during fatigue test was measured continuously. Moreover material change caused by fatigue was tried to catch, using the deflection-modulus equation derived here, but this trial was disturbed by thermal softening and gradual crack development. It was found that change of dynamic deflection and temperature rise of specimen are characteristics of material and stress condition, so these can be a usufull measure to show fatigue behavior.

(2) By using differential transformer and wire strain gauge, phase difference between load and deflection was tried to catch. As the difference was very small, it can not be measured quantitatively, but the vibrating condition of fatigue test can be known by watching the waves of vibration.

(3) From the results of ten kinds of plastics, the types of temperature rise, change of dynamic deflection, and fatigue rupture of plastics can be classified into several patterns as shown in Fig. 7.

(4) Fatigue process of plastics are considered to be the following three types on the point of dynamic deflection change; thermal softening by heat evolution, local thickness decrease by crack development, and quality change of specimen material.

With the aid of analytical experiments for deflection change, Table 3 shows the connection of the types of fatigue behavior to fatigue process with examples and typical data of them are shown in Fig. 8.

(5) Applications of this method are an accelerated fatigue test by alternating load for plastics and a detaching test by alternating deformation for adhesives and coating materials.

(Report No. 698, 1969)

Table 3 Relation of the type of fatigue behaviors to fatigue process

Type of fatigue behaviors	Fatigue Process	Examples
(d, t)	N	PC2-1 PC1-2 PVC1-1 PH1-1
(d, t)	Q	EP3-1
	S	ES4-2 PVC5-1
	T	4 FE1.5-1
(d, t)	Q	PS3-1
	S	PVC3-1
(d, t)	Q	EP5-1
(d, t)	Q	EP4-1 EP3.5-1 PC4-2
(d, t)	T	MMA7-1 ACC7-1
(d, t)	Special	PAm2-1

N: No apparent change
Q: Quality change of material
S: Shape change by crack
T: Softening with temp. rise

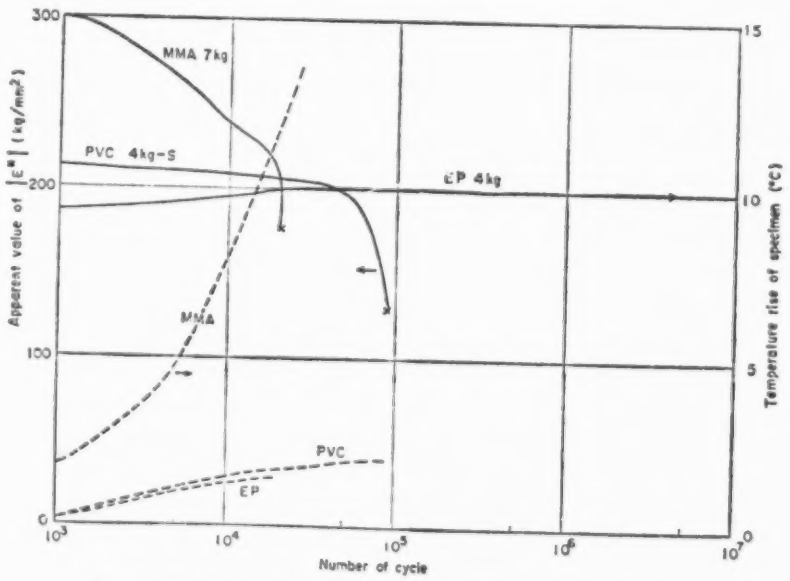

Fig. 8 Typical example of fatigue behavior for plastics
MMA: softening, PVC: cracking, EP: quality change

621.791.019 : 625.151.811 : 15'74

Some Data on Damage to Manganese Steel Crossing in Service

Ichiro OOI, Dr. Eng. *, Noboru KIMATA *

Occurrence of withdrawal of manganese steel crossings out of the track on account of damage is not fully eliminated, though it has become less frequent through various improvements tried lately. Besides, a problem of extending their service life through repair welding still remains unsolved. Further, occasional cracks, though slow in propagation, of welded metal are observed in the butt-welded portion of the movable rail in manganese steel crossings of SHIN KANSEN track. Some investigations have been carried out to collect accurate data on this situation.

Up to the end of March 1968, 366 new sets of manganese steel crossings had been laid in the track within the territory of Nagoya Operating Division and 43 sets of them have been withdrawn out of the track. Among the factors mentioned as the reasons for withdrawl in Table 1, transverse crack at head and tail ends, particularly at tail end, is predominant; it almost invariably occurs in the portion 450–675 mm from the end face and it is said that the crack is more liable to be initiated in the end facing against the train running direction. Substantial increase in the service life of manganese steel crossings will be possible, if this type of cracking can be successfully stopped by specifying a higher design strength of their head and tail ends or by revising the present casting procedure.

Table 1 Reasons for with ldrawa of 50 N manganese steel crossings

Types of defect	Head end	Wing rail	Nose	Tail end	Others	Total
Transverse crack	4	1	0	23	0	28
Horizontal crack	2	2	5	1	0	10
Crush, Chip, Wear	0	1	2	1	1	5
Total	6	4	7	25	1	43

Table 2 Toonnage carried vs. withdrawal rate

Cumulative tonnage carried from laving to withdrawal (million tons)	With-drawal unmber	Number of sets laid	With-drawal rate
Less than 50	4	147	2.7
0 ~ 100	4	106	3.7
0 ~ 150	11	70	15.7
0 ~ 200	7	21	33.3

Table 2 lists the withdrawal rates per class of cumulative tonnage carried of 187 new sest of these crossings laid in tracks carrying over 40 million tons per year (within Nagoya Operating Division). From this Table it is seen how sharp is the increase in the withdrawal rate, beginning from 100 million cumulative tons carried.

Out of the 43 sets withdrawn, 19 were put to use again after repair welded and of these 19, 10 sets were again withdrawn after an average of 7.3 months of re-service. It is especially notable that in 6 out of the rejected 10 sets the repaired part again developed a defect, which was again a transverse crack.

On the other hand, the cracked state in 7 repair-welded spots on three 50 PS crossings was investigated. These crossings were originally mamufactured in the period 1952—1958 and after the first 2—6 years of service they were repair-welded two or three times; two of them served again for about 2 years and 4 months after every repair welding and the purpose of repair was practically satisfied. Thereby the defect necessitating their withdrawal turned out almost invariably a transverse crack at similar position to the one which developed before the last repair. This defect is traced to some design problems or to insufficient removal of shrinkage cavities in the last repair and it is nothing related to welding. Conceivable countermeasures for such defect are practice of nondestructive inspection on the cracked portion and perfect removal of casting flaws as well as strengthening of end portion; adoption of these measures will be able to realize a considerable extension of service life for repair-welded parts.

Three movable rails (containing one welded joint) were checked for cracks in butt-welded joint; all of them had been withdrawn for reasons other than a failure of welded part after 3—4 years of service. Scrutiny, however, revealed presence of a fine crack in the welded metal. In most cases, the crack originated at the bevel root of rail top and bottom or side of bevel part. All cracks are intercrystalline ones and unlike in the case of repair-welded part, they do not propagate to the base metal. The Si and P contents in the welded metal are rather high, being respectively 1.05 and 0.030 % in one case.

Countermeasures for it would be stricter control of chemical composition in base metal and electrode, improvement of welding procedure, and post treatments such as low temperature stress removal of weld (400°C, 2 hours), shot peening of the whole surface.

The conclusions are as follows:

(1) 50 N crossings before repair: After 100 million cumulative tons carried, their withdrawal

* Welding Laboratory

rate makes a considerably steep rise. Defects are predominantly transverse cracks at the end. Improvement of design strength is desirable.

Results of repair welding are not satisfactory.

(2) Repair welds on 50 PS crossings: Cracks are traced to insuffcient design strength and or incomplete removal of shrinkage cavities in repair welds. Welding effect is secondary.

(3) Butt-welds: Crack development is limited to welded metal. Thereby the problem lies in the chemical composition of electrode and welding procedure.

(Pre. Report No. 11, 1970)

624.131.211.001.5

Rock Breaking with High Speed Water Jet Stream

Toyohiro KINOSHITA *
Kenzo HOSHINO, Dr. Eng. *

For developing the tunneling machine using the high speed water jet stream, we have to proceed the basic experiments with regard to that.

So we have manufactured the second stage testing plant for breaking the hard rock with high speed water jet stream under pressure up to 5,000 kg/cm².

As shown in the Fig. 1, this testing plant is made up of oil power unit, hydraulic power unit, accumulator and pressure amplifier etc.

The pressurized oil up to 250 kg/cm² (maximum) by the oil power unit is accumulated in the accumulater, and it flows instantaneously to the pressure amplifier by opening the stop valve.

The cylinder portion in this pressure amplifier consists of two chamber A and B, whose area ratio is about 20 : 1.

So pressurized oil which indicates 250 kg/cm² in the chamber A can augment the weter pressure up to 5,000 kg/cm² in the camber B, and water jet can flow with the velocity of 1,000 m/sec through the nozzle.

The chracteristic properties of this testing plant are as follows.

(1) As for the sealing of high pressure water, which is the most difficult in the problem of this category, we have successfully developed the original technique which makes use of the mechanism of pressurizing the outer surface of the packing in proportion to the pressure within the cylinder (namely chamber B) by means of guiding the pressurized water to it.

(2) As the result of adopting the cone-type nozzle which has the cylindrical portion in the tip of it, the flow rate coefficient of nozzle indicated the value of 0.94 ~ 0.95 in the case of 0.25 mmϕ nozzle and 0.90 ~ 0.91 in the case of 0.15 mmϕ nozzle.

We have put the test piece of sandstone, dicerite, granite, basalt, andesite, gabbro etc. to the "traversing digging test" using the above testing plant, and got the following result. (see. Fig. 2)

(3) Referring to the dimensional analysis, if we put

ρ_1 : density of water
σ : surface tension of water (in the air)
μ_1 : dynamic viscosity of water
ρ_2 : density of rock
μ_2 : dynamic viscosity of rock

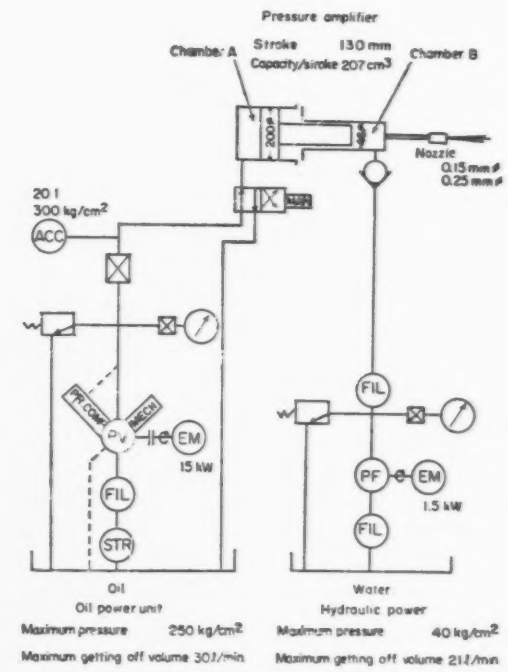

Fig. 1 2 nd-stage testing plant for breaking the hard rock with high speed water jet stream ; oil, hydraulic power system block diagram

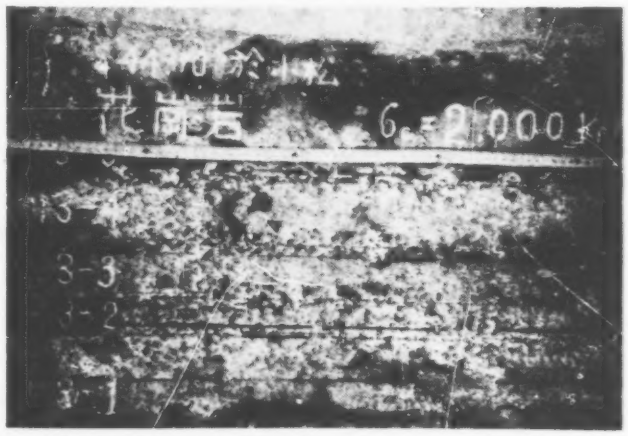

Fig. 2 Traversing ditches digged on the surface of granite (σ_c = 2,000 kg/cm², c_j = 5,100 m/sec) using 0.15 mmϕ nozzle

* Maintenance & Construction Machinery Laboratory

V_W : water jet speed at the nozzle outlet
l : distance between the nozzle outlet and the surface of rock
V_t : relative traversing velosity between the nozzle and the surface of rock
f : plotdzakonoph coefficient
d : outlet diameter of nozzle

We can put the depth of traversing ditches digged on the surface of the rock in the following way.

$$\frac{h}{d} = C_1 \times \frac{W_W{}^{\alpha}}{W_t{}^{\beta} \times (l/d)^{\gamma} \times \phi^{\delta}}$$

where

$W_W = V_W{}^2 \frac{\rho_1 d}{\sigma}$: weber unmber of the water jet

$W_t = V_t{}^2 \frac{\rho_1 d}{\sigma}$: "weber unmber of traversing nozzle"

$\phi = f \frac{d}{\sigma}$: coefficient of strength

α, β, γ, δ : constant

As the result of experiments, we find that $\alpha > 0$, $\beta > 0$, $\gamma > 0$, $\delta > 0$, $C_1 > 0$.

So we can conclude that the depth of traversing digged ditches h/d increases as the distance between the nozzle outlet and the surface of rock l, the traversing nozzle speed V_t $(= \sqrt{W_t \times \sigma/\rho_1 d})$ and the strength of rock f $[= \phi\,(\sigma/d)]$ decrease, and the velocity of water jet V_W $(= \sqrt{W_W \times \sigma/\rho_1 d})$ increases.

(Pre. Report No. 18, 1970)

624.27.072.2.014.2 : 625.143.59

Measurement of Stress of Railway Bridge Stringers to which the Rail is Fastened without Sleeper

Fumihito ITOH *
Toshio OKUDA *

In order to decrease the maintenance of railway track, new types of stringer for steel bridge to which the rails are fastened without sleeper have been designed. The upper flange of the stringers are directly connected to rail fastenings with bolts.

As the result of previous test on similar steel girders, it was found that large distortion occured at the upper flange and the upper part of web plate. Since upper flanges on both side of the girder are deformed independently under lateral load acting on a rail, large local stresses appeared at the distorted portions mentioned above.

For the purpose of decreasing these local stresses, four types of reinforced structures were designed for Daiichi-Hirakawa Bridge in Oou main line. On two types of these structures, the stresses under statical test car loading and dynamical steam locomotive (type D 51) passage were measured. The test car could apply required lateral and vertical load. The purpose of our measurement was to investigate the problems on strength of such structures and to get some useful data for coming design.

Figure 1 shows outline of such stringers; the SA type has box shape reinforcement at upper of stringer, and the type SC has large T shape reinforcement welded between web plate and upper flange.

Table 1 shows statical stresses per ton of test car loading. Table 2 shows impact stresses under steam locomotive passages. From these field tests, we can get the following results.

(1) No serious problems on strength of these stringers can be expected unless stress far larger than considered in design acts, since measured stresses under full loading were smaller than half of allowable stress.

(2) The impact stresses increase linearly with velocity of passage, but no problem on strength of these stringer was found. However, it remains unknown what will happen under higher velocity than 80 km/h, since no measurements under such high velocity were carried out.

(3) The results of these measurements could not give us any knowledge on fatigue strength. But the fact that stress at upper part of web plate, which shows larger stress value and experiences layer number of stress cycles than other parts of the stringer, of AS type was about twice of the one of SC type may be worth noting.

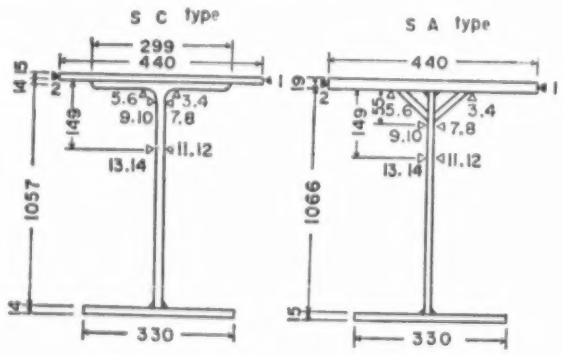

▲ One direction gage
△ Two direction gage

No.	Direction
1	P
2	P
3	P
4	P
5	O
6	P
7	O
8	P
9	O
10	P
11	O
12	P
13	O
14	P

P : Parallel to axis of bridge
O : Orthogonal to axis of dridge

Fig. 1 Outline of Daiichi Hirakawa Bridge

* Structure Laboratory

Table 1 Stress per ton (kg/cm²/t)

No.		1	2	3	4	5	6	7	8	9	10	11	12	13	14
Vertical load	S C	−2.0	−15.8	−22.8	−49.8	−20.0	−47.0	−7.8	−11.0	−10.5	−20.0	−5.0	−8.8	−6.8	−9.8
	S A	−4.4	−7.4	−9.4	−10.8	−9.7	−12.8	−4.0	−11.8	−5.4	−18.1	−3.4	−11.7	−2.2	−10.6
Lateral load	S C	36.0	−34.5	2.0	−30.3	−9.8	−16.3	−8.3	−33.5	14.3	37.8	−7.8	−23.8	14.5	22.3
	S A	46.5	−42.3	−3.5	−60.0	−17.3	−0.8	−8.8	−35.0	11.8	24.3	−5.0	−19.3	12.0	20.3

Table 2 Impact rate per velocity

No.		1	2	4	6	8	10
Stress value at 0 velocity kg/cm²	S C	−85	−72	−349	−431	−69	−182
	S A	85	74	−60	−55	−222	−151
Impact rate/velocity $\times 10^{-3}$	S A	5.53	2.08	0.97	2.51	11.11	6.54
	S C	3.88	2 03	3.50	8.55	5.86	3.58

(4) Since the measured results could not give us any definite informations in choosing between the two types of stringer, facility for erection and manageability in maintenance will make a discrimination between them.

(Pre. Report No. 24, 1970)

621.316.57.015.3 : 656.2.022.81

Surge Test on Test Car in SHIN KANSEN

Kohichi ARAI*, Kimiharu WATAHIKI*
Torajiro FURUHATA*, Tatsuo TAJIMA*

The test car in Shin Kansen, whose form was changed for the first time since Shin Kansen was operated on business, was manufactured for trial with the view of business running at the maximum speed of 250 km/h and was equipped with various kinds of new technics. Main differences between the test car and the present car are 4 divided thyristor control, the vacuum circuit breaker (for short, VCB) with long life, and the resonance shunt type filters accompanied with thyristor control. This report deals with the results of the surge characteristics test which was carried out stationarily in Hamamatsu Factory prior to the running test.

The surge transfer test and the switching surge test were carried out. In the former test, the impulse or the sine wave of 50 Hz ~ 200 kHz was impressed on the pantograph and the transfer voltages were measured at the secondary of the main transformer, each part of the thyristors, and the ternary. In the latter test, about 30 kV with commercial frequency was impressed, VCB was switched on and off, and the abnormal voltage at each part was measred. In each case, the surge absorption effect of the filter and the maximum value of the abnormal voltage were measured under the conditions that at the secondary of the main transformer the load was cut off at LB of DC side, and at the ternary the air-conditioner and the air-compressor were switched off and the other machines were switched on, and the conditions of the filter at the secondary were changed variously.

Surge transfer

Concerning the impulse, the transfer ratio was measured with about 2 kinds of wave-forms, namely $1 \times 40\ \mu s$ and $1 \times 200\ \mu s$, and the ratio under the latter wave-form was larger, but there was little difference in the transfer wave-forms. The following examinations are for the case of the impulse $1 \times 200\ \mu s$.

(1) The transfer ratio between the secondary with CR filter ($5\,\Omega + 80\ \mu F$, or $5\,\Omega + 40\ \mu F$) is about 1.6 %, while the ratio with CR filter ($20\,\Omega + 20\ \mu F$) or without CR filter is 2.1 ~ 2.3 %. These results make the absorption effect of CR filter clear.

(2) The transfer ratio into the secondary with CR filter ($5\,\Omega + 80\ \mu F$) and the 5th harmonic shunt filter is 1.5 ~ 1.6 % and is less than the turn ratio 1.86 %.

(3) The maximum transfer ratio from the secondary to the earth when the thyristor is not ignited is as much as that between the secondary. The transfer ratio by the diode, on the simulation of the ignition of thyristor, is 2.7 % at maximum.

(4) The transfer ratio between anode and cathode, when the thyristor is not ignited, equals to that between the secondary. The ratio between the lines of DC side, when the thyristor is ignited, is 4.3 %.

(5) The transfer into the ternary is not effected by the condition of the 2nd circuit, and the ratio between the lines is 1.8 %, and the voltage between the ternary and the earth is divided equally.

(6) The transfer ratio of the sine wave is as follows.

(a) Owing to the effect of the 5th CR filter at the secondary, the resonance point occurs near 250 Hz, but that near 7 kHz is removed.

(b) The transfer ratio of sine wave at each

* Electric Power Laboratory

part has the resonance points at 250 Hz, 7 kHz, and 180 kHz, but it is generally flat and it is especially good when CR filter, is inserted.

Switching surge

The switching surge test was carried out at three conditions (i.e. closing—5 cycles—breaking, breaking of the exciting current, and reclosing). The abnormal voltage at breaking is smaller than that at closing, and it scarcely occurs when there is no reignition.

The maximum abnormal voltage through the test at the primary of the main transformer is 2.1 times as much as the normal voltage, and it is rather small when there are the 5th and the 7th shunt filter. The abnormal voltage at closing presents high frequency vibration and has no relation with the condition of the circuit of the closing. This is the phenomenon characteristic of VCB and the predischarge between the poles of VCB seems to repeat the extinction and the ignition owing to the strong extinctive action of VCB.

The transfer ratios into the secondary and the ternary circuit are not constant and scatter at random, but the maximum ratio is 2.4 times as much as the normal voltage at the secondary circuit and 2.6 times at the ternary circuit.

According to the above results, both the switching surge and the surge transfer at this test were better than that at the surge test on the operating car in Shin Kansen and the effective data on the design of the car in Shin Kansen hereafter were obtained.

(Pre. Report No. 226, 1969)

621.355.8

Discharge Characterististics of Nickel-Cadmium Cells Charged at Constant Voltage

Shiro OKUMA*, Kuranobu SUGITA, Dr. Eng.*

Alkaline storage batteries are often used at the constant voltage charging system. In this case, capacity of car starting and lighting batteries which are frequently charged with a certain amount of load, apart from the batteries for emergency use in which appreciable load is not required in normal state, tends to be decreased as compared with the capacity that can be delivered after constant current charging. Alkaline storage batteries including pocket type and sintered plate batteries have generally such a property, but it seems not to be well known. So, the discharge characteristics of Nickel-Kadmium cells charged at various conditions of constant voltage charging methods are compared with discharge characteristics after constant current charging.

Test cells are mainly pocket type cells having about 20 Ah capacity, which are prepared by a representative manufacturer in Japan. In an experiment, sintered plate cells having the same capacity are also tested. The experiments are all carried out in a water bath at 30° ± 1°C. The results are as follows:

(1) Change of capacity with repeated cycles of constant voltage charging and successive deep discharging

Seven cycles of charge and discharge is repeated. The current of discharge is 10 A and the final voltage of discharge is 1.0 V. The charging is carried out for 45 h at a constant voltage of 1.500 V ± 5 mV. Although the capacity of the pocket type cells is decreased rapidly with repeated cycles of such a charge and discharge, it becomes to be stabilized after 5 cycles. The stabilized capacity is 74 % to the capacity after initial constant curront charging. Single electrode potential of the cells is measured by a Keithley-electrometer (Rin ≒ 10^{14}) using a Cd° standard electrode and it is found that the decrease of capacity is due to incomplete charge of the positive plate.

(2) Charge of capacity with repeated cycles varying the depth of discharge

A stabilized capacity was obtained after 5 cycles in previous experiment and the total quantity of discharge amounts to 100 Ah. Then, this experiment is carried out so that the total quantity of discharge may be 100 Ah. Voltage of charge is 1.5 V/cell and charging hours 10 h. The results are shown in Table 1. Table 1 shows that the degree of capacity decrease in shallow discharging cycles is not so large as in deep discharging cycles.

(3) Relation between charging voltage and capacity or final charging current

At first, a stabilized capacity and a final charging current are measured at charging voltage of 1.40 V according to the method as described in (1), then the same measurement is carried out in turn changing the charging voltage from 1.45 V to 1.60 V. The results are shown in Fig. 1. The broken line in Fig. 1, means a charging current that is required for a charged lead-acid storage cell having 20 Ah capacity

Table 1 Effect of the depth of discharge to variation of capacity after constant voltage charging and successive discharging cycles

Condition of discharge	To 1.0 V 5 cycles	5 A, 2 h *10 cycles	2.5 A, 2 h *20 cycles	1 A, 2 h *50 cycles
Proportion of the capacities to a capacity after constant current charging (%)	74	77	85	92

* The repetition of cycle is carried out by an automatic apparatus.

* Electrical Testing Laboratory

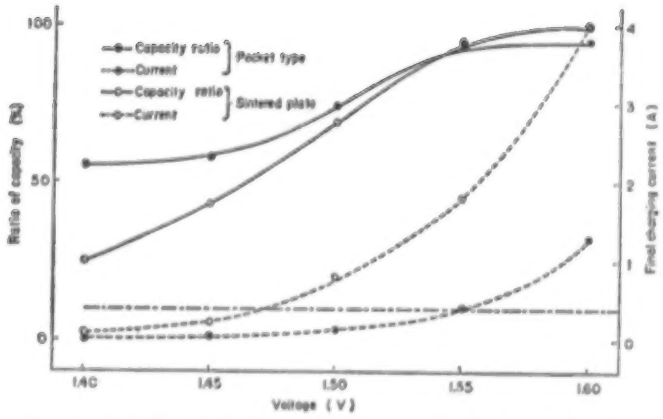

Fig. 1 Relation between charging voltage and the ratio of capacity or final charging current

$$\text{Ratio of capacity} = \frac{\text{capacity after constant voltage cycle}}{\text{capacity after constant current charging}} \times 100)$$

in order to maintain the cell in a range from 2.4 V to 2.5 V. The value agrees nearly with "50 percents of the finishing rate" by G. W. Vinal. As a field condition corresponding with it has been established in a charging system of diesel-car starting lead acid storage batteries, the final charging current shown in broken line, Fig. 1, might be considered as the allowable upper limit taking account of the trouble of adding water to the electrolytes. Thus, the upper limit of chrging voltage is 1.55 V on a pocket type cell and is 1.46 V on a sintered plate cell. In these charging voltages, the ratio of capacity after cycles of constant voltage charging and deep discharge to initial capacity is 93 % on pocket type cell, while it is not more than 50 % on sintered plate cell. It should be noted in this experiment that some of LiOH had been added to the electrolyte of the former but the electrolyte of the latter contains no LiOH.

(Pre. Report No. 70, 1970)

621.431.72.05 : 662.614

Analysis of Combustion Process of DML 61 Series Diesel Engine

Toyoharu UCHIBORI *, Eiichi KAWASHIMA *
Takehira ARAI *

General performance of the DML 61 series diesel engine for locomotive has been investigated repeatedly, but work done process of the engine has never been analysed yet. One of the reasons is considered to be that a sufficiently accurate cylinder pressure diagram could not be obtained under the condition of high engine speed and high temperature. A piezo-electro indicator of the best accuracy and good thermal stability has been developed recently. From the cylinder pressure diagram measured by applying this new type indicator to DML 61 series precombustion chamber type diesel engine, the factors, related to combustion, such as rate of heat release, ignition delay and rate of pressure rise, were obtained, and their influence on various engine operations was analysed.

This indicator consists of a piezo-electro pressure transducer and an amplifier for exclusive use. Results of test showed its linear sensitivity within the range of 0 to 130 kg/cm², good stability at high temperature, and reliability during long period of measurement.

In calculating the heat generated by combustion at some crank angle, the heat loss into cylinder wall and the gas leakage from combustion chamber must be taken into consideration. Rate of heat release was therefore calculated from the value of cylinder pressure and volume at each step of crank angle, by a stepwise procedure, based on the first law of thermodynamics, together with the perfect gas equation.

The followings are some of the results.

(1) Compression pressure under the motoring condition showed its peak value at only a few degrees before TDC, and would increas by about 4.6 kg/cm² with the increase of the intake pressure of 0.1 kg/cm². This relationship at 1,000 rpm was nearly equal to that at 1,500 rpm, however the absolute value was rather large at higher engine speed. Friction loss was nearly constant even if the intake pressure had changed.

(2) Rate of trapped air mass (calculated) to charge air mass (measured) was about 55 % at 1,000 rpm and 68 % at 1,500 rpm, showing that air mass per engine cycle blown through cylinder at the state of valve overlap was less at higher engine speed.

(3) Figure 1 shows a typical example of the obtained indicator diagrams, in which CA stands

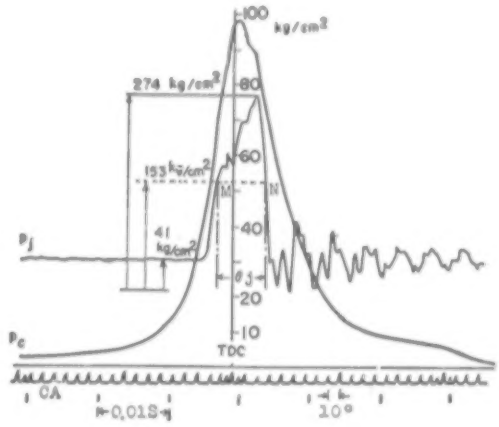

Fig. 1 Example of indicator diagram (1,000 rpm)

* Car Equipment Laboratory

for crank angle, p_e for cylinder pressure, p_j for supply pressure in fuel pipe before fuel injection valve, and M for beginning of injection, respectively.

Injection beginning pressure in fuel pipe (pipe length 2 m, static valve opening pressure 130 kg/cm²) was about 160 kg/cm² at 1,000 rpm and about 190 kg/cm² at 1,500 rpm. Maximum pressure in fuel pipe and period for injection duration would increase with the increase of fuel supply rate. After one injection closed, pressure vibration occurred in fuel pipe, but it damped by the time of the next injection beginning. The propegating speed calculated from this phenomenon was about 940 m/s.

(4) The injection delay, that is the period between static and actual injection beginning, was 3 ms at 1,500 rpm, 3.3 ms at 1,000 rpm, and it was rather small at higher engine speed. The ignition delay, that is the period between actual injection beginning and combustion beginning, tended to increase with the increase of injection advance.

(5) The peak cylinder pressure was nearly constant for the change of fuel supply rate and engine speed, however, it was affected largely depending on ignition advance, and it increased by 7 to 8 kg/cm² with the increase of injection advance of 10 degrees. Maximum value of peak cylinder pressure showed 108 kg/cm² when the engine generated maximum power at the intake pressure of 1.3 kg/cm². Maximum rate of pressure rise were hardly affected by the change of fuel supply rate and engine speed, except it increased with the increase of injection advance. However, these values were comparatively small (max. 4.3 kg/cm² per unit crank angle), and this fact means lower engine noise.

(6) As shown in Fig. 2, pattern of the rate of heat release is closely similar to isosceles triangle, and specific fuel consumption has a tendency to decrease with the increase of ratio of height to base on this triangle, therefore this ratio on the heat release pattern can be taken as a criterion of thermal efficiency of a precombustion chamber diesel engine.

(Pre. Report No. 13, 1970)

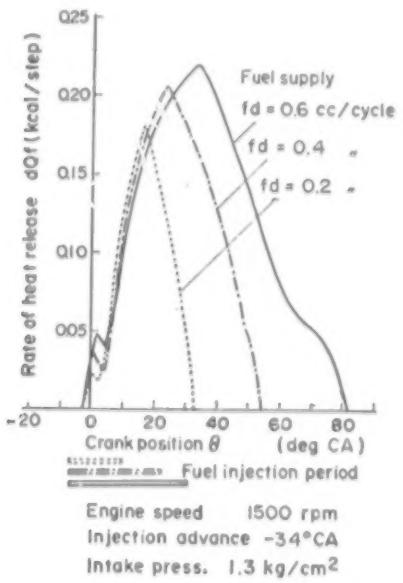

Fig. 2 Comparison of heat release rate for each fuel supply rate (1,500 rpm)

621.436 : 621.646.2—52

Experiment of the Automatic Valve Clearance Adjusting Device of the Diesel Engine for Rail Car

Toyoharu UCHIBORI*, Takehira ARAI*

An experiment was conducted to get the operating characteristics of the valve mechanism equipped with the automatic valve clearance adjusting device, and also to find out the cause of the cam surface trouble when equipped with the device. Easier maintenance would be expected about the new series diesel engine with the device for rail car.

As shown in Fig. 1, the pressure oil is fed through the oil passage of the rocker arm shaft and the holder to the oil inlet hole at the bottom of the oil cylinder. Then it enters to the oil cylinder though the non-return valve, so the arm of the eccentric ring is pushed upward and the ring is rotated.

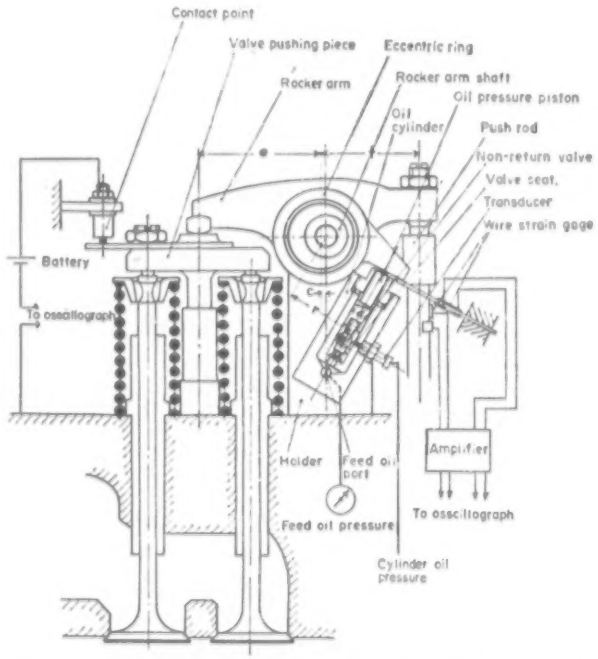

Fig. 1 Test device and apparatus for measurement (type A)

* Car Equipment Laboratory

Table 1 Dimension of test devices

Type		A	B
Eccentricity of eccentric ring	e (mm)	3	5
Arm length of eccentric ring	r (mm)	40	22
Diameter of oil pressure piston	d (mm)	11	8
Area of oil pressure piston	a (cm²)	0.95	0.50
Oil capacity of oil cylinder	v (cc)	0.85	0.45
Non-return valve spring		yes	no

By the mechanism of eccentricity, the rotation center of the rocker arm is pushed downward, so that the valve clearance is diminished automatically and the oil pressure in the cylinder sustains the reaction force on the piston during valve opening.

Two kinds of devices, i. e. type A and type B as shown in table 1, were examined.

(1) On type A device, the piston displacement was small, so the automatic adjusting effect was good at the range over 1,000 rpm of engine speed. But the valve push-up (the phenomena, the valve is kept open) was observed at the lower feed oil pressure. Especially, when the valve pushing piece contacts only to the one side of valve during valve is closed, the oil pressure, at which the valve push-up will occur, would tend to lower than in the normal contact condition, and would be about 4 kg/cm² throughout the engine operating speed.

This valve push-up oil pressure would be reduced at the lower oil temperature, and if the non-return valve spring is removed or the piston clearance is increased, the valve push-up would not occur even at oil pressure 8 kg/cm².

(2) The valve push-up oil pressure in type A was 7 kg/cm² in the static condition, but during operation it was reduced according to the engine speed. It will be influenced by the relative effects between the frictional force at the eccentric ring caused by the dynamic forces of the valve mechanism and the oil leakage caused by the piston clearance and the non-return valve jump.

(3) On type B device, the piston displacement was larger than type A, and the effect of the valve clearance adjusting was not sufficient, as the period of the valve timing was reduced. It seems that they come from larger eccentric valve, smaller eccentric ring arm length, smaller diameter of oil cylinder and larger oil leakage due to the lack of non-return valve.

(4) When the adjustable clearance S_0 (clearance between the oil cylinder and the arm at no oil pressure) was kept constant, the valve clearance in operation in type B was larger than in type A.

At larger S_0, the period of the valve timing in type B is reduced while that in type A is kept constant. If S_0 becomes too large and the piston arm not follow in operation, then the impact between cam and tappet will occur, and it will lead to the severe wear.

(5) For the design of these devices, it must be noticed to make the valve push-up oil pressure higher than the normally used oil pressure, and to keep the period of the valve timing normal by the quick response of the automatic adjusting mechanism.

(Pre. Report No. 173, 1969)

625.2.073.23 : 620.1.05.001.57 : 625.2.012.3.071.53

Construction of the New Alternating Load Type Adhesion Testing Machine

Hiroshi MARUYAMA *, Tadao OHYAMA *

The friction phenomena under oscillation have been recently interested in various categories of engineerings. In the field of adhasion phenomena of the railway, oscillation takes part in friction in the form of alternating load of the wheel. But the adhesion problems have been hardly investigated from this point particularly by experiments.

We made a new type testing machin by which adhesion force (friction force) under alternating load could be measured. The followings are the construction and the results of preliminary experiments with this machine.

This machine includes two discs corresponding to rail and the real wheel. The former drives the latter with frictional force. The axis with the smaller drived disc is free in principle up and down as well as right and left about the spherical roller bearing set on the remote side of the disc, playing the role of fulcrum. The friction force can be measured from the tangential force which is generated on the disc surface as a result of slip between both discs caused by putting the brake on only the smaller disc. The brake force can be adjusted by the hydraulic pressure of the disc brake attachment. The larger diriving disc is equiped with a flywheel which drives the smaller disc through the power of inertia after the commutator motor has been switched off simultaneously with braking action. The vertical load is imposed on the roller bearing box of the smaller disc, both statically and dynamically through an electro-hydraulic servo valve and a servo amplifier. In addition, a differential gear type slip detector is equiped for the purpose of preventing serious slip damage between both discs. The principal specifications are shown in Table 1 and the general view of this machine in Fig. 1.

* Machinery Eqipment Laboratory

Table 1 Specifications of the machine

Dia. of the drived disc	440 mm
Dia. of the driving disc	660 mm
Contact length	20 mm
Peripheral speed	0 ~ 300 km/h
Revolution of the drived disc	0 ~ 3,620 rpm
Max. braking torque (continuous)	40 kg-m
Vertical load	
Statical load	300 ~ 600 kg
Dynamical load	± 50 ~ ± 300 kg
Frequency of dynamical load	5 ~ 100 Hz

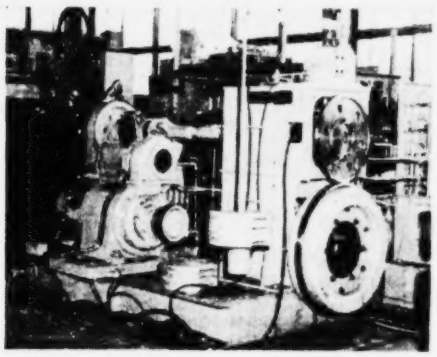

Fig. 1 General view of the machine

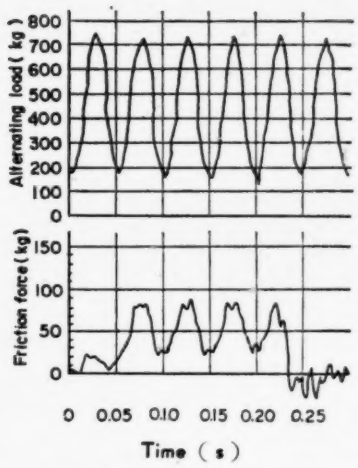

Established Condition

Statical load	400 kg
Dynamical load	± 300 kg
Frequency of dinamical load	20 Hz
Hydraulic pressure of disc brake	30 kg/cm²
Peripheral speed	50 km/h

Fig. 1 Example of measurements of friction under alternating load

The results of preliminary experiments with this machine are as follows. The friction force on the surface of the drived disc was related with the hydraulic pressure of the disc brake almost linearly under the particular pressure but it tended to saturate after that. And also the slip increased with brake pressure. The hydraulic pressure of the brake corresponding to maximum friction force between both discs was recognized to increas according as the peripheral speed of the disc. Coefficient of friction under dry condition after cleaned with chemicals on both surfaces was about 0.10 ~ 0.15, which was fairly lower than the value obtained commonly in such experiments. But this value might correspond to considerably lower slip of both discs which was set up with the slip detector. An example of friction measurements under alternating load is shown in Fig. 2. In case of larger amplitude of alternating load the corresponding friction varies in proportion to imposed load. On the other hand the smaller amplitude hardly influences on friction. In addition to this, it was recognized that this experimental equipment resonated at the frequency of about 60 Hz and so it was necessary to increase the resonance frequency by improvang the rigidity of this machine in order to perform the experiments under alternating load of higher frequency.

At present we made some experiments concerning the relation between slip ratio and coefficient of friction under some kinds of surface condition, i. e. dry and lubricating with oil, by imposing both statical and oscilating load.

(Pre. Report No. 218, 1969)

625.243.015 : 621.54 : 624.04

Effect of Air Bag Type Car Holder on the Side Structure of Freightcar

Masuo IZUMI *

With a view to mechanizing the car lashing aimed at prevention of derailment or overturning due to ship's rolling of railway vahicles carried on board the train ferry, a remote-controlled simultaneous action car-holder utilizing air bags has been developed as a substitute for the conventional turnbuckle type car lashing apparatus.

Not to get in the way of vehicles being loaded or unloaded on the wagon deck, the air bags are deflated flat within a vertical plain ; after the vihicles have been loaded, they are simultaneously inflated by remote-control to extend to full length of car and softly hold the top side of car (about 2.5 m above the rail top) from both sides, thereby preventing the car from overturning, These bags are made of neoprene-coated nylon cloth which can be swiftly inflated or deflated.

Using a cylindrical air-bag and a square cushion type one, the effect of the proposed car-holder using such air bags on the side structure of the JNR typi-

* Ferry-boat Laboratory

cal freight car WAMU 80000 series was investigated with the following results. The cylindrical air bag, when inflated, assumes a cylindrical shape (cylinder 1.4 m long, with 700 mm cross-section) and the square cushion type one, when deflated, becomes flat with dimensions: 1.4 m long × about 1.1 m wide.

(1) In the cylindrical air bag, a maximum stress develops at the guide to the top door rollers for the middle sliding door of car, when the middle part is pushed by the bag.

(2) In the square cushion type air bag, a maximum stress develops at the guide to the top door rollers for the middle sliding door when the part just beneath the door rollers of this door is pushed by the bag.

(3) As between the cylindrical air bag and the square cushion type one, the former exerts less effect on the side structure of car and has a greater bearing ability (Fig. 1 and Fig. 2). Thus, for the car holding purpose, the former is more suitable, because this bag has structurally a greater contact area with the car; particularly its contact length in the longitudinal direction of car (in the sliding direction of doors) can be ample and accordingly its load on the sliding doors can be spread over the two door rollers.

(4) Estimating the stress developed in the guide of door rollers for the freight car WAMU 80000 series in reference to the yield point (23 kg/mm²) of SS 41, i.e., the structural material of this part, the reaction of one air bag is about 1.7 t for the cylindrical type and about 1.3 t for the square cushion type. Considering the estimated reaction of the air bag during a voyage on the Aomori-Hakodate ferry route, 5 air bags on each side of a freight car of WAMU series will suffice with respect to the load bearing ability. Since one air bag is about 1.4 m long, one freight car of WAMU series will be able to have 5 air bags on each side.

(5) When an emergency is supposed when the ship has been damaged and is rolling at ± 15 degrees in the state of tilting to 25 degrees, there is high risk of the car getting derailed even if held by air bags; or there is a likelihood of the guide to door rollers of the sliding doors suffering plastic deformation or coming to a failure.

(6) It is desirable that the air bag to be actually provided on the ferry route have its compression characteristic such that the reaction of 0.8 t per m in the longitudinal direction of freightcar may be secured within 50 mm of its compression.

(Pre. Report No. 199, 1969)

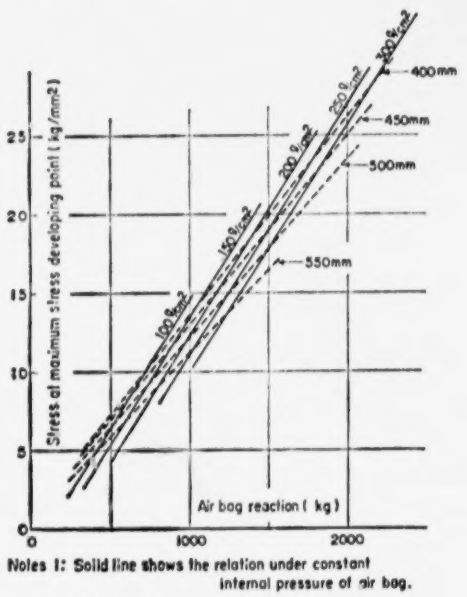

Notes 1: Solid line shows the relation under constant internal pressure of air bag.
2: Broken line shows the relation under constant gap between air bag

Fig. 1 Stress vs. air bag reaction at maximum stress point when cylindrical air bag pushes center of middle door of car

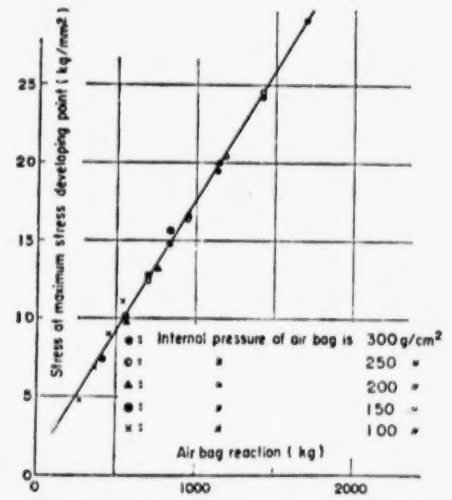

Fig. 2 Stress vs. air bag reaction at maximum stress point when square cushion air bag pushes the part just beneath door rollers of middle door of car

539.37.082.7 : 563.53 : 621.394.6

Noncontact Transmission of Signals Measured on Rotating Objects with Mutual Induction

Hiroshi SUGIYAMA *, Seijiro WADA †

In order to transmit to measuring instruments weak signals measured on rotating objects, the device which transmits 2 channels frequency modulated waves by mutual induction between opposite concentric ring coils is proposed and the inductively coupled circuit is analyzed.

The device is operated with satisfactory stability and S/N characteristics, because the carrier can be modulated at wide ranges of a frequency deviation.

* Physics Laboratory, † Intrumentation Center

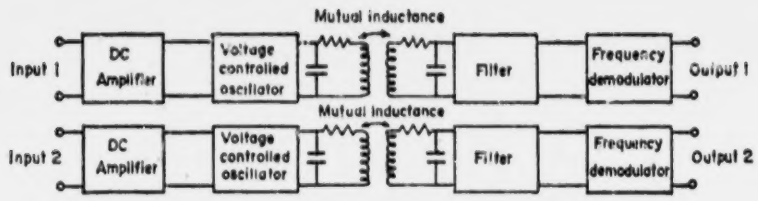

Fig. 1 Block diagram of noncontact transmissive device

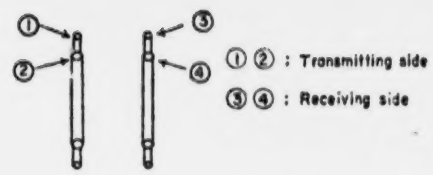

Fig. 2 Ring coils

Furthermore the transmitter is constructed so small, light and robust that it has high resistance to shocks, vibrations, temperatures and aging effects.

The block diagram of this device is shown in Fig. 1. The signals from pick-ups (strain gauges: resistance thermometers) are amplified at about 60 dB gains by a DC amplifier of microstructures. The voltage controlled oscillater is an astable multivibrator of high density assembly and generate frequency modulated waves of ± 40 % frequency deviations. As indicated in Fig. 2, transmitting and receiving coils are concentric ring coils and are arranged opposite to each other. The circuit of pulse counter type is used in this frequency demodulator.

It is desired that the output voltage of the receiving coil is as high as possible within the range that the amplitude variation in the bandwidth as well as the amplitude outside the bandwidth remains small.

The equivalent circuit of inductive coupling between two ring coils can be expressed in the inductively coupled resonance circuit.

In fact the output part of the voltage controlled oscillator forms the imput source of this resonance circuit. The output part of the voltage controlled oscillator can be looked upon either as the constant voltage source or the constant current source. The relation batween the gain and the frequency, in the former case, and the relation between the open transfer impedance and the frequency, in the latter case shows explicitly the amplitude characteristics of the inductively coupled circuit. The relation is easily calculated; it is function of Q-value, coupling coefficient K, selfinductance L and resonant frequency f_0. On the other hand Q, K, L are determined by ring coils dimensions.

Therefore the value of all elements of the inductively coupled circuit can ba determined by mean of graphic syntheses, providid that the amplitude characteristic of the inductively coupled circuit and the values of K, L, and Q are determined by dimensions of ring coils through graphical method.

Table 1 shows an example of the values of elements of the inductively coupled circuit that are determined according to above stated procedure and this trensmitting ring coils are installed on a shaft end. The center frequency is based upon the single-carrier FM record parameter of the magnetic tape record standards for telemetry applications.

From experiments of this device for strain measurement the following results was obtained.

Table 1 Major values of inductively coupled circuits

	First channel	Second channel
Carrier center frequency (kHz)	54	13.5
Maximum frequency deviation (± %)	40	40
Diameter of ring coil (cm)	14.5	10
Distance between ring coil (cm)	8	8
Selfinductance of transmitting side (mH)	15.4	64.4
Selfinductance of receiving side (mH)	0.91	13.5
Coupling coefficient	0.08	0.06
Q-value	8	8

(1) Sensitivity: 250×10^{-6} strain on four arms of a 120 Ω strain gauge with a gauge factor of 2 producing full scale output.

(2) Frequency response: 0~1,000 Hz

(3) Linearity over-all: ± 2 %

(4) Signal to noise ratio: 40 dB

(Pre. Report No. 221, 1969)

656.226.073.58

Package form Survey of JNR Baggage

Ryoichi IMANISHI *, Toshimasa OHNUMA *
Kazuo MAEDA *, Kakuji YAMANAKA *

An actual package form survey of baggages is a necessary condition for the mechanization of baggage handling. The baggage condition changes according to the season and the locality. We carried out a survey at Shiodome and Sumidagawa station, which are principal bases, handling a quarter of all baggages in JNR. We made five surveys last year under the seasonal conditions as shown in Table 1.

The items, which are connected to the mechanization, are size, weight, packing material and the binding material.

Results of the survey are as follows.

* Freight Transportation Laboratory

Table 1

	Main object of the package form survey
From the latter part of March to the beginning part of April	Baggages of employment seekers and new students
From the middle part of May to the middle part of June	Standard baggage
From the beginning part of July to the beginning part of August	Baggage for seasonal gifts
From the middle part of August to the latter part of August	Baggage of home visitors in Bon-season and summer vacationers
December	Baggage for year-end gifts

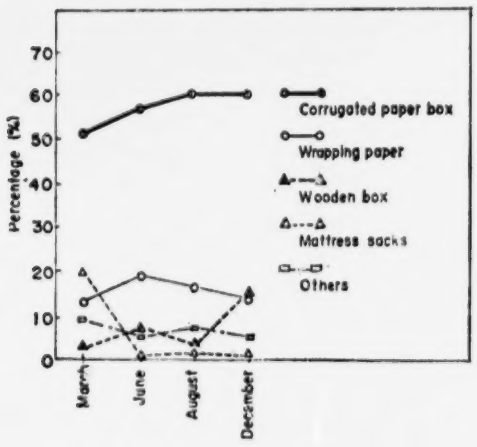

Fig. 1 Packing materials

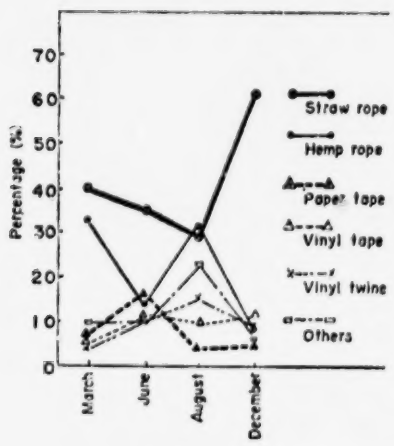

Fig. 2 Binding materials

(1) Packing material

The packing material is classified into corrugated paper boxes, wrapping paper, wooden boxes, straw-mattings, mats, mattress-sacks, wrapping cloth, basket, trunk bags, bamboo-baskets, cans, and barrels. Figure 1 shows percentages of packing materials for baggages at Shiodome which have been carried from Western Japan to Tokyo. The corrugated paper boxes are most popular in all seasons and all places, followed by wrapping paper and wooden boxes. In March, mattress-sacks are used more than in other seasons.

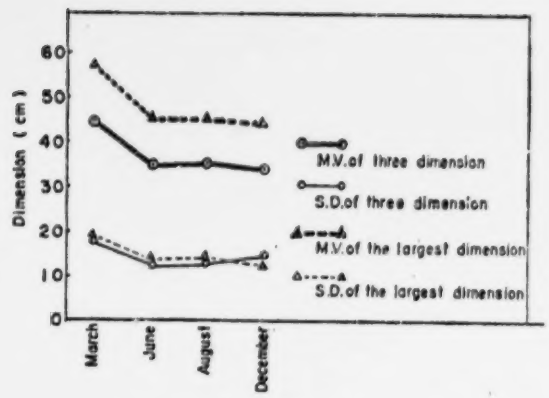

Fig. 3 Dimension of baggage

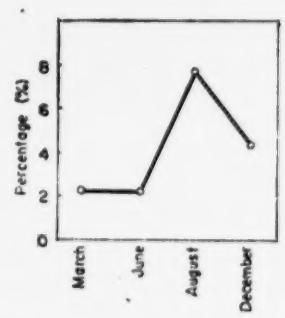

Fig. 4 Baggages to be handled with care

(2) Binding material

Straw rope, hemp rope, hemp yarn, paper tape, paper twine, vinyl tape, and vinyl twine are used for binding purposes. Figure 2 shows the results of the survey.

(3) Size

The three dimension were surveyed.

Mean value of three dimensions and mean value of the largest dimensin are shown in Fig. 3. The volume of a baggage is larger in March than in other seasons.

(4) Baggage which should be handled with care

Baggages to be handled with care such as Fragile baggages and animals, are very difficult to handle by machine. The percentage of these baggages is shown in Fig. 4. According to the above results the conditions for mechanization of the baggage are as follows:

(a) The maximum length of baggage is 120 cm.

(b) The maximum width and height are 70 cm, respectively

(c) The minimum height is 3 cm.

(d) The machine should be able to handle smoothly such baggages, as packed in corrugated paper box, wrapping paper, wooden box and mattress-sack, and bound with various materials.

(Pre. Peport No. 217, 1969)

519.283 : 65.012

Statistical Estimates of Cumulative Failure Rate and Conditional Reliability from Short Term Observations

Shun-ichi ABE*

On observing lifetimes of certain devices (parts or systems) in some fields, we are often met with the situation that each one is subject to withdrawals due to such causes as accidental damage, preventive maintenance and so on. The data used to estimate the probability distribution of wear-out failure, for instance, are necessarily truncated from the right by these withdrawals.

Moreover, if a number of devices of the same kind are being used in the field and if the period or cost of observing their lifetimes is limited, it may be possible and convenient to take, as a sample from the population, n elements whose present ages are $s_1, s_2, \cdots\cdots, s_n \geq 0$ and to observe them during certain periods $l_1 - s_1, l_2 - s_2, \cdots\cdots, l_n - s_n > 0$ respectively, as far as the data are analyzed reasonably.

Our stochastic model of multiple-cause failure is described by C 1° ~ 3° as follows:

C1° Each element of a population is subject to two kinds of failure-causes denoted by 1 and 2. The times, X_1 and X_2, to their respective occurrences are mutually independent random variables with probability laws

$$P(X_i > t) = R_i(t) \quad (i = 1, 2) \qquad \cdots\cdots(1)$$

which are assumed to satisfy $R_i(0) = 1$ $(i = 1, 2)$ and to have no common discontinuity.

C2° The lifetime X_0 of each element is determined by

$$X_0 = \min\{X_1, X_2\} \qquad \cdots\cdots(2)$$

C3° Let the age interval of our interest be $(0, t_0]$ and it is assumed that

$$P(X_0 > t_0) = R_0(t_0) > 0. \qquad \cdots\cdots(3)$$

We assume the data to satisfy the following conditions D1° ~ 3°:

D1° Let the n elements whose ages are $s_1, s_2, \cdots\cdots, s_n$ be given at the starting point of the observation, where $0 \leq s_i < l_0$ for each i.

D2° Let the observation of the i-th element which is started from the age s_i terminate at the age $t_i = \min\{X_{i1}, X_{i2}, l_i\}$, where $l_i\ (> s_i)$, the limit of observation, is a predetermined constant for each i at the beginning of the observation of the n element, and where X_{ij} is the time to the occurrence of the cause j on the i-th element $(i = 1, 2, \cdots\cdots, n;\ j = 1, 2)$. Let the age t_i as well as its causality, i.e., either of

$$\left.\begin{aligned} t_i &= X_{i1}: \text{ failure of cause 1,} \\ t_i &= X_{i2}: \text{ failure of cause 2,} \\ t_i &= l_i \ : \text{ no failure in the period,} \end{aligned}\right\} \qquad \cdots\cdots(4)$$

be observed for each $i(= 1, 2, \cdots\cdots, n)$.

D3° The number of such elements that satisfy $s_i \leq \theta < l_i$ is sufficiently greater than 1 for every $\theta \in (0, t_0]$.

Given the data satisfying the conditions D1° ~ 2°, we define the "number of remainders", $N(\theta)$, as the number of such elements that satisfy $s_i \leq \theta < t_i$ among the n observed, for an arbitrarily given $\theta \in (0, t_0]$. Similarly let $N(\theta-)$ be, except the special case defined by (6), the number of such elements that satisfy

$$s_i < \theta \leq t_i \qquad \cdots\cdots(5)$$

among the n observed. Now pick up all of the cause 1 failure data mentioned in (4) and assume that they are $\theta_1 \leq \theta_2 \leq \cdots\cdots \leq \theta_M$.

If occasionally two or more of them coincide with each other, i.e., if the relation $\theta_{j-1} < \theta_j = \theta_{j+1} = \theta_{j+2} = \cdots\cdots\ (\theta_0 = 0)$ holds for certain positive integer j, then we define exceptionally

$$\begin{aligned} N(\theta_{j+1}-) &= N(\theta_j-) - 1, \\ N(\theta_{j+2}-) &= N(\theta_j-) - 2, \ \cdots \end{aligned} \qquad \cdots\cdots(6)$$

as far as the equality signs hold among θ_{j+k}'s, where $N(\theta_j-)$ is as usual the number of elements satisfying (5), putting $\theta = \theta_j$.

Let us define the "cumulative failure rate" $Q_i(s, t)$ and "conditional reliability" $R_i(s, t)$ by

$$\begin{aligned} R_i(s, t) &= R_i(t)/R_i(s) \\ &= \exp\{-Q_i(s, t)\} \quad (0 \leq s < t). \end{aligned}$$

Now let the nonparametric statistics $Q_1^*(s, t)$ and $R_1^*(s, t)$ be defined by

$$Q_1^*(s, t) = \sum_{s < \theta_i \leq t} N^{-1}(\theta_i-), \qquad \cdots\cdots(7)$$

$$R_1^*(s, t) = \prod_{s < \theta_i \leq t} \{1 - N^{-1}(\theta_i-)\}, \qquad \cdots\cdots(8)$$

where the right hand sides of the above represent, respectively, the summation and product over such subscripts i that satisfy $s < \theta_i \leq t$.

We can prove that the statistics $Q_1^*(s, t)$ and $R_1^*(s, t)$ are almost unbiased for $Q_1(s, t)$ and $R_1(s, t)$, i.e.,

$$\begin{aligned} 0 < Q_1(s, t) - E\{Q_1^*(s, t)\} \\ \leq Q_1(s, t) \exp(-n_{st}), \end{aligned} \qquad \cdots\cdots(9)$$

$$\begin{aligned} 0 < E\{R_1^*(s, t)\} - R_1(s, t) \\ \leq \{1 - R_1(s, t)\} \exp(-n_{st}). \end{aligned} \qquad \cdots\cdots(10)$$

The variances of the statistics are evaluated by

$$\begin{aligned} V\{Q_1^*(s, t)\} = \int_s^t \frac{1}{n(\theta)} \left\{1 + \frac{v(\theta)}{n^2(\theta)}\right\} \\ \cdot \frac{dF_1(\theta)}{R_1(\theta)} + O(n_{st}^{-3}), \end{aligned} \qquad \cdots\cdots(11)$$

* Operations Research Laboratory

$$V\{R_1^*(s,t)\} = R_1^2(s,t) \cdot \int_s^t \frac{1}{n(\theta)} \frac{dF_1(\theta)}{R_1(\theta)} + O(n_{st}^{-2}), \qquad \cdots\cdots(12)$$

where we assume the continuity of $F_1(\theta) = 1 - R_1(\theta)$ $(\theta \in (s, t])$ and put

$$I(\theta-) = \{i \mid s_i < \theta \leq l_i, \quad 1 \leq i \leq n\},$$
$$n_{st} = inf_{s<\theta\leq t} \sum_{i \in I(\theta-)} R_0(s_i, \theta),$$
$$n(\theta) = \sum_{s_i \leq \theta < l_i} R_0(s_i, \theta),$$
$$v(\theta) = \sum_{s_i \leq \theta < l_i} \{1 - R_0(s_i, \theta)\} R_0(s_i, \theta).$$

Furthermore, we can show that $\sqrt{n}\{Q_1^*(s,t) - Q_1(s,t)\}$ and $\sqrt{n}\{Q_1^*(u,v) - Q_1(u,v)\}$ are, asymptotically, independently as well as normally distributed as n increases $(0 \leq s < t \leq u < v \leq t_0)$.

Thus, using the statitsics $(7 \sim 8)$ we can estimate the failure characteristics cause by cause from multiply and stochastically truncated data obtained by short term observations.

(Report No. 636, 1968)